Sequential 3D Read-Out Integrated Circuit for Micro-Bolometer

Alireza Eskandari Turk

Thesis submitted for the degree of
Master in Master's Program Name
60 credits

Department of Physics
Faculty of mathematics and natural sciences

UNIVERSITY OF OSLO

Spring 2021

Sequential 3D Read-Out Integrated Circuit for Micro-Bolometer

Alireza Eskandari Turk

Sequential 3D Read-Out Integrated Circuit for Micro-Bolometer

http://www.duo.uio.no/

Printed: Reprosentralen, University of Oslo

Preface

This Master's thesis was submitted for the degree of M. Sc. at the University of Oslo, dept. of Informatics. The work has been carried out in the period between spring 2020 and spring 2021 at the Nano electronic systems group under the supervision of Professor Philipp Dominik Häfliger.

Oslo, June 25, 2021

A.R. eskandari

Alireza Eskandari Turk

Acknowledgement

First and foremost, I would like to express my sincere gratitude to my supervisors, Philipp Dominik Häfliger. Your continuous guidance and scientific deep insights during our countless discussions have been invaluable. You have shown great enthusiasm and patience in my work, which has allowed me to develop both my knowledge and confidence. I would also like to thank Joar Martin Østby for your undisputed support and help in Cadence and circuit design.

A.E.

Abstract

In this thesis, a novel integrated read-out circuit (ROIC) for uncooled microbolometers is presented. It features in-pixel pre-amplification instead of just one amplifier per column or even just a single amplifier for the entire frame. The 3D-sequential integration (3DSI) process is used with two tiers (bottom and top) for designing, simulating, doing the layout, and evaluating the area optimization. Two types of Pre-amplifier are designed ,implemented and simulated based on the limited area under each pixel which is approximately 17 x 17µm in dimension on the layout and passive elements availability for each tier. The first amplifier is designed on the bottom tier and the second one is on the top tier while both amplifiers use resistor and capacitor from the bottom tier. A Size evaluation and optimization performed on both tiers while the functionality is almost the same with some adjustments. A decoder for selecting related pixel and Current sources for driving operational amplifiers in an example ROIC for 4x4 pixels are designed and simulated. This project is limited to simulation, and there is no tape out for this work because of some time limitations for actual production.

Contents

List of Figures

Chapter 1

Introduction

1.1 Thermal Monitoring

Different types of vision systems are used to cover our sight limitations. Principally , we can divide them in to two main categories: daylight vision and night vision. Ability to see in low-light conditions will give us many opportunities as humans have poor night vision compared to many animals, additionally, night vision has many industrial applications also. Infrared imaging science is the key tool for recognising objects and totally getting information about the facts without visible illumination since infrared radiation is emitted by all objects with a temperature above absolute zero . Temperature is defined as the energy level of matter which can be observed by some change in that matter. Temperature measuring sensors come in a wide variety and have one thing in common: they all measure temperature by sensing some change in a physical characteristic. A temperature sensing can be categorized in to two basic physical types: (a) Contact Temperature Sensing Types which is required to be in physical contact with the object being sensed. (b) Non-contact Temperature Sensing Types, These type of sensors use convection and radiation to monitor changes in temperature [57].

In general, the basic common types of temperature measurement sensors in industries are thermocouples, resistive temperature devices (RTDs, thermistors), infrared radiators, bimetallic devices, liquid expansion devices, molecular change-of-state and silicon diodes[57].

Remote sensing is the science of obtaining information about an object, area, or phenomenon through the analysis of data acquired by a device that is not in contact with the object, area or phenomenon under investigation. The process uses physical characteristics of an area or object by measuring its reflected and emitted radiation at a distance. Thermal imaging is a very powerful remote sensing technique for a number of reasons, thermal imaging data is collected at the speed of light in real time from a wide variety of platforms, including land, water, and air-based vehicles. It is superior to visible imaging technologies because thermal radiation can penetrate smokes, aerosols, dust, and mists more effectively than visible radiation. It is a completely passive technique capable of imaging under both daytime and night-time conditions. Fig. 1.1

shows one application of night vision system. The development of such systems is interested from the first applications and so much continuous works are done to update the quality and performance of the IR imagers till now.

Figure 1.1: Crew-1 Dragon return, night vision checking camera(4 main parachutes vision)[18].

Imaging based on temperature or Thermal imaging goes all the way back to year 1800 when infrared was discovered as a form of radiation beyond red light. Infrared light or for short (IR) , is a type of radiant energy that's invisible to human eyes but we can feel it as heat. IR wavelengths start from the edge of red color of the visible spectrum around 700 Nanometers (frequency 430 THz), to 1 millimeter (300 GHz). Infrared technology has many uses. One of the most notable usage of it is for thermal imaging cameras.A standard camera captures the light we can see with our eyes or visible part of it, but a thermal camera captures "invisible" infrared light, this ability is used for making technologies such as night vision goggles. The first thermal camera is almost 100 years old, and it used in the earlier wars of the 20^{th} century. But today, they're using as household and industrial items. Anybody can buy a camera with a thermal imaging sensor for a fair price and use it as a hobby or recreation [60]. Thermography, the process of using heat and infrared light to create an image goes back as far as early cameras. Hungarian physicist Kálmán Tihanyi first invented thermal imaging or “night vision” for British anti-aircraft defense following World War I. The new camera technology was so useful that it didn’t take long time to cross the Atlantic where it grew rapidly in the United States throughout the rest of the 20^{th} century. After its success with British anti-aircraft defense in the 1920s and 1930s, the U.S. Military and Texas Instruments created the first infrared line scanner in 1947 that allowed cameras to produce a single image (however, that process took one hour at the time). As image processing speed improved over time, cameras were used for more practical applications, such as seeing through smoke when firefighters are trying to locate people trapped in burning buildings. Thermal cameras wouldn’t reach the consumer market level until the late 20^{th} century, but they quickly became popular and used with different agencies, and companies. Fig. 1.2 shows one of the first IR camera in use [58].

Figure 25.2 1969: Thermovision Model 661. The camera weighed approximately 25 kg (55 lb.), the oscilloscope 20 kg (44 lb.), and the tripod 15 kg (33 lb.). The operator also needed a 220 VAC generator set, and a 10 L (2.6 US gallon) jar with liquid nitrogen. To the left of the oscilloscope the Polaroid attachment (6 kg/13 lb.) can be seen.

Figure 1.2: Outdoor substation infrared scan, circa 1969. Photo: FLIR Systems(Forward Looking Infrared).

1.2 Work Motivation

Detection and tracking in thermal infrared imagery has historically been of interest mainly for military purposes. Increasing image quality and resolution combined with decreasing price and size during recent years opened up new application areas. Thermal cameras have advantages in many applications due to their ability to see in total darkness, their robustness to illumination changes. There are currently two types of thermal imaging sensors on the market, cooled and uncooled.

(a)Cooled systems are maintained at a very low temperature by a cooling system. The fact that they are cooled presents them from being "blinded" by their own infrared emissions. Each time the system starts up, it must be cooled. These cooled sensors are the most sensitive to tiny differences in temperature between objects in the scene being observed. Cooled imagers are often bigger in size and heavier than uncooled imagers, but they offer very high image quality and are compatible with longer-range lenses.

(b) Uncooled (bolometer-based) systems are compact , and usually, they are not heavy. They are especially suited for mobile applications where weight is more important than image quality. Microbolometer-type detectors are much less expensive than their cooled equivalents, making them compatible with compact, affordable devices. These sensors are also more reliable in similar operating conditions. For surveillance applications, for example, microbolometers require much less maintenance than cooled sensors.

Uncooled (thermal) infrared sensors are one of the most typical MEMS-based devices [1]. They are a light weight and low cost alternative to their cooled counterparts also these IR focal plane arrays (IRFPAs) use in many applications such as medical imaging, thermography, night vision, surveillance and industrial process control which is under focus recently.

Also they can detect infrared radiation in the long wavelength infrared spectral band roughly between 8µm to 14µm. This ability gives them a wide rage of applications. Since objects near room temperature emit electromagnetic waves around a wavelength of 10µm so we can detect them in complete darkness and obtain information on their temperature with uncooled infrared sensors [1].

Fig. 1.3 illustrates the infrared sensor market. Both single-element infrared detectors and large-format infrared focal plane arrays (IRFPAs) have already been marketed. But a very large undeveloped market exists between them that cannot be filled with existing devices because of high cost and inadequate specifications. Over the past 20 years, although major efforts for uncooled infrared sensor development have concentrated on performance improvement. the interest is growing in the intermediate market. Recently, many researchers and some companies have been working on small-format infrared array sensors that are suitable for the new market.These new type of sensores are mainly include microbolometers . Based on end user, the market is categorized into military and defense, industrial, commercial, healthcare and life sciences, residential, automotive, and oil and gas [74].

---

[1] Microelectromechanical systems

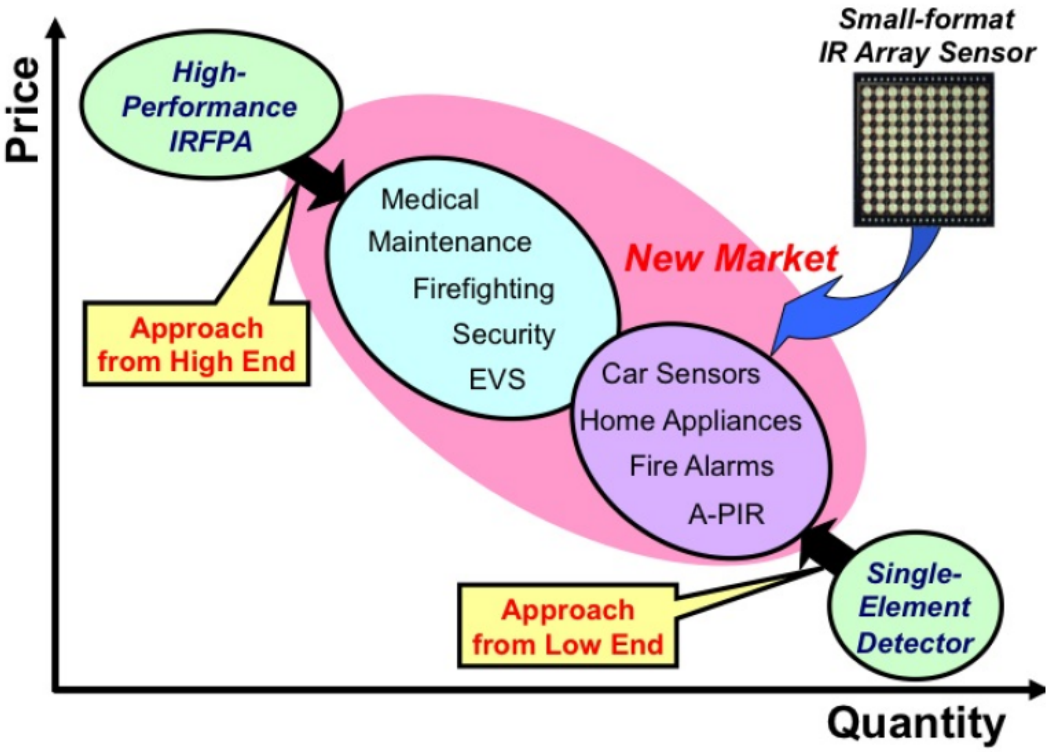

Figure 1.3: Structure of infrared sensor market. Large new market is expected between two existing markets: high-performance IRFPA and single element detectors [48].

Fig. 1.4 shows market evaluation for IR camera and up warding trend for both military and commercial applications at a CAGR of 8.8% over the forecast period (2021 - 2022) [2]. The IR camera market was valued at USD 4 billion in 2020 and expected to reach a value of USD 10 billion by 2026. With the increasing demand for advanced driver assistance systems (ADAS) in the future and investments in autonomous cars, IR cameras are expected to use significantly in vehicles [40].

---

[2] Compound annual growth rate (CAGR) is the rate of return that would be required for an investment to grow from its beginning balance to its ending balance, assuming the profits were reinvested at the end of each year of the investment's life span.

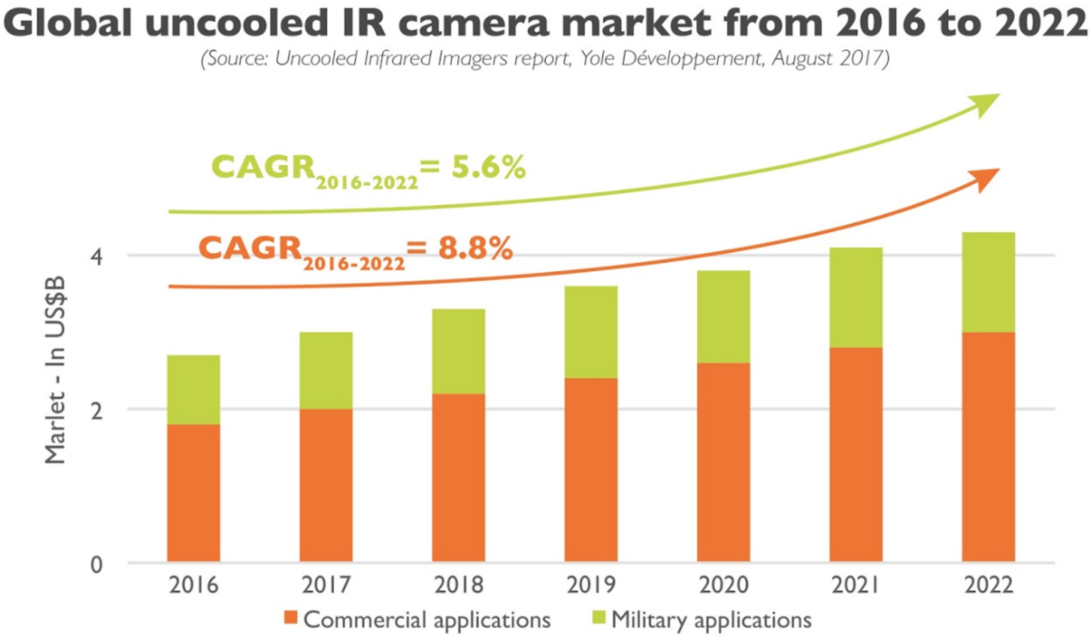

Figure 1.4: Market evaluation for IR sensors between the years 2016 and 2022 [40].

1.3 Thesis Proposition

In this thesis, the structure and principle of Bolometer will be discussed and take look at the microbolometer as a specific type of Bolometer which is used in many applications as thermal detector. Also a novel readout circuit is proposed with the cell integrated amplifier for improving noise issue of the existing methodes [47].

By using long metal interconnects as a part of the pre-digitization readout circuit, we should use buffers and, potentially we need to apply some noise cancellation techniques because of long metal routing increase noise. So that result in increasing power consumption and area overhead in the Layout. Thus re-thinking at the architectural level is crucial to meet these demands [61].

Accordingly, in this work by using an in-build amplifier for each IR cell in readout circuit , we can make short signal path (by shortening the metal interconnections) before amplification, which is always beneficial for noise reduction. Since this structure is rarely use for the pixel readout topology today, we can not compare it with the other examples. By reducing the noise, power consumption can be also reduced as a result of ignoring extra noise cancellation circuitry. Transimpedance amplifier (TIA) added for each cell with full voltage swing and pre-amplification can reduce the noise which can be an effective method for small size IR sensors [21]. In addition, in the readout circuit after pre-amplification there is source follower (SF) in each pixel which increase the signal current (will be discussed in readout implementation part). Most of the readout circuits use amplifier for every column or one for all pixels (we will cover this in the readout topology chapter 3.5). Adding amplifier has some advantages like , noise reduction and digitization possibility at the pixel level. But it has some drawbacks also. Firstly, by increasing the number of amplifiers, power consumption increases. Secondly, MOSFETs suffer from random, microscopic variations and hence mismatches between the equivalent lengths and widths of two transistors that are identically laid out. Device mismatch leads to dc offsets, which reduce the performance of circuit and increase nonlinear operation. Generally, most of the TIA amplifiers use differential pair and current mirror design configuration. Some techniques can be used to minimize mismatching effects at the transistor level by implementing common centroid layout , degeneration design and adaptive biasing [50]. Width and length of the transistor can effect overdrive voltage result in improving mismatch. Also some Electronic Mismatch cancellation methods can be used at circuitry level.

In mobile applications the size of sensor is important. Decreasing IR sensor size result in the pixel size decreasing. As the pixel size is decreased, low sensitivity rises severely. Fig. 1.5 shows the thermal response simulations of conventional microbolometer design with various pixel sizes.

If the pixel design is maintained the same, the short thermal conduction path at small pixel size show very low responsivity which is the gradient of the output signal as a function of the light intensity (The responsivity depends on how the light is hitting the pixel. The result is shading.)

In addition, the small pixel size requires more design in terms of mechanical and electrical characteristics. IR imaging sensors need a small-sized pixel for high resolution as well as for small form factor[3]. For the effective pixel design with high fill-factor[4], the anchor and leg area should be minimized because these spaces proceed to low thermal resolution by reducing IR absorption area [8]. The most efficient way to use these spaces by shared-anchor structures, which used to minimized the anchor and leg for more effective pixel with high fill-factor.

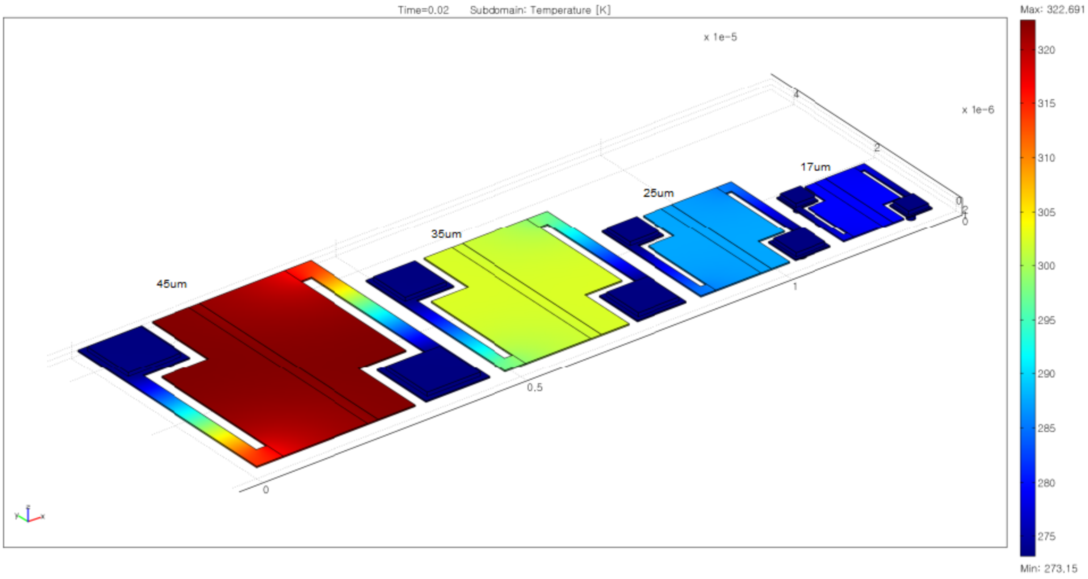

Figure 1.5: Thermal response of conventional microbolometer with various pixel sizes(form-factor).temperatures are in kelvin [45].

---

[3] hardware design aspect that defines and prescribes the size, shape, and other physical specifications of components, particularly in electronics devices or elements

[4] The fill factor of an image sensor array is the ratio of a pixel's light sensitive area to its total area. It will be explained in detail later on section 2.1.

Chapter 2

Background

2.1 IR Sensors and Bolometer Structure Overview

Infrared radiation was discovered by Herschel [34] using a mercury-glass thermometer to detect sunlight that distributed or spread over a wide area by a prism. Thermal detectors have played an important role in the exploration of infrared radiation to the present date Fig. 2.1 shows radiation spectrum. All thermal radiation detectors include an absorbing element with heat capacity C which converts the incident electromagnetic radiation to heat, and which is attached to a heat sink at temperature T_s via thermal conductance G. After the incident radiation power P is turned on, the temperature T_B of this absorbing element initially increases with time at rate $dT_B/dt = P/C$ and approaches the limiting value $T_B = T_S + P/G$ with the thermal time constant $\tau = C/G$ [64].

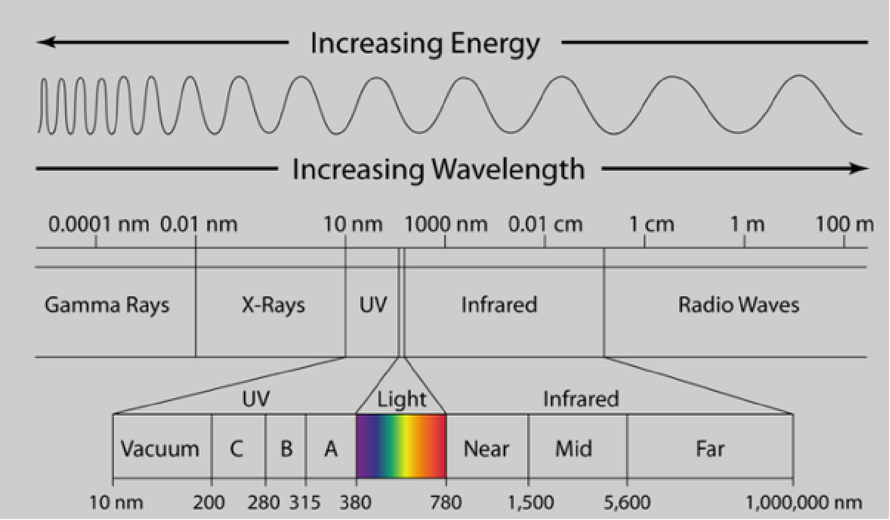

Figure 2.1: Different types of electromagnetic radiation spectrum.

When the radiation is turned off, it relaxes back to T_S with the same τ. Thermal detectors are different by the method they use to readout the temperature from the radiation absorber. The following frequently used examples illustrate the range of possibilities (methods which was used before bolometer invention).

1) In the radiation thermopile, the thermoelectric effect is used as the temperature readout. The output impedance of this thermometer is increased by using many thermocouples[1] in series, the hot junctions on the absorber, and the cold junctions on the heat sink Fig. 2.2 shows an example thermopile [5].

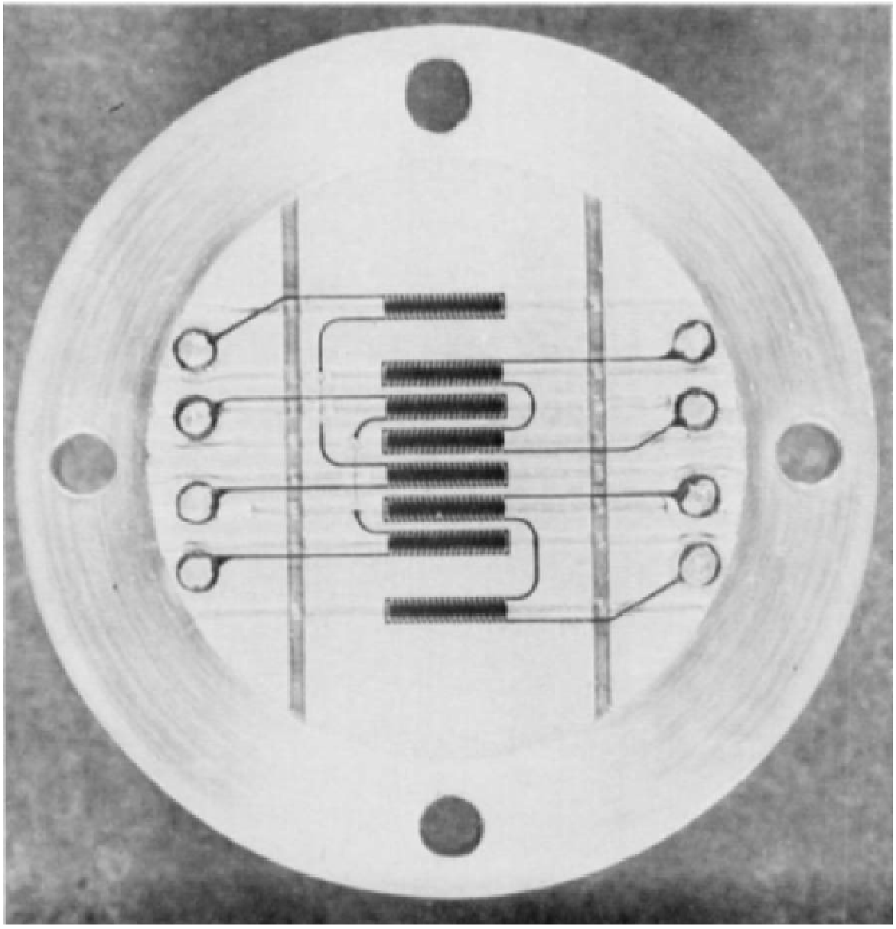

Figure 2.2: Eight thermopile arrays. Each 0.4 mm x 6.0 mm thermopile contains 40 junctions. [5].

---

[1] A thermocouple is a sensor for measuring temperature. This sensor consists of two dissimilar metal wires, joined at one end, and connected to a thermocouple thermometer or other thermocouple-capable device at the other end. When properly configured, thermocouples can provide temperature measurements over wide range of temperatures.

2)In the Golay pneumatic detector, the heat absorbed in a thin metal film is transferred to a small volume of gas. The resulting pressure increase changes the angle of a mirror in an optical amplifier Fig. 2.3 shows Golay Cell Schematic [32].

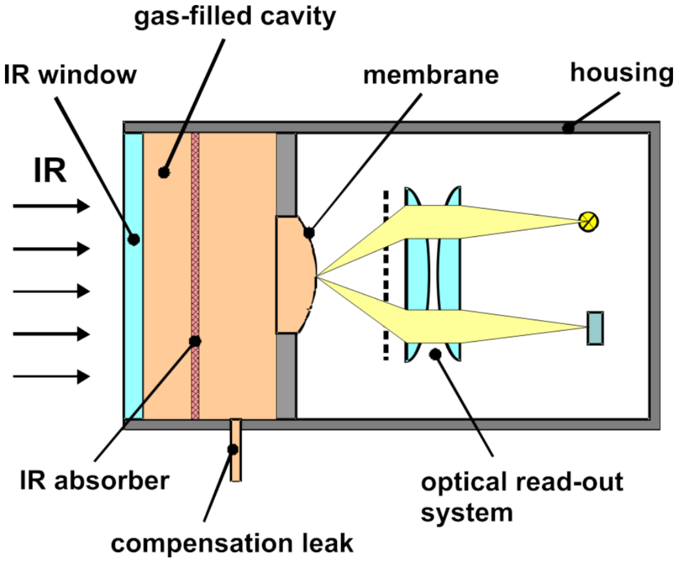

Figure 2.3: Golay Cell Schematic)[32].

3)In the pyroelectric detector, the absorbed heat increases the temperature of a material whose dielectric constant is a sensitive function of temperature. This pyroelectric material is contained in a voltage-biased capacitor which acts as a source of current proportional to the time rate of change of the dielectric constant.Both the Golay and the pyroelectric detector have been widely used in laboratory infrared spectrometers since the 1960s Fig. 2.4 shows Pyroelectric sensor structure [64].

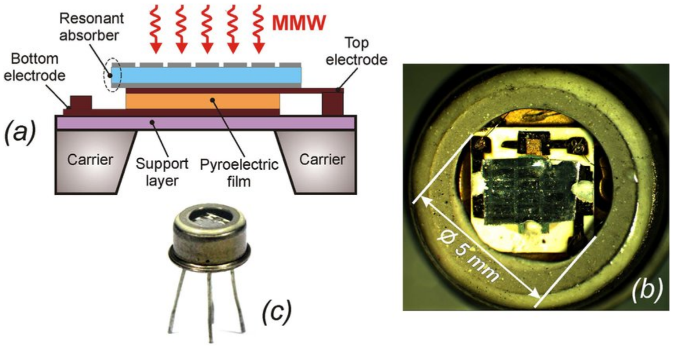

Figure 2.4: Pyroelectric sensor. (a) Sketch of the pyroelectric sensor with an integrated resonant absorber. (b) Photo of the sensor structure through the sapphire window. (c) Appearance of the accomplished sensor in the standard KT-3 package [51].

The bolometer, which was developed by S. P. Langley (1981) is a thermal infrared detector which employs an electrical resistance thermometer to measure the temperature of the radiation absorber.

In general, Bolometer is a device for measuring the power of electromagnetic radiation via the heating of a material with a temperature-dependent electrical resistance. Electromagnetic radiation (EM radiation or EMR) includes radio waves, microwaves, infrared, (visible) light, ultraviolet, X-rays, and gamma rays, as shown in Fig. 2.1. A sensitive thermometer with electrical resistance varies with temperature is used for detecting and measuring of thermal radiation.[64].

A bolometer structure is made up an absorptive element, like a thin layer of metal which is connected to a thermal reservoir which is a heat sink or a body with constant temperature through a thermal conductance. Absorber element hits by radiation and it's temperature raises above the thermal reservoir's temperature. Absorber change the radition power to the temperature.

The speed of the detector is set by thermal time constant which is defined by The time required for a thermistor to change 63.2% of the total difference between its initial and final body temperature when temperature changed by step function from T_a (ambient temperature) to T_∞ (final temperature) Fig.2.5 . The intrinsic thermal time constant is defined by τ_w:

$$\tau_w = \frac{heat\ capacity\ of\ the\ absorptive\ element}{thermal\ conductance\ between\ the\ absorptive\ element\ and\ the\ reservoir}$$

Changing in the temperature can be measured directly with an attached resistive thermometer(thermistor), or by the resistance of the absorber element itself. Thermistor is a type of thermal resistor made of semiconductor material and has a negative temperature coefficient. The negative temperature coefficient means their resistance decreases with the increases in temperature.

Usually, metal bolometers don't need cooling system and they are made of thin foils or metal films. Semiconductors or superconductors use as absorptive elements in stead of metals with greater sensitivity. These devices can be operated at very low temperature with significantly better sensitivity.

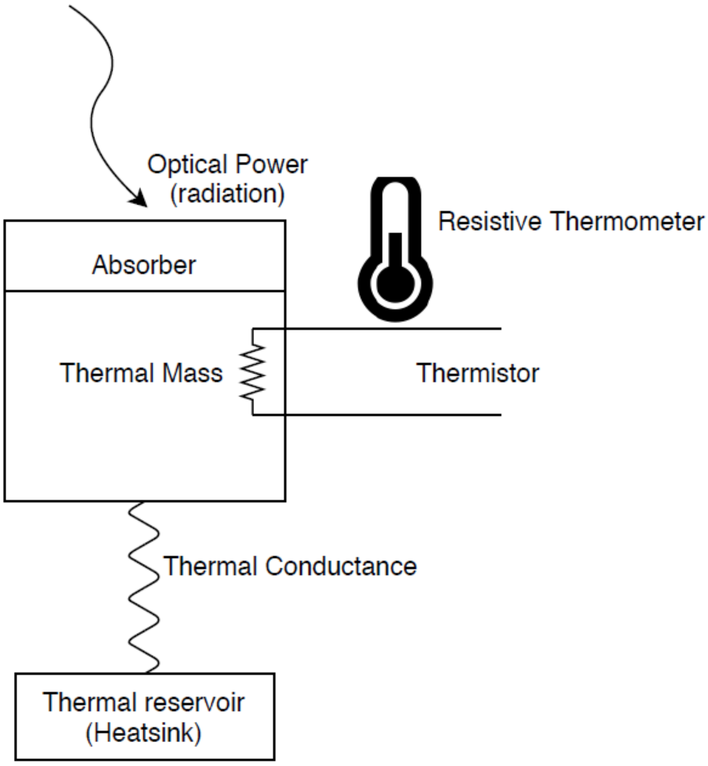

Figure 2.5: Structure of Bolometer [28] .

Before moving to the microbolometer structure, two important definitions will be discussed, in order to evaluate the detector properties[23].
The first one is fill-factor which is the detection area to the detector area; its values depend on the structure and the shape of the supporting leg. In a sensor with the high fill factor pixels, more number of photons is captured in comparison to a sensor with the low fill factor pixels. Hardware innovations in image sensor technologies are achieved to increase the fill factor by decrease of occupied area of the pixel transistors. One of the effective way to in-crease the fill factor is to put a microlens or an umbrella above each pixel which converges light from the whole pixel unit area into the absorber in order to capture more number of photons as shown in Fig.2.6. Since 90s, various techniques have been developed for increasing fill factor and they are widely used in different type of sensors. But it is still impossible to make fill factor 100% in practical production due to the physical limits in digital camera development [24, 26]. Fig. 2.7 shows various microbolometer topologies for improving fill factor.

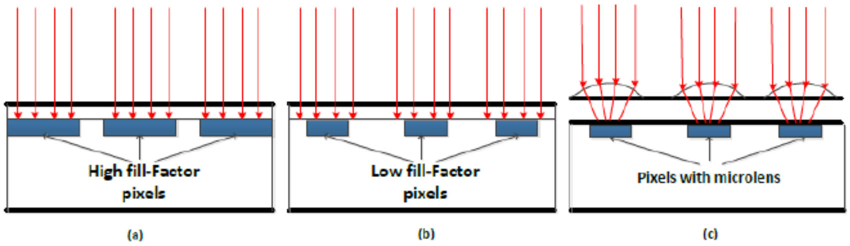

Figure 2.6: Light incident on sensor with high and low fill factor pixels are shown in (a) and (b) respectively. (c) Pixel with the micro-lens is used to compensate the entering light [16].

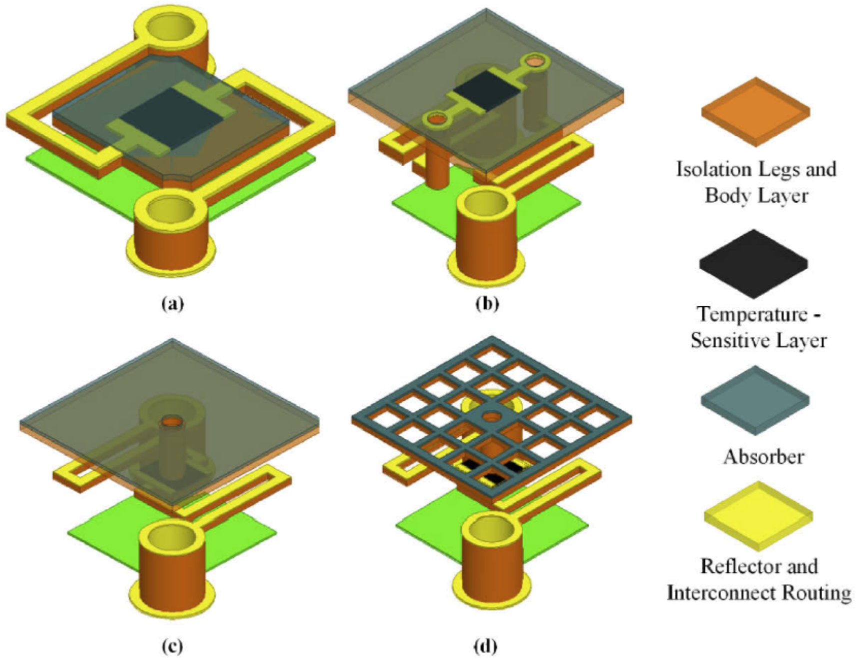

Figure 2.7: 3D illustrations of various microbolometer topologies.(a) A typical one-level topology involves the absorber layer, the temperature-sensitive part, interconnect routing, and the thermal isolation legs on the same vertical space, with which either the filling factor is too small or the thermal isolation is too low . (b) Isolation legs are vertically spaced apart from the temperature-sensitive part and the absorber layer in order to make more room for longer isolation legs with a typical two-level topology . (c) Umbrella solution leaves the interconnect routing in the first level and helps increasing the filling factor in the second level , and (d) perforations to the umbrella layer is introduced to further enhance the overall detector performance [12].

The second definition is Amorphous silicon (a-Si) which is the non-crystalline form of silicon used for solar cells and thin-film transistors.As mentioned a-Si is also used in thin films for variety of substrates and flexible substrates, such as glass, metal and plastic [11]. The principal advantage of amorphous silicon is their lower manufacturing costs, which makes cells very cost competitive. One of the main advantages of a-Si over crystalline silicon is that it is much more uniform over large areas.

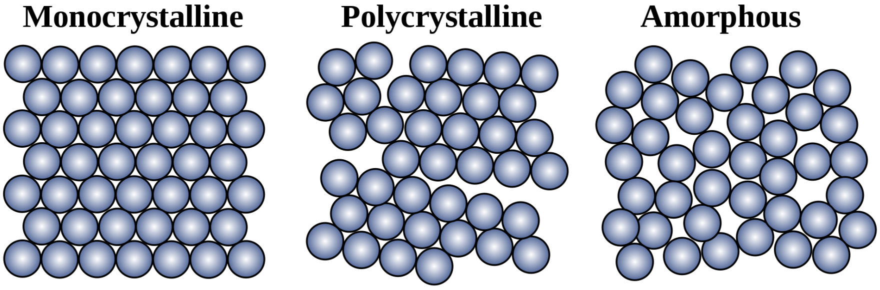

Figure 2.8: Schematic of allotropic forms of silicon: monocrystalline, polycrystalline, and amorphous silicon

The two most commonly used IR radiation detecting materials in bolometers are amorphous silicon and vanadium oxide (V_2O_5 Vanadium(V)oxide or vanadium pentoxide). Amorphous Si (a-Si) works well because it can easily integrated into the CMOS fabrication process, it is highly stable, has a fast time constant, and has a long mean time before failure (MTBF). A thermal imaging camera with Vanadium Oxide Micro-bolometer detector is more stable, compact, sensitive compare with any other technology although VOx is older technology. VOx market share is closely 70% where as Amorphous Silicon is about 13%. Also, VOx technology based thermal cameras are being used in Defence Sector due to its sensitivity, image stability and reliability [22, 81].

A *microbolometer* is a specific type of bolometer which is used in many mobiles or stationary applications as a thermal detector. Microbolometer belongs to the group of thermal detectors and consist of temperature sensitive resistor which is exposed to measured radiation flux. Bolometer array employs a pixel structure prepared in silicon micromachining technology (MEMS) is called microbolometer. When radiations hit the detector, it makes heat and changes its electrical resistance. This resistance change is measured and processed into temperatures that can be used to create an image or data. Usually, microbolometers do not need cooling system, unlike other types of radiation/infrared detecting equipment [87].

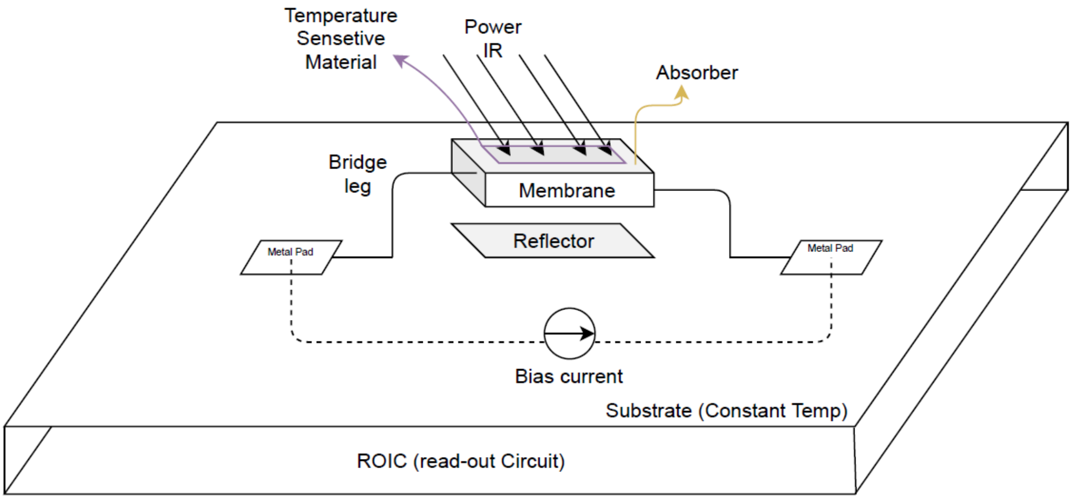

Figure 2.9: Basic structure of an uncooled microbolometer pixel.

The sensitivity of the microbolometer can increase by using semiconductors or superconductors as absorptive elements rather than using metals film. In comparison to the conventional high-resolution thermal sensors which required expensive cooling methods like liquid nitrogen or helium gas coolers. These cooling methods make early thermal imager sensors expensive to operate with limited mobility. Additionally, most older thermal imagers required a cool down time before being usable.
A microbolometer consists of an array of pixels and each pixel is made up of several layers. Basic structure of microbolometer shown in Fig.2.9. Different procedure will be used for producing microbolometer also a variety of different absorbing materials used in the structure. In Fig.2.9 the bottom layer consists of a silicon substrate and a readout integrated circuit (ROIC) as an example. Also Fig.2.10 shows schematically the structure of such a pixel , and Fig.2.11 represents a Scanning electron microscope(SEM) view of an active pixels processed on a ROIC substrate.

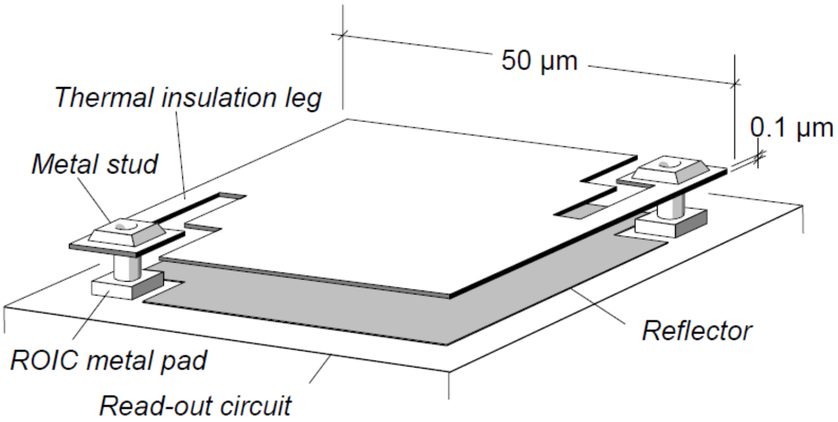

Figure 2.10: Schematic of microbolometer pixel.

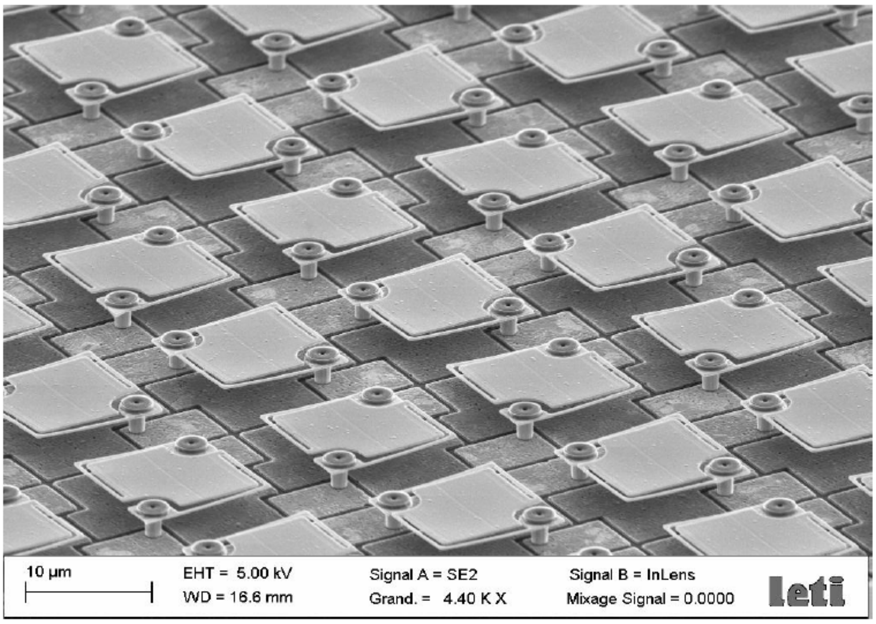

Figure 2.11: SEM photography of an active pixels processed on a ROIC [69].

2.1.1 Pixel architecture

Usually, the microbolometer has at least 2 anchors and 2 legs with λ/4 (quarter wave length) resonant cavity structure for fully absorbing of infrared or electromagnetic waves. Fig. 2.12 shows 4 kinds of 3D geometric single–element microbolometer structures [35].

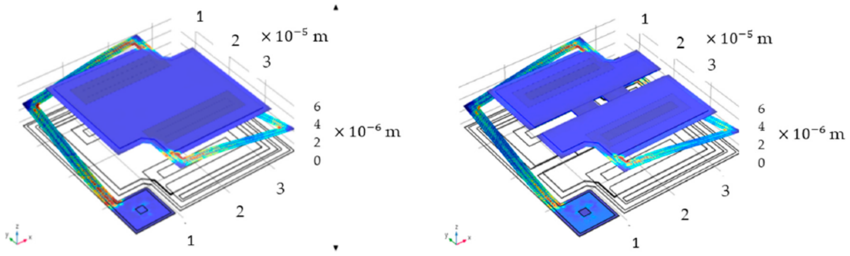

(a) Design 0 (b) Design 1

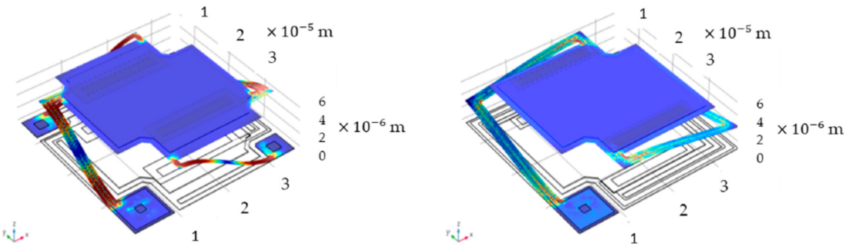

(c) Design 2 (d) Design 3

Figure 2.12: The 4 kinds of top-view 3D geometric 35 µm pixel pitch single-element microbolometer structures, where (a) Design 0 is the standard L-shaped dual-leg structure for reference; (b) Design 1 with 2 µm × 2 µm central square hole and two 7.5 µm × 2 µm slits on the suspended area; (c) Design 2 with 4-leg structure used for strengthen the suspended supporting and (d) Design 3 is the structure with increasing the gap between two contacts, from 14.5 to 20.5 μm as an example design [89].

In general, an infrared detector generates temperature changes by absorbing infrared light from the external environment and converts those changes into an electrical signal, so the infrared absorption structure plays an important role in enhancing detector sensitivity[14, 31]. Most infrared detectors consist of a metal reflector, a quarter wave floating membrane, and an absorption film because 50% of the incident radiation is absorbed and the rest of infrared light is transmitted or dispersed. Therefore, in order to achieve efficient infrared light absorption, a gap design (2.5 µm for quarter wavelength at 10 µm) without loss of incident or reflected light is necessary for 100% absorption in the ideal case.

When the pixel size is large (45 µm for example), the area of the anchors and legs are not as important for determining the responsivity as the IR absorbing area is sufficiently large. However, the responsivity at pixel sizes below 25 µm is more affected by the area of the anchors and legs. In this case, the anchor and leg areas should be minimized to increase fill factor. When the neighboring pixels share the same anchor, this area will be also shared by the pixels. As a result, it is possible to design a single-anchor-per-unit-pixel structure by sharing the anchors with four neighboring pixels. Unit pixels have four legs, only two of which are electrically conductive in order to isolate electrically and thermally from the neighboring pixels [45].

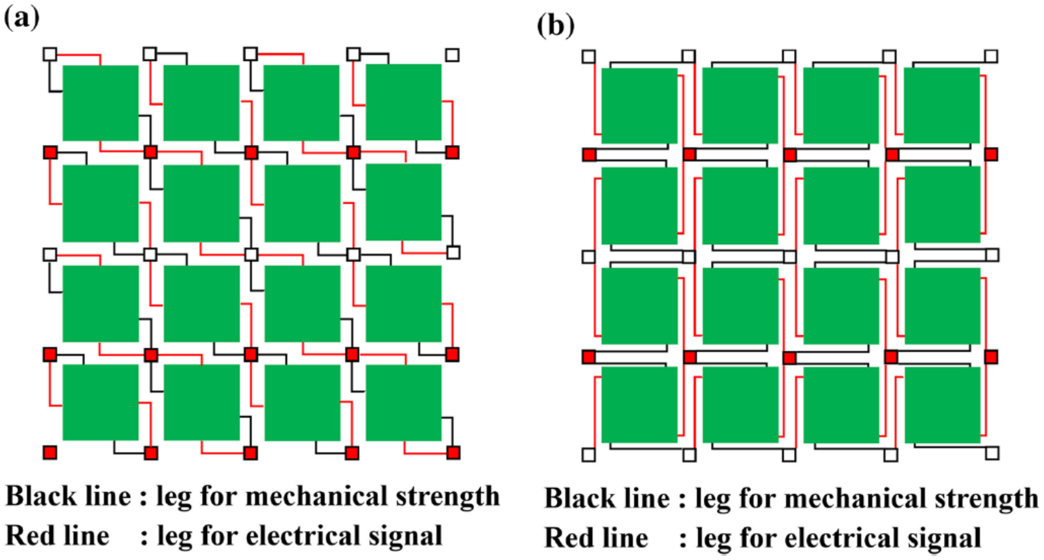

Figure 2.13: Design concepts of the proposed microbolometer using shared anchor structure 2 typologies a and b suggested [45].

As shown in Fig. 2.13, two types of pixel designs are suggested and their fill factors increase by 10% compared to the normal unshared-anchor design.

2.1.2 Mechanical and Thermal Design

Mechanical deformation of unit pixel should be minimize. This is important to maintain the optically resonant cavity structure and electrical uniformity through the membrane. The detecting area is defined by a size of thin membrane. Focal plane array (FPA) is made of a large number of detector elements, where each individual detector has different responsivity and offset due to detector-to-detector spread in the FPA fabrication process, and additionally can change with sensor operating temperature, biasing voltage variation or temperature of the observed scene. The difference in responsivity and offset among detectors (which is called nonuniformity) with its high sensitivity, produces fixed pattern noise (FPN) on produced image [7] [83].

Fixed pattern noise degrades parameters of infrared cameras like sensitivity or NETD (Noise Equivalent Temperature Difference will be discussed in section 2.1.4) [59]. Additionally it reduces image quality and temperature resolution. As an example structure, new shared anchor designs have 4 anchors around unit pixel to minimize the free-end corner and edge which show high mechanical deformation in normal unshared anchor design [42].

Under the same thickness and material properties, the simulation results show that shared anchor structures have lower mechanical deformation than that of unshared anchor structure as shown in Fig. 2.14 Minimization of free-end edge is more effective to decrease the mechanical deformation and design 1 has the lowest deformation.

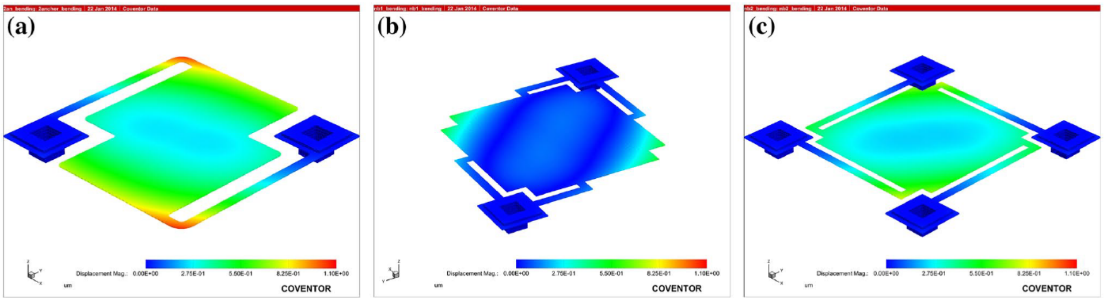

Figure 2.14: Mechanical deformation simulation of the proposed microbolometer using shared anchor structure: a 2 anchor, b design 1 and c design 2

Thermal simulation is performed with the assumptions of ambient temperature, vacuum condition and the irradiated IR power condition of 2nW/μm^2. The transient thermal response depends on the leg length and parameter like fill factor. Membrane temperature is determined by leg design and design 1 reaches at the highest temperature at the same irradiated IR power with the highest fill factor [45].

2.1.3 Fabrication

Amorphous Si based microbolometer is popular to fabricate. The previous microbolometers have fabricated using typical MEMS (micro-electro-mechanical systems) process using polymeric material and wet process. Polymeric sacrificial layer has many problems such as degassing during post process which is an important key-step in polymer processing, during the process low-molecular-weight components are removed from a polymeric system and make it pure. Also other problem with using this method is limitation of processing temperature [45].

MEMS processes such as wet cleaning and lift-off process can give yield problems. yield is the percentage of the devices on a wafer that function properly. high yields are difficult with MEMS devices due to their mechanical complexity and their integration with the necessary microelectronics also reliability of fabricated MEMS due to the phenomenon known as stiction which is about the sticking of structural elements either to the substrate or the adjacent elements. Fig. 2.15 shows some typical MEMS process for microbolometer.

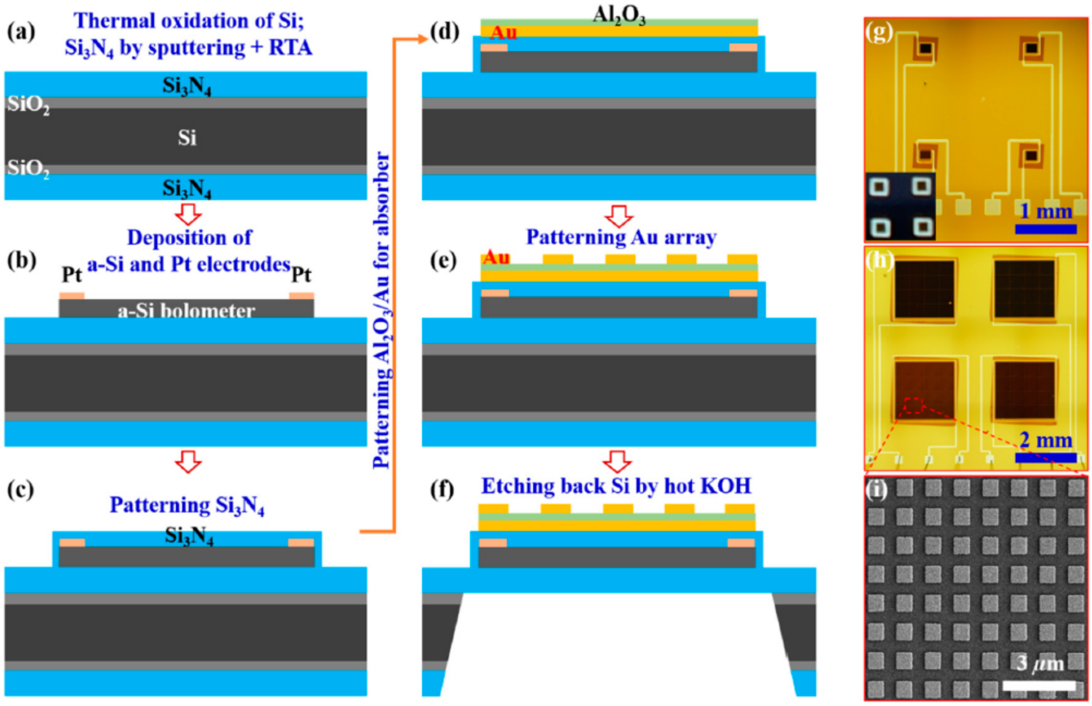

Figure 2.15: (a)–(f) Fabrication procedure of the MEMS-based wavelength-selective absorbers. (g) and (h) Top-view optical microscope images of the fabricated MEMS wavelength-selective bolometers with different square antenna sizes of the individual sensors. The inset in (g) reveals a photo of the MEMS-based quad-wavelength bolometer with the clear transparent Si_3N_4 membrane around each bolometer. (i) Top-view SEM image of the typical MEMS sensor [73].

By applying completely dry process using CMOS compatible materials and process without any problems of degassing and temperature limitation. Membranes are consisted of SiNx substrate (SiNx thin films have good properties and advantages as low temperature processed barrier layers, and they can be adopted in the thin film transistor (TFT) type), a-Si resistor and Ti(Titanium) absorption layer is used so, when fabricated devise is checked by SEM(scanning electron microscope), It shows very clean surface and high mechanical robustness. Fig. 2.16 shows microbolometers with 25 µm pixel size [45].

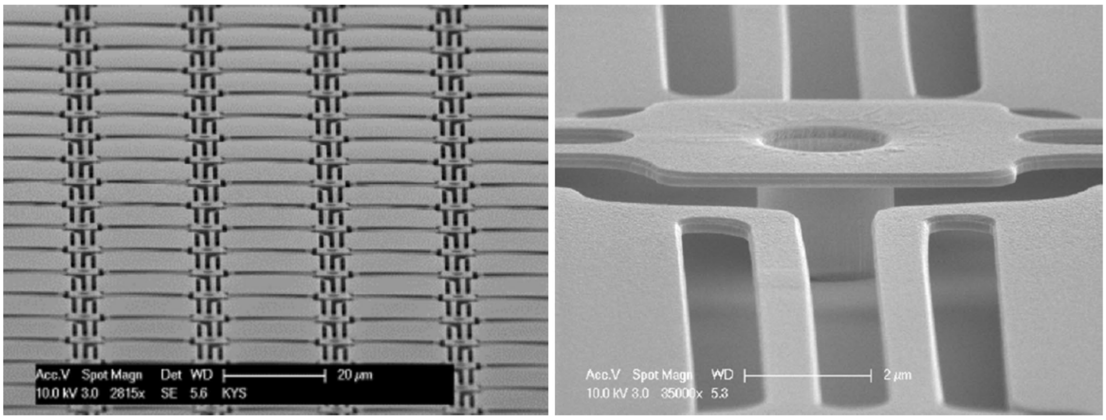

Figure 2.16: SEM image of released microbolometers with 25 µm pixel size [45].

A titanium mirror can be used as a reflector, which is placed beneath the IR absorbing material for increasing absorption. Since some light is able to pass through the absorbing layer, the reflector redirects this light back up to ensure the greatest possible absorption and, allowing a stronger signal to be produced.
The Next layer is a sacrificial layer. this layer is based on fundamental technology for creating movable parts so later in the process a gap can be created by pseudo-3D μmachine to thermally isolate the IR absorbing material from the ROIC(readout circuit). on top of sacrificial layer A layer of absorbing material is made. In order to create the final bridge like structure (leg) shown in Fig. 2.17, the sacrificial layer is removed so that the absorbing material is suspended above the readout circuit. Membranes consisted of a SiN_x substrate, an a-Si resistor, and a TiN absorption layer.
Since microbolometers do not need any cooling system so the absorbing material must be thermally isolated from the bottom ROIC and the bridge structure. After the array of pixels is created the microbolometer is encapsulated under a vacuum to increase the longevity of the device. In some cases the entire fabrication process is done in vacuum.

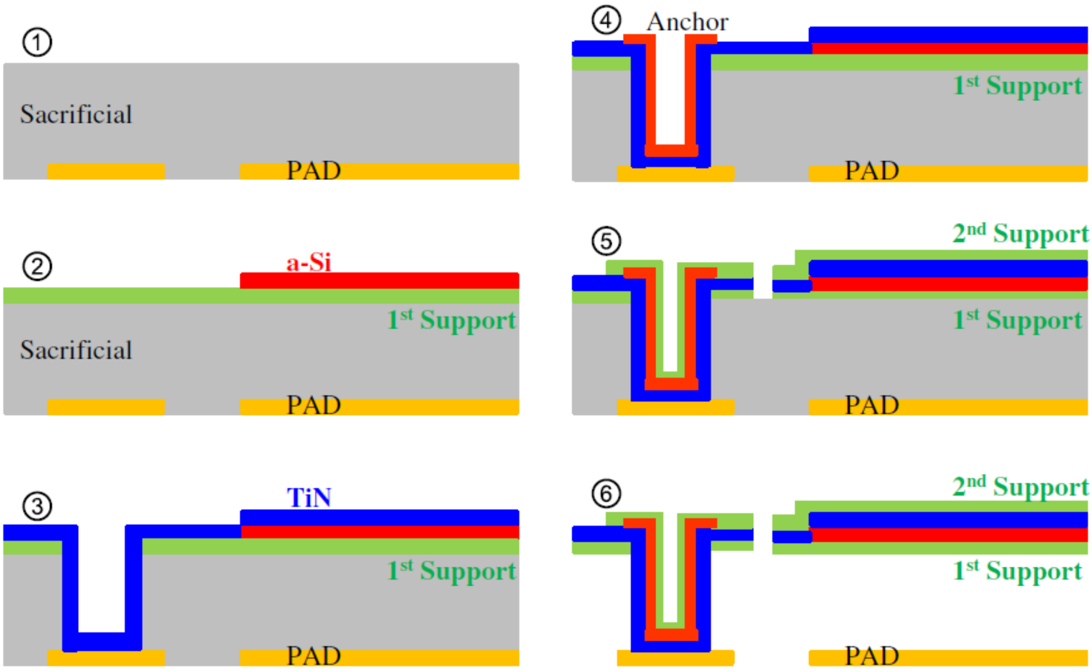

Figure 2.17: Typical process flow of microbolometer [45].

Some of the challenging points in designing of the new microbolometer are mentioned below.

-The quality of images created from microbolometers has continued to increase. As the pixel size is decreased and the number of pixels per unit area is increasing proportionally, an image with higher resolution is created, but with a higher NETD (Noise Equivalent Temperature Difference) due to smaller pixels being less sensitive to IR radiation. NETD or thermal sensitivity is importance for the process of evaluating and comparing performances of thermal imagers which are essentially non-contact temperature measurement devices.
These systems have small pixel pitches ($< 25\mu$m) and require power effciency, low noise equivalent temperature difference (NETD) (< 50 mK, "milli-Kelvin"). Low NETD demands excellent microbolometer and readout noise performance [55] (NETD will be discussed in detail in section 2.1.4. It has effect on image quality which is important in the thermal imager development.).

-Temperature coefficient of resistance (TCR) The material used in the detector must represent large changes in resistance as a result of changes in temperature in a short time. When the material is heated, due to the incoming infrared radiation, the resistance of the material decreases. This is related to the material's temperature coefficient of resistance (TCR) specifically its negative temperature coefficient. Manufacturers of microbolometers try to use material with TCRs near $-2\%/K$. However many other materials have far higher TCRs that need to be taken into consideration when producing optimized microbolometers. The resistance of the metal increases with the rise in temperature. So, the temperature coefficient of resistance is positive for metal. but for semiconductor or other non-metal, the number of free electrons increases with an increase in temperature. so the resistance of non-metallic substances decreases with an increase in temperature. therefore temperature coefficient of resistance is negative for non-metallic substances and semiconductors[82]. Fig. 2.18 shows The electrical resistance for metal and semiconductors.

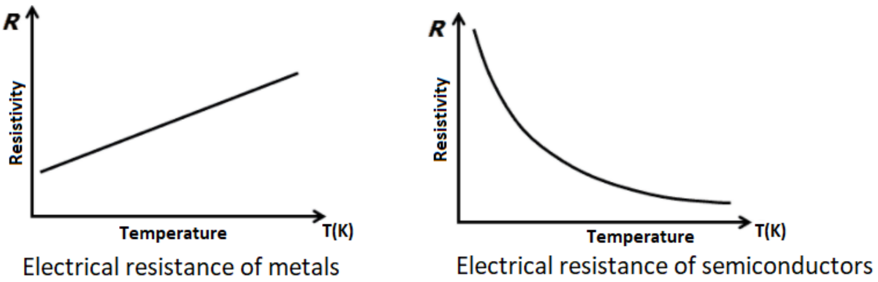

Figure 2.18: The electrical resistance for metal and semiconductors

-Flicker noise or 1/f noise, Changes in temperature across the absorbing material are determined by changes in the bias current or voltage flowing through the detecting material. If the noise is large then small changes that occur may not be seen clearly and the device is useless. Using a detector material that has a minimum amount of 1/f noise allows for a clearer signal between IR detection and the output. Detector material must be tested to evaluate the effect of this noise on the signal[36], [37].

-Power consideration, by using a material that has low room temperature resistance is also important. Lower resistance across the detecting material mean less power. Also, there is a relationship between resistance and noise, the higher the resistance the higher the noise. so low resistance can meet the low noise requirement.

2.1.4 Noise Equivalent Temperature Difference

NETD is one of the important parameters at the technical details of a thermal camera. The expression stands for "Noise Equivalent Temperature Difference". it represented the ability to distinguish between very small differences in thermal radiation in the image by thermal detector. NETD is typically expressed in milli-Kelvin (mK). It is also sometimes referred to as "Thermal Contrast". When the noise is equivalent to the smallest measurable temperature difference, the detector has reached its limit of its ability to resolve a useful thermal signal. The more noise there is, the higher the NETD value of the detector.

Typical values for uncooled, micro-bolometer detector thermal cameras are about 45 mK. Scientific cameras with photon based and cryogenically cooled detectors can achieve NETD values of about 18 mK. The noise measurement value should be specified at a particular object temperature, as this impacts the measurement. Example: NETD at 30C° is 60 mK.

For measuring the noise equivalent temperature difference of a detector, the camera must be pointed at a temperature controlled black body. The black body needs to stabilize before starting the measurement. Also a black body is a physical material with zero reflectivity and perfect emission. This means that a blackbody at constant temperature absorbs all incident radiation at all angles and the spectrum of radiation it emits is based on only temperature and no other physical property. The noise equivalent temperature difference is then being measured at a specific temperature. It is not a single snapshot measurement, but using a time related measurement of noise.

Fig. 2.19 shows the same scene recorded by two different cameras. One camera has an NETD of 60 mK and the second has value of 80 mK. The areas in the image with very low temperature show significantly more noise in the image taken with the 80 mK camera. 20 mK difference doesn't seem like much, but it has a potentially huge impact on the image quality and measurement accuracy [80].

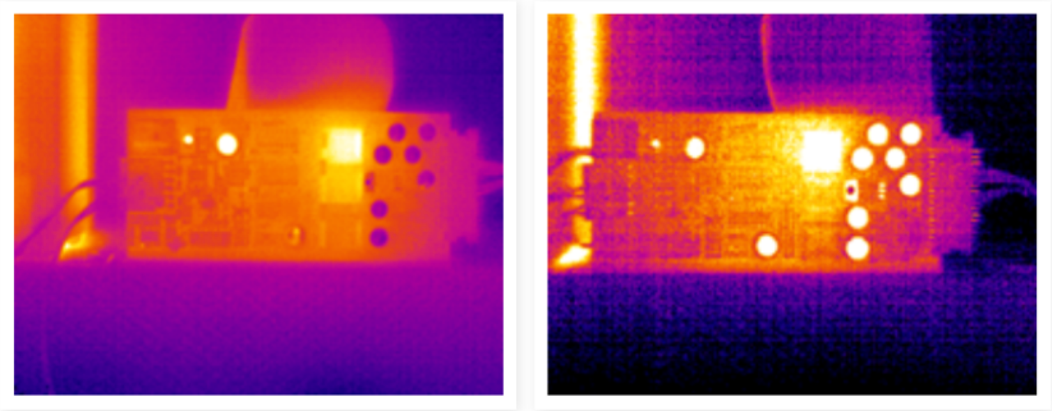

NETD 60mK NETD 80mK

Figure 2.19: NETD affect [80].

There are several factors that can affect NETD. Thermal cameras sometimes come with more than one calibrated temperature measurement range. The noise reading can vary based on the selected range and also the object temperature. As long as there is significant thermal contrast in the image and the temperature of interest is a lot higher than the background temperature, then this won't affect the measurement accuracy much. The noise level can also be affected by the detector and/or camera temperature. If the camera is exposed to a high ambient temperature, the system noise may increase. This depends on how well the camera is internally stabilized. Another variable that can affect NETD is the f-stop (Focal-STOP) of the lens. The f-stop or aperture of the lens determines how thermal radiation reaches the detector. Generally, a lower f-stop will lead to a better noise value [3, 88].

In brief, the lower NETD value has these features:
-Good image quality.
–Simple to understand and easy to focus on the camera.
-Higher efficiency with a better image.
-Ease of identifying the objects in a thermal image.
Fig. 2.20 represents other example picture differences between two cameras with different NETD.

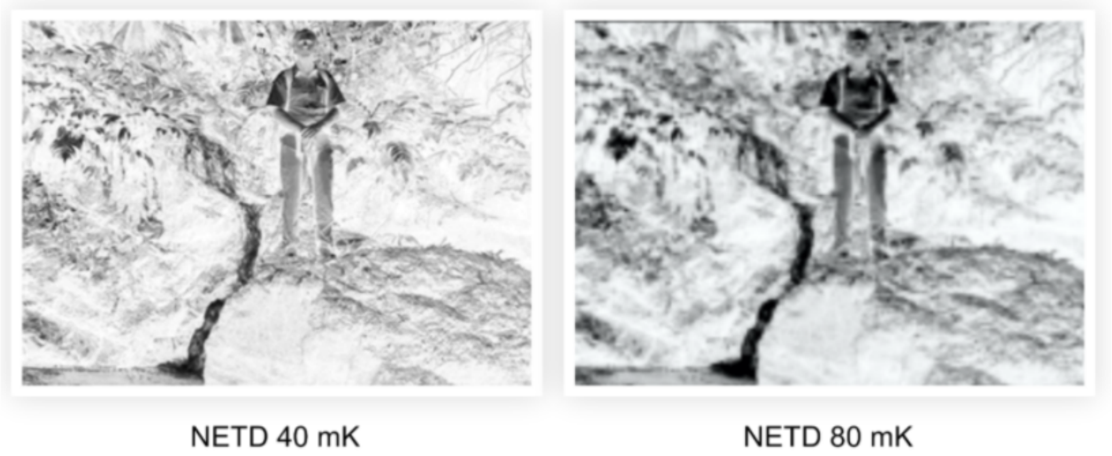

Figure 2.20: Comparative illustration of thermal images captured by the thermal camera of different NETD values [30].

2.2 Applications

The major applications of the bolometer include the following.
- A bolometer is an extremely sensitive device used for detecting electromagnetic radiation or heat. Many devices use thermal camera which is based on microbolometer. Fig. 2.21 shows some products with uncooled infrared technology.
- Emerging applications of this device are thermal imaging, scientific, monitoring of the remote environment, solar probes, and THz communication.
- It is used in particle detectors, thermal cameras, scanners of fingerprint, forest fire detection, concealed weapons detection, air surveillance, and astronomical applications.

Application requirements of microbolometer based imaging systems are pointed out in Fig. 2.22 and 2.23. While recent developments in microbolometer detector technology have allowed the reduction of cost and size, improvements are still required on the readout circuits and lower the overall power consumption. The Figures of merit, related to microbolometer imagers, that are directly affected by these requirements include NETD and readout dynamic range (digital resolution).

Figure 2.21: New uncooled infrared products in 2018.

Uncooled microbolometers also use in industerial monitoring and medical imaging. Thermal cameras use microbolometers to get accurate infrared images with high quality. Particle detectors for measuring radiation levels is another application. Security services, such as the police and military, use to detect concealed weapons. Some types of fingerprint scanners, Air surveillance to survey concealed areas and Forest departments use bolometers to detect and study forest fires.

By using smarter IR sensors made thermal cameras more practical and affordable for the consumer market such popular usage listed below: -Night vision (popular with hunters)
-Building inspection (checking for hot water pipe leaks and insulation) Roof inspection
-Law enforcement (helicopter units following a suspect on foot)
-Medical testing and diagnosis
-Automotive night vision
-Paranormal tracking (debatable if it works but a popular hobby nonetheless)
-Hobby photography
-Security.

Law enforcement and medical uses might not sound very “consumer,” but the affordability of these devices makes them available to even small-town police departments and hospitals. Some other advancements in thermal imaging today and in the future can

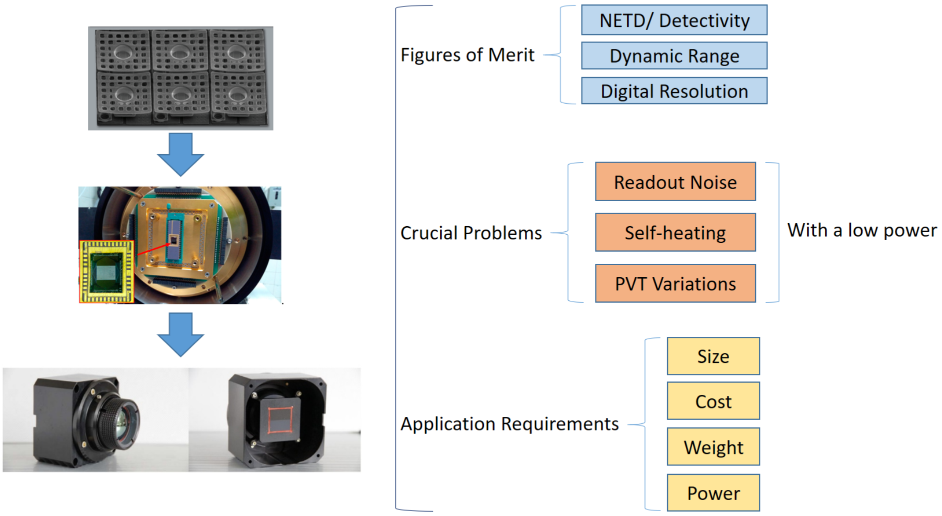

Figure 2.22: Applications of thermal IR cameras

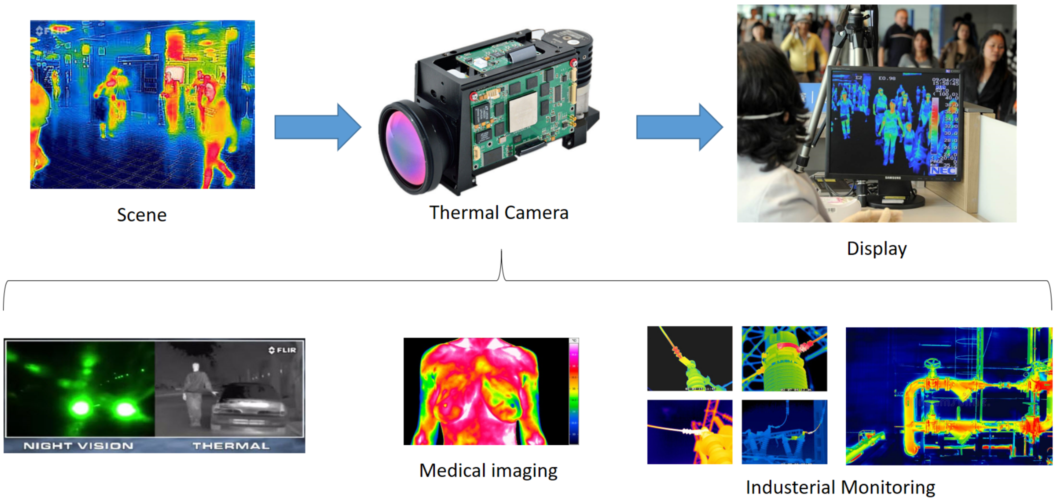

Figure 2.23: Application Requirements and Figures of Merit of Microbolometer Imagers

be distance measurement as right now, a good consumer thermal imaging camera can detect heat signals across a football field and expects that distance to increase rapidly

and sensors grow and processors improve. It's not unreasonable to expect something similar to a telephoto lens for thermal cameras in the very near future. Also usage in drones, right now a thermal camera and exploring an area where normal drone cameras are legal. As drones get better, so with their uses with a thermal imaging camera attached to the bottom.
Agencies such as NASA and ESA, which are involved in astronomical studies, make use of these equipment in their observation devices to study outer space in the far-infrared spectrum. Bolometers are directly sensitive to the energy which is left inside the absorber so they can be used for variety purposes with different type of input such as ionizing particles, photons, non-ionizing particles, any sort of radiation, and even to search for unknown forms of mass or energy. for example BGO scintillating bolometer as dark matter detector prototype Fig.2.24 [17].

Figure 2.24: BGO scintillating bolometer

Bolometers can also measure microwaves that are emitted by a pulsing power source. This technology uses in automotive safety by detection of moving objects in front of a vehicle. specially when we don′t have so much light another application can be security cameras Fig 2.25 shows some night vision application [49].

Figure 2.25: Automotive night vision

2.3 Biasing Circuits for the Uncooled IR Detectors

The readout circuits used for the uncooled infrared detector arrays perform two basic operations:
1) pixel addressing in the detector array.
2) low noise amplification before and any signal processing stages.
The addressing circuitry (usually, A decoder is used for this purpose.) can be common for different detector types, however pre-amplifier structure differs for different detector types. Pre-amplifier must be able to read out different detectors with minimum signal loss and minimum noise contribution.
Basically, there are two types of uncooled microbolometer detectors: resistive microbolometers and diode type microbolometers. The continuous improvement in the uncooled infrared detectors quality and their readout circuits improved the performance of the uncooled imaging arrays at reduced device size, power consumption, and overall cost.
Biasing circuitry needs for all types of the uncooled detector except for the thermoelectric and pyroelectric detectors. Resistive and diode type microbolometers need to be biased by a voltage or current source in order to sense the changes in the detector parameter by absorbing infrared radiation. The simplest and most direct method of reading out a resistive microbolometer is to apply a voltage or current bias and to measure the pixel current or voltage for resistance measurement. Fig. 2.26 (a) and (b) show the two basic methods to measure the resistance value of the resistive microbolometer detectors, which use constant voltage biasing with current reading and constant current biasing with voltage reading methods, respectively [72].

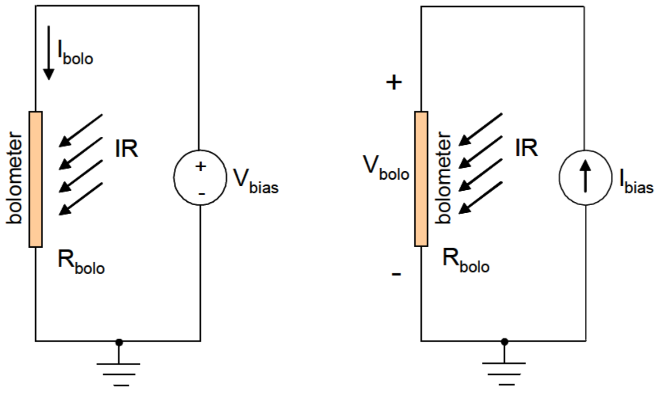

(a) (b)

Figure 2.26: Two basic methods to measure the resistance value of the resistive microbolometer detectors: (a) constant voltage bias-current reading and (b) constant current bias-voltage reading methods [72].

Constant voltage bias can be implemented easily with minimum additional noise, since the implementation of stable and low-noise current sources is not so easy. Although constant voltage or constant current biasing methods are very simple, But these biasing methods have some major drawbacks. Firstly, the resistance in these circuits measurements absolute temperature while relative temperature is used for most of applications also resistance readings are sensitive to temperature and process variations. Secondly, the detector temperature starts rising with the application of bias pulse, which is known as self-heating effect. The detector voltage changes related with the changes in the detector resistance due to the self-heating effect, and usually the self-heating induced change in the detector voltage is much larger than what can be achieved with infrared radiation. The ratio based measurements is performed to reduce the effect of process and operating temperature variations which can be obtained by using resistive divider circuits operating in half bridge or full bride modes. These bridge circuits can also be used to compensate the self-heating effect. Figure 2.27 shows the half bridge and full bridge circuits used for the resistive microbolometers, where R_{bolo} and R_{load} are the resistance of the microbolometer detector and the resistive load, respectively. For the half bridge circuit, load resistances are implemented on the substrate without any thermal isolation so they are insensitive to infrared radiation. R_{load} used as reference resistor also. For full bridge circuit, an optically shielded microbolometer is used which is electrically identical to the bolometer pixel, and it is suspended and made insensitive to infrared radiation. This optically shielded detector is mainly used to cancel the variation in the detector voltage due to the self-heating effect. These characteristics of shielded bolometer (suspended and being identical to the actual bolometer detector) cause similar rising of temperature for both bolometers, and self-heating generated signal component at the detector output is canceled by using a differential readout circuit. Since the optically shielded bolometer can not respond to the infrared radiation, there is no loss in the actual infrared induced voltage at the detector output.

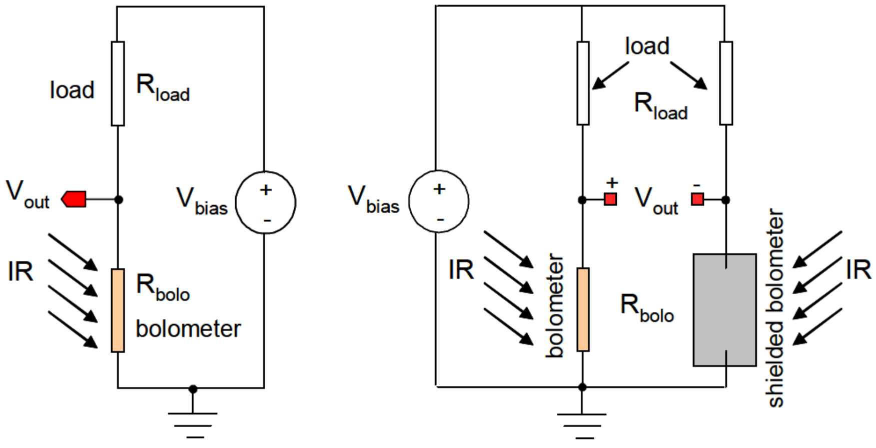

(a) (b)

Figure 2.27: Bridge circuits for the resistive microbolometers: (a) half bridge and (b) full bridge circuits, where R_{bolo} and R_{load} are the resistance of the microbolometer detector and the resistive load, respectively.

2.4 Pre-amplification Architectures for the Resistive Microbolometers

A Readout integrated circuit (ROIC) is an integrated circuit (IC) for reading detectors signals. ROIC circuits are compatible with different types of detectors such as infrared and ultraviolet. The main purpose of ROICs is to accumulate the image-current from each pixel and transfer the signal for readout. Conventional ROIC technology stores the signal by sample and hold circuit for each pixel and then send the signal for readout. Fig. 2.28 shows A simplified sample and hold circuit diagram. AI is an analog input, AO is an analog output and C is a control signal.

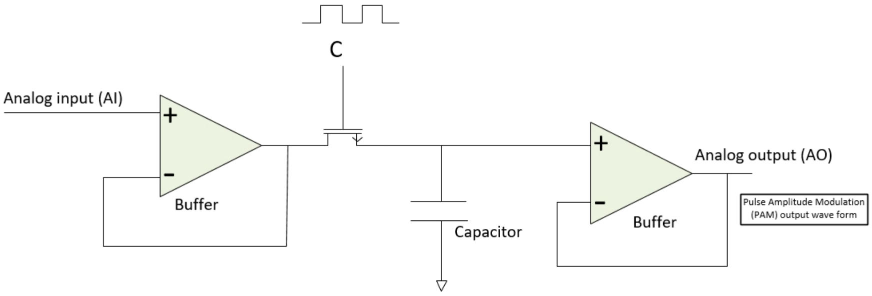

Figure 2.28: Typical Sample and Hold circuit

This technique requires storing large signal charge for each pixel. A ROIC has high-speed analog outputs to transmit pixel data outside of the integrated circuit. If digital outputs are implemented, the IC is referred to as a Digital Readout Integrated Circuit (DROIC). A digital readout integrated circuit (DROIC) is a class of ROIC that uses on-chip analog-to-digital conversion (ADC) to digitize the accumulated image-current in each pixel of the imaging array. DROICs are easier to integrate into a system compared to ROICs as the package size and complexity are reduced, also they are less sensitive to noise and have higher bandwidth compared to analog outputs. Fig. 2.29 shows an example of comparison between ROIC and DROIC betwwen CCD [2] and CMOS readout architecture [29, 79].

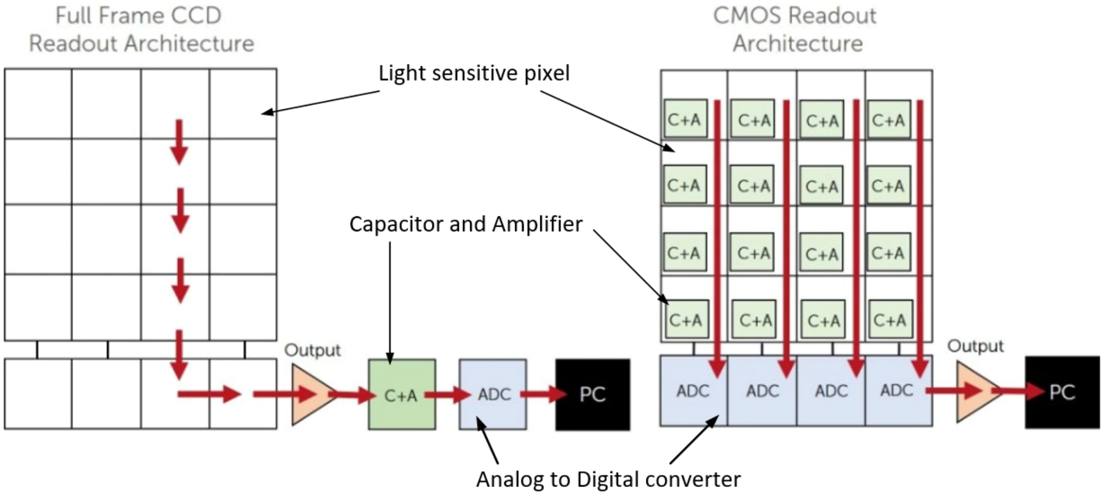

Figure 2.29: An Example comparison between ROIC and DROIC architecture.

A Digital pixel readout integrated circuit (DPROIC) is a ROIC that uses on-chip analog-to-digital conversion (ADC) for each pixel to digitize the accumulated image-current within the imaging array. DPROICs have an even higher bandwidth than DROICs and can significantly increase the capacity and dynamic range of the device[6, 41, 46].

Usually, resistive microbolometers use pre-amplifier with a a simple biasing circuit which is followed by an integrator. The pre-amplifier senses and amplifies the detector current or voltage with minimum noise contribution. Generally, there are four types of pre-amplifiers use in resistive microbolometer imagers:

---

[2] A charge-coupled device (CCD) is an integrated circuit containing an array of linked, or coupled, capacitors. Under the control of an external circuit, each capacitor can transfer its electric charge to a neighboring capacitor. CCD sensors are a major technology used in digital imaging.

1) Bolometer current direct injection (BCDI): This circuit is based on constant voltage biasing. R_b is the active microbolometer, whereas R_r is the reference microbolomter(reference blind). R_r is thermally shorted to substrate, therefore, it is not sensitive to IR radiation. This configuration converts the detector current to voltage and helps to cancel out any DC offsets and also reduces self-heating induced change in resistance. Before integration starts, rst(reset) discharge the capacitor. The difference current of the two microbolometers is integrated on the load capacitor.The main advantage of the integration is that it limits the electrical bandwidth, and it amplifies the signal with a certain gain. Lack of buffering at the output is the main drawback of the BCDI amplifier Fig. 2.30 [76].

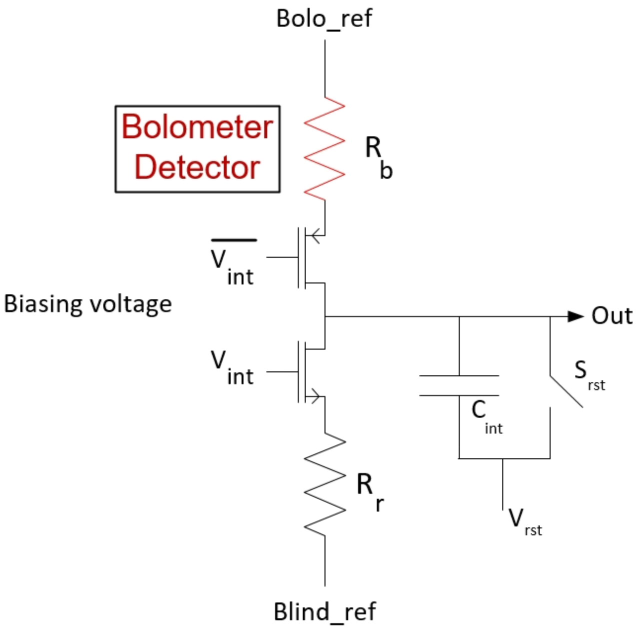

Figure 2.30: BCDI pre-amplifier circuit

2) capacitive transimpedance amplifier (CTIA) constant voltage biasing is used , and the detector current is integrated using a switched capacitor to reset the integrator. This configuration is similar to BCDI, but the use of operational amplifier (opamp) based reset integrator provides output buffering. this pre-amplifier Converts the detector current to voltage through an integration process Fig. 2.31 [25],[75] .

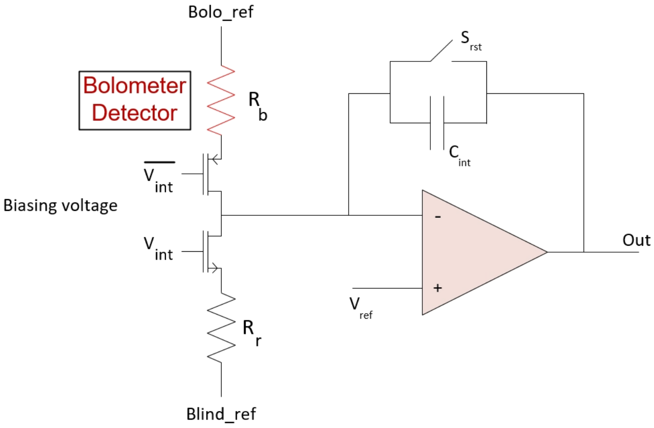

Figure 2.31: CTIA pre-amplifier circuit

Before going forward to the next type of pre-amplification, structure of readout circuit based on mixing the two first type of pre-amplification will be discussed. Generally, The IRFPA (Infrared Focal Plane Array) readout architecture is illustrated in Fig. 2.32.

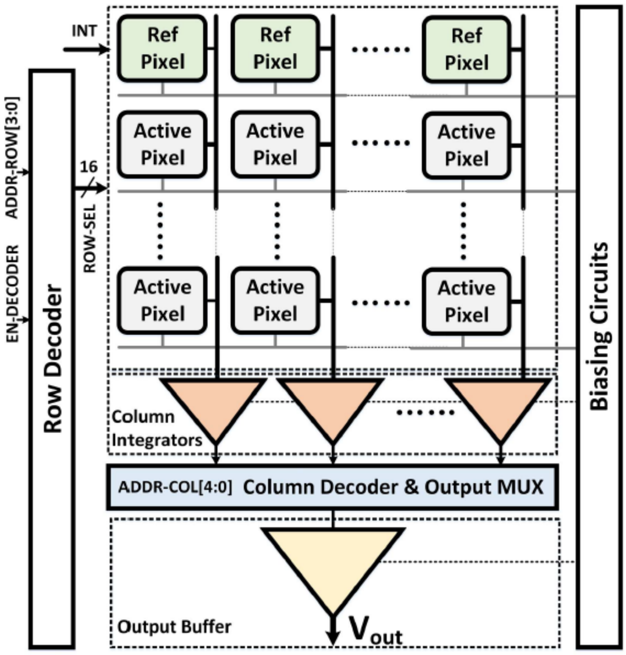

Figure 2.32: Readout architecture [4].

Every active pixel in a column shares an optically isolated reference blind bolometer and an integrator to prepare column parallel readout. The bolometer bias signals are shared in a row and blind bolometer is used as a reference bolometer. The column parallel readout is a good combination between pixel parallel and serial readout in terms of circuit layout and operational speed. The pixels in each row are integrated simultaneously (one row at a time) and then serially readout in a rolling line using the column multiplexer.

The readout circuit is based on the commonly used capacitive transimpedance amplifier (CTIA) where the detector is biased by a constant voltage and the current difference between the active and blind bolometers is summed with an integrator. The CTIA configuration with bridged reference and active bolometers is suitable for highly resistive bolometer detectors because of the high output resistance of the direct injection biasing circuit [75].Fig. 2.33 shows the readout example pre-amplifier schematic circuit which is commonly used for resistive types of bolometers.

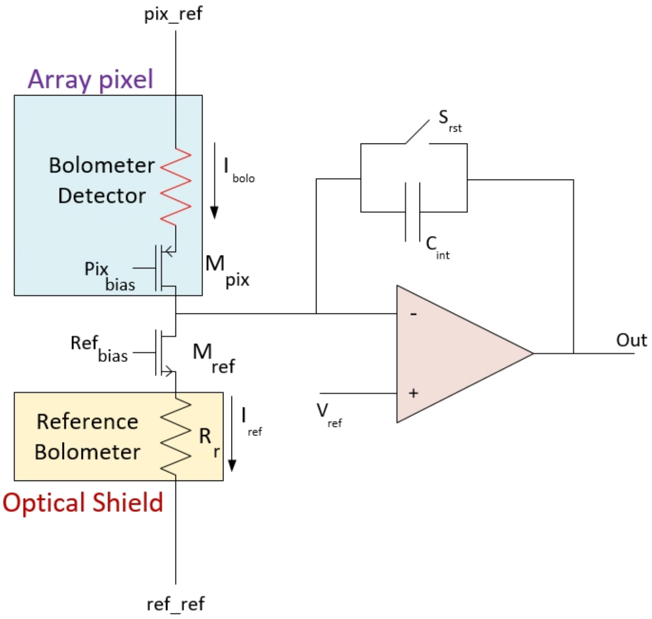

Figure 2.33: Simplified schematic of a preamplifier circuit called capacitive transimpedance amplifier (CTIA), which is commonly used in the readout circuits of the resistive uncooled detector arrays [75].

The detector bias in the CTIA pre-amplifier is using a p-channel CMOS transistor M_{pix} acting as a direct injection transistor. One terminal of the array pixel is at the pixel reference potential pix_{ref}, and the other terminal of the array pixel is at a potential which is one source-to-gate V_{GS} potential higher than the applied pixel bias voltage pix_{bias}. Since the change in the detector current is slightly small as compared to its DC level, so the change in the source-to-gate potential of the direct injection transistor is providing a stable bias voltage to the array pixel.

The DC portion of the detector current is cancelled by using a reference pixel, which is biased similar to the array pixel, but in reverse polarity. To bias the reference pixel in reverse polarity, an n-channel CMOS transistor is used as a direct injection transistor. The reference bias potential ref_{bias} and reference potential ref_{ref} for the reference pixel are adjusted so it can sink the DC current of the array pixel before entering the CTIA circuit. The negative input of the opamp follows the DC potential at the positive opamp input terminal making the input stay at the signal ground with zero input impedance. Therefore, theoretically the entire infrared induced detector current is integrated in the integrator without any loss in the gain [75]. For implementation and analysing of this model, The ROIC structure that is mentioned in Fig. 2.33 , dummy detector model and transmission gates for switching are used . Transmission gate (TG) has a better threshold voltage and higher switch resistance. Fig. 2.34 shows The circuit of the bridge type pixel readout with TG and dummy detectors. It is based on the CTIA topology in which the detector is biased by a constant voltage and the current difference between the active and reference branches is summed with an integrator. PMOS and NMOS transistors are biased in triode region as a dummy detector and blind bolometer respectively [4]. The readout sequence follows bellow structure. The INT signal is set for controlling the transmission switch in the reference bolometer branch (M3 and M4) before integration starts. This provides a ground path for C_{INT} resetting the V_{INT} output to VDD. Next stage, the RS[X] (row select) is set to enable the active pixels via (M1 and M2) of row X. Row select addresses are set by row decoder (set EN signal on Decoder). This enables the corresponding active pixels and a difference current $I_{diff} = I_{bolo} - I_{blind}$ is generated. At the end of integration period, the voltage on V_{INT} node represents the change in detector resistance and is read out. The CTIA configuration with bridged reference and active bolometers is suitable for highly resistive bolometer detectors because of the high output resistance of the direct injection biasing network. If we neglect the effect of bulk-to-source in the biasing transistors (M2 and M3), the output resistance of the biasing network (R_{out}) is :

$$R_{out} = (g_{m2} r_{ds1} r_{ds2}) || (g_{m3} r_{ds3} r_{ds4}) \tag{2.1}$$

where, $g_{m2,3}$ are the input transconductances of the PMOS and NMOS biasing transistors (M2 and M3) and r_{ds1-4} are the intrinsic darain-to-source resistances of the transistors M1 to M4 in the biasing network.R_{out} is much higher than the detector resistance rds1 and rds4 (drain-to-source resistances of the dummy detectors). The high output resistance reduces the contribution of op-amp/integrator input noise current to the detector input noise current which makes CTIA suitable for using. However, the current responsivity of the detectors biased with the direct injection transistors is decreased as a result of negative feedback; a small decrease in the detector resistance upon incident radiation increases the detector current which, increases the gate overdrive voltage of the direct inject transistor and causing a small signal voltage drop in the actual detector bias voltage. This drop in detector bias leads to lessen the current increase, decreasing responsivity of the detector. It should be noted that maximum responsivity does not necessarily result in minimum NETD which is the indication of maximum detector performance.

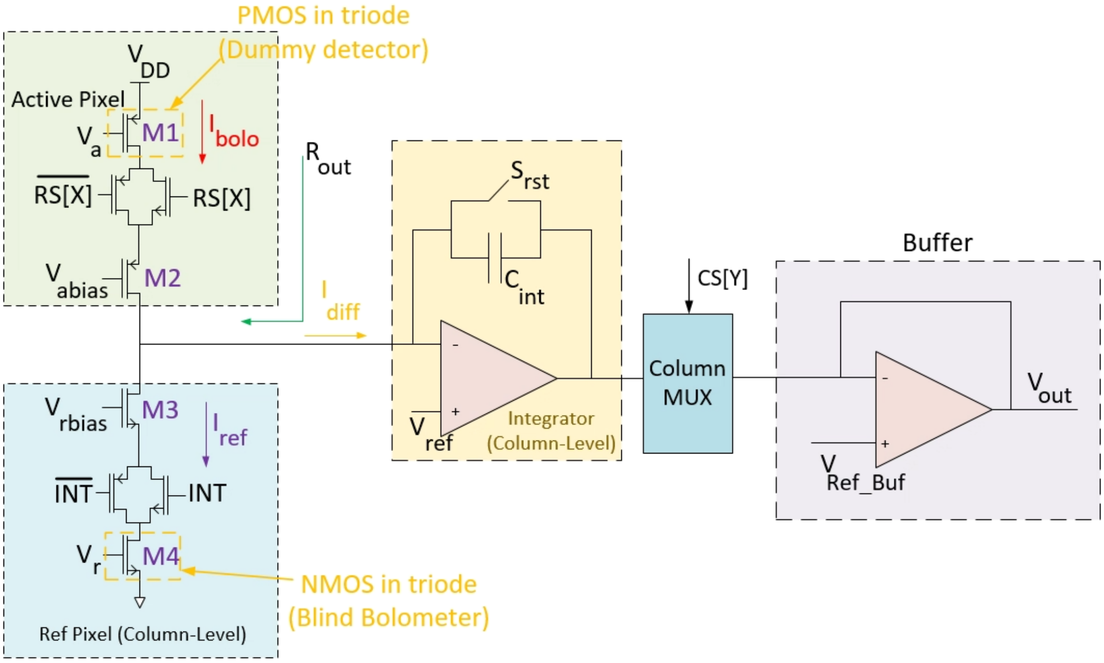

Figure 2.34: ROIC signal chain including the pixel and column circuits.

The readout operation is controlled by *INT* and *RS* switches implemented as transmission gates enabling pulsed bias operation as seen in Fig. 2.34 The active and blind detector biases are set by the V_{abias} and V_{rbias} signals using the direct injection transistors, respectively. The small signal current resulting from the resistance change of the active pixel due to IR heating can be shown by changing the V_a signal. This example shows the combination principle of the two first methods for readout circuit(BCDI+CTIA) [4].

3)Wheatstone bridge differential amplifier (WBDA), pre-amplifier structure uses a wheatstone bridge. Differential detector biasing circuit followed by a low noise differential pre-amplifier and an integrator circuit. The detector voltage is sensed by a differential amplifier. In this configuration, most of the errors coming from PVT variations(includes process, voltage and temperature (PVT) variation effects of circuit) and self-heating are cancelled out. The output is filtered and amplified through the integration circuit . This configuration require both optically isolated and thermally shorted so detectors which is made by this approach is complex to implement thus there is limited applications which are using WBDA. this approach converts the detector voltage to current with a low noise differential pre-amplifier [70].

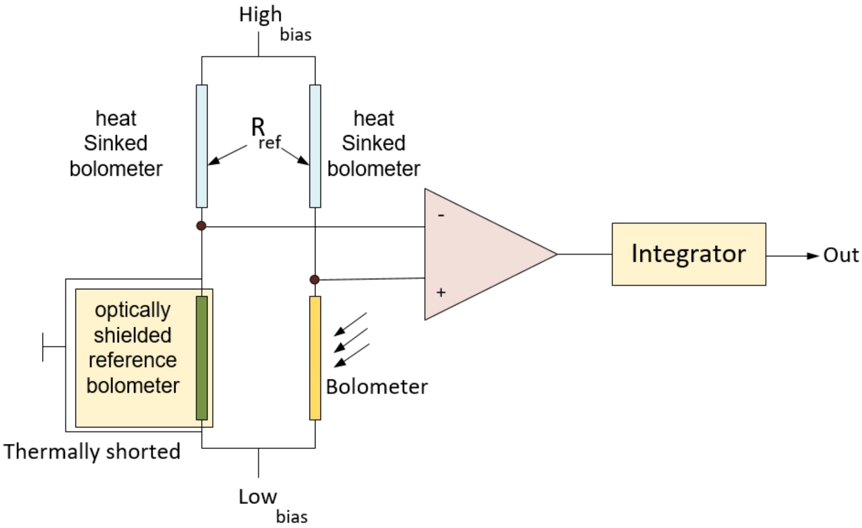

Figure 2.35: WBDA pre-amplifier circuit

4)Constant current buffered direct injection (CCBDI), Unlike previous approaches, CCBDI uses constant current biasing. this configuration converts the detector voltage to current with a low noise differential pre-amplifier. Constant current biasing has the advantage of increased responsivity and improved linearity. By using constant current biasing , it is necessary to use a transconductance amplifier to convert the detector output voltage to current before an integrator circuit. the main challenge of the CCBDI is that the design of low noise and stable current sources is difficult [13].

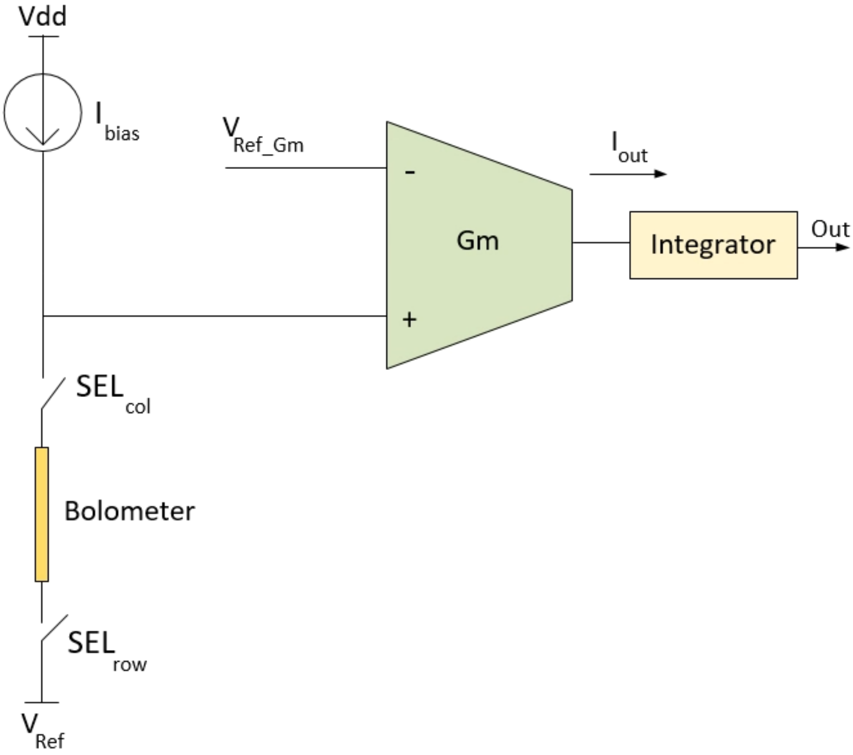

Figure 2.36: CCBDI pre-amplifier circuit

2.5 Preamplifiers for the Diode Type Microbolometers

Diode type uncooled microbolometers use forward biased p-n junction diodes instead of high TCR (Temperature Coefficient of Resistance) resistors as temperature sensitive elements. Since the I-V characteristics of the diode type detectors are exponential, readout circuits that read the detector current upon voltage bias are not suitable [43]. In the constant voltage biasing, a small variation in the bias voltage may cause a large variation in the detector current, increasing the non-uniformity of the array. The bridge type circuits are also not practical due to the non-linear I-V characteristics of the diode type detectors. Furthermore, the diode type detectors have both less temperature sensitivity and reduced impedance compared to the resistive and capacitive devices. Therefore, the noise level of the corresponding pre-amplifier should be very low, which is quite difficult to implement in CMOS technology. There are two types of diode FPAs: SOI diode (silicon on insulator) and n-well diode FPAs. The first FPA uses gate modulation integration (GMI) circuit, and second FPA uses differential buffered injection-capacitance transimpedance-amplifier (DBI-CTIA) circuit [65–68].

2.6 Readout Integrated Circuit example works

Infrared focal plane arrays have a wide range of industrial, military, medical, and scientific applications. A high performance readout circuit of IRFPA should have a large dynamic range to increase the maximum charge storage capacity. In order to achieve this requirement, a large integration capacitor should be used, which contradicts with the small pixel area and high resolution requirements. Some techniques will be used to achieve this feature like direct-Injection (DI) pixel cell structure with only four MOS transistors and provides four different readout sequences to enlarge the range of system application or make a wide dynamic range (WDR). Usually, there is a build-in temperature sensor to detect the temperature of the chip for shutting down the process in case of intolerable temperature. Fig. 2.37 shows typical example of schematic diagram of the ROIC (in this case for 128x128 pixels)[10, 78].

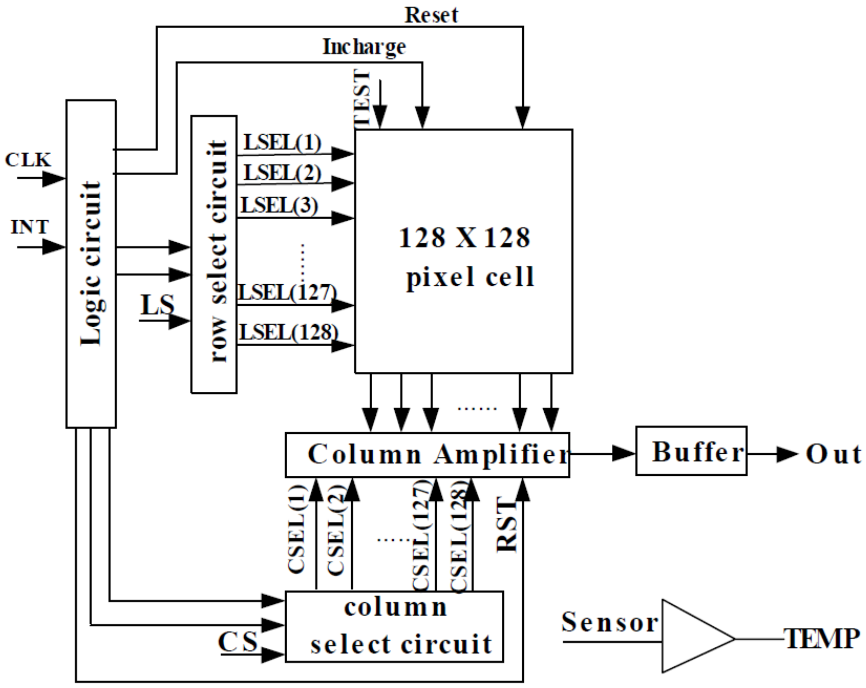

Figure 2.37: Block diagram of the ROIC [85].

Usually, the logic circuit generates all internal control signals, this can minimize the applied external signals to the ROIC part which has only two input signals, one is the main clock (CLK) and the other is INT (variable integration time function). A synchronous sequential circuit uses clock signal and level inputs (or pulsed) (with restrictions on pulse width and circuit propagation). The output pulse is the same duration as the clock pulse for the clocked sequential circuits. So these two signals by using logic circuit produce other necessary signals. Row select circuit provides the

row addressing clocks and the row readout sequence. Column select circuit has the same signals. The outputs of pixel cells at the same column are connected to their column buses. The column addressing clocks multiplex the output analog signals of the column amplifiers to the output buffer. The voltage of column bus is V_{ref} and keeps constant during pixel charge is transferred to column amplifier. Generally, the ROIC chip has a build-in temperature sensor for monitoring the temperature of the device. As we can see the main amplifier is out of the pixels or it can be used for each column. In this work, we designed the Pre-amplifier in-pixel so there are more possibilities such as noise improvement and speed rather than conventional ROIC [9].
The common ROIC schematic is represented in Fig. 2.38 it uses a direct injection input circuit designed to have large integration capacitor [33, 54].

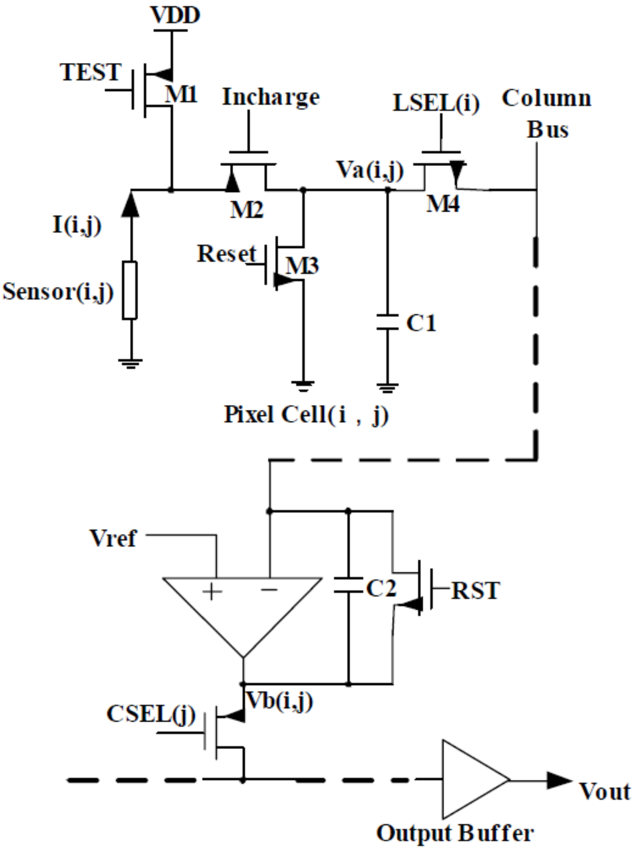

Figure 2.38: Schematic diagram of ROIC [85].

The pixel circuit includes only four transistors (4T). According to the picture the detector current flows through the transistor M2 and charges up the integration capacitor. The bias of detector can be adjusted by the low voltage level of signal *Incharge*. Integration time is controlled by the input signal *INT*. M1 is a test transistor used to simulate the detector for testing of the readout chip. M3 transistor is used to reset the pixel for beginning of the new frame. Also All M2 gates in the column are driven at the same time for snapshot operation mode. M4 is an addressing transistor. All the transistors M4 of the same row are driven together by the clock *LSEL(i)*. Fig. 2.39 shows an example ROIC circuit schematic.

Various type of ROIC circuit design topology is used for different IR systems and purposes. Modern IR imagers are developed by variety of methodologies. Several approaches are considered for demanding applications in terms of high speed, low power, and ultra-low noise. For example improving process of the electrical signal and speed to stream-out video signal. The choice of detectors depends upon wavelength of interest, quantum efficiency, noise, and cooling requirements specific to the application. While, the majority of ROICs are fabricated with CMOS technology so they are compact ,low power, and have an integration capabilities [39].
Fig. 2.39 Shows different pixel readout circuits examples, (a,b) 3T and 4T , (c) Global shutter pixel for moving objects with fixing time lag between columns , (d) pixel share structure.

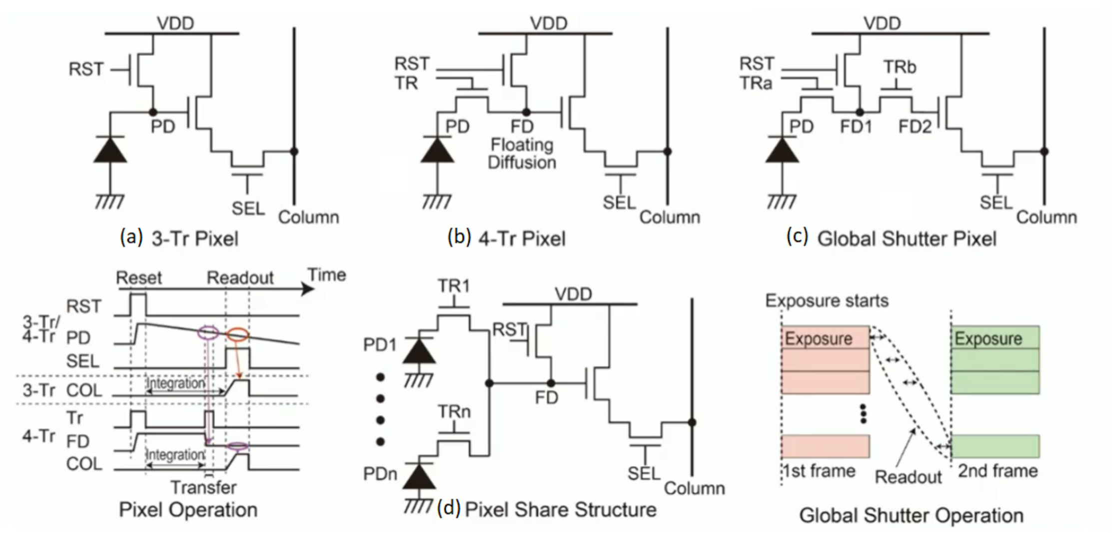

Figure 2.39: different ROIC typologies, (a,b) 3T and 4T , (c) global shutter, (d) shared pixel [39].

2.7 Summary and proposed circuit solution

In recent years, much research has focused on uncooled infrared (IR) imaging systems [20, 56, 62]. These systems have small pixel pitches usually ($< 25\mu$m) and require power effciency, low noise equivalent temperature difference (NETD) ($<$ 50mK) and adequate scene dynamic range ($>$ 200K).

A low NETD demands excellent readout noise performance which becomes a challenge if noisy analog circuits are to be implemented off-pixel. This is because long metal interconnects commuting analog signals. Also noise cancellation circuits that can be an additional power and area overhead. Moreover, high readout dynamic range also requires adequate performance on multiple fronts.

In addition to circuit imperfections such as offset and noise, self-heating of the microbolometer detector also makes the required dynamic range unnecessarily large, resulting in a higher power consumption and potential complexities in the readout circuit chain. As a result , achieving a low NETD and a large readout dynamic range becomes a challenge with power and size constraints. Low noise performance could be achieved with a pixel-parallel readout architecture in which the digitization takes place inside the pixel. However, with a small pixel pitch, this approach severely limits the achievable design size of digitization circuitry. Fig. 2.40 shows traditional IRFPA and microbolometer structure.

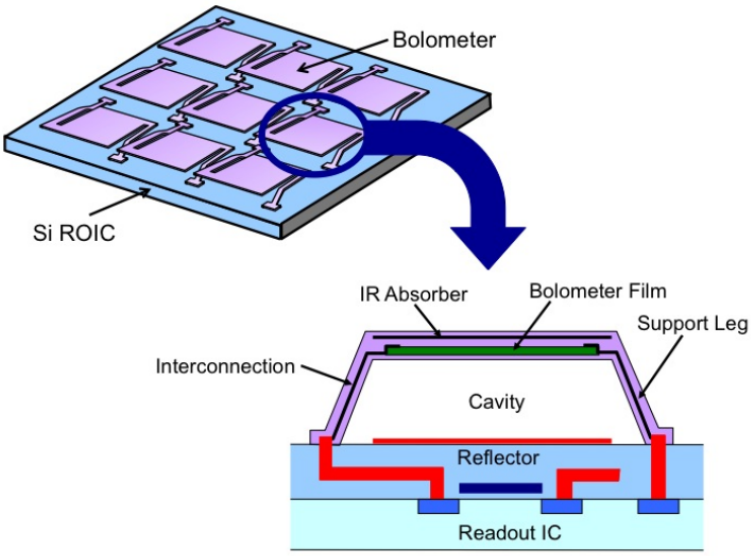

Figure 2.40: Structure of microbolometer uncooled IRFPA and its pixel. Lower right figure is a cross section of a pixel, showing microbridge structure fabricated over readout circuit.

By using advantages of the sequential 3D circuit implementation, realization of the readout circuit for a small pixel pitch is possible. The main challenge for the small pixels with size of ($< 17\mu$m [45]) is designing a pre-amplification circuit for each pixel which is possible by the mentioned technology in two transistors layer (top tier and bottom tier). Special TIA (transimpedance amplifier) is designed to fulfill the pixel size criteria. Our main design is limited to simulation and most of the works are focused on designing of different parts of the circuit such as: amplifier, decoder, current sources and making an example 4x4 ROIC. For this matter Layout of the circuit is important regarding to the fitting to the pixel size. Usually, transistor sizes don't take so much places but capacitor and resistors, so we need to use as much as possible small size of these elements in order to reduce the size of the circuit as long as keeping the functionality of the circuit. The proposed circuit has a better noise performance, and it can keep self heating due to added in-pixel circuits under control(By using more TIA in each pixel, we will use more energy and as a result heating but by reducing noise , we don't need to design some extra circuits as noise cancellation). Also the long signal connections in more classical ROICs are partially avoided and if not avoided then at least further away from the sensor in implementation phase.

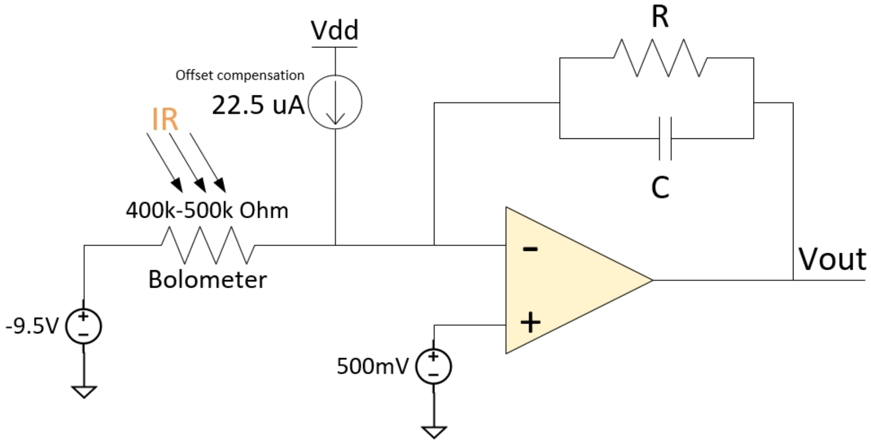

Figure 2.41: proposed TIA circuit with offset compensation for in pixel amplification.

Chapter 3

Implementation

3.1 Bolometer sensor characterization

In this work, we design TIA circuit for the a-Si-based micro-bolometers with shared-anchor structure Fig. 2.13 and 2.14 [44]. The thermal simulation is performed with the assumptions of ambient temperature, vacuum condition and the irradiated IR power condition of $2\frac{nW}{\mu m^2}$ [45]. Fig. 3.1 shows the thermal response simulations of the conventional micro-bolometer design with various pixel sizes. If the pixel design is maintained, the short thermal conduction paths at small pixel sizes lead to very low responsivity. In addition, small pixel size requires more sophisticated design with regard to resulting mechanical and electrical characteristics. For an effective pixel design with high fill factor, the anchor and leg areas should be minimized as these spaces contribute to low thermal resolution by reducing the IR absorption area. Therefore, it is necessary to develop a new pixel design and fabrication process for small sizes and high performance. The efficient way to use these spaces is shared-anchor structures for developing costeffective micro-bolometers for various mobile applications.

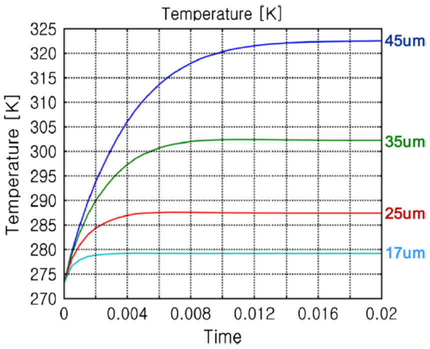

Figure 3.1: Thermal response simulation of conventional microbolometer design with various pixel sizes: from 45 to 17 µm [45].

By redesigning of the bolometer structure, the transient thermal response depends on the leg length, number of legs, and fill factor changes. The membrane temperature is determined by the leg design and Design 2 reaches the highest temperature under the same incident IR power as shown in Fig. 3.2 as we can see for 17 µm bolometer, using three different structure results in different response by keeping the same size. three structures are : Unshared 2 anchor , Design 1 (shared 2 anchor) and Design 2 (shared 4 anchor).

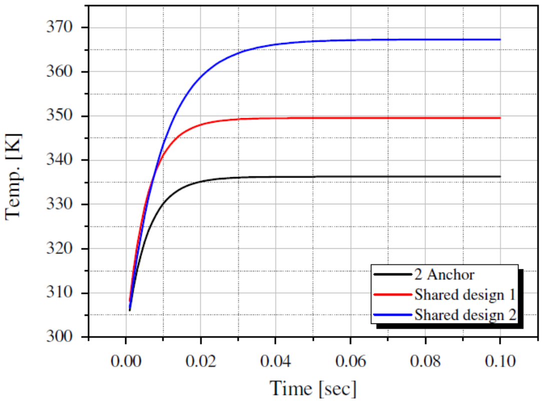

Figure 3.2: Transient thermal response simulation results of three designs (IR power : $2\frac{nW}{\mu m^2}$) [45].

Fig. 3.3 shows transient characteristics of various design under 0.5V bias and thermal time constants for each design. As we can see from Figure, resistance value changes from 500KΩ till 400KΩ approximately.

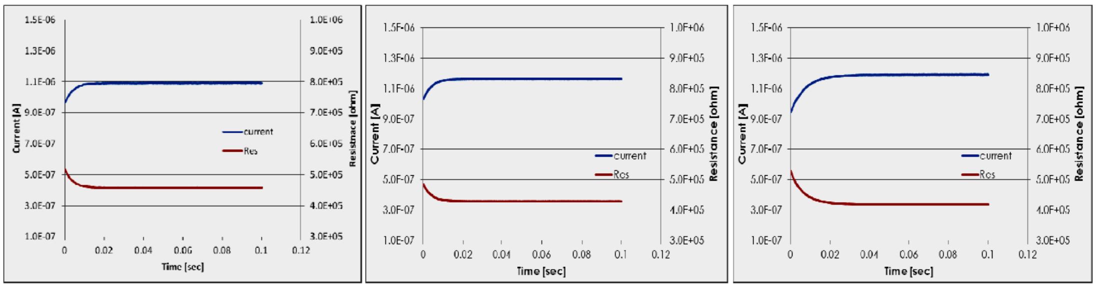

(a) 2anchor design

(b) Shared design 1

(c) Shared design 2

Figure 3.3: Comparison high vacuum t-I,R curve of three different design split [45].

3.2 Transimpedance amplifier

A transimpedance amplifier (TIA) is a current to voltage converter. TIA presents a low impedance to the Pixel and isolates it from the output voltage of the operational amplifier. In its simplest form TIA has just a large valued feedback resistor, R_f. The gain of the amplifier is set by this resistor and because the amplifier is in an inverting configuration, has a value of $-R_f$. Fig. 3.4 shows a simple TIA configuration [52].

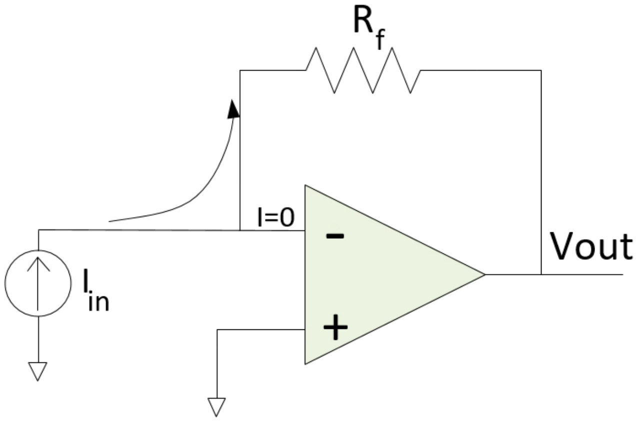

Figure 3.4: Simplified form of transimpedance amplifier

There are several different configurations of transimpedance amplifiers, each suited to a particular application. The one factor they all have in common is the requirement to convert the low-level current of a sensor to a voltage. The gain, bandwidth, as well as current and voltage offsets change with different types of sensors, requiring different configurations of transimpedance amplifiers. For our design parameter, it is important for amplifier to cover full swing of input current while the size is limited to the pixel size.

In the circuit shown in Fig. 3.5 the bolometer (shown as a changeable resistor) is connected between constant voltage source and the inverting input of the op-amp. The other input of the op-amp is connected to ground which makes the invertering terminal virtual ground. The gain of the opamp depends on the feedback current through R_f. The DC and low-frequency gain of a transimpedance amplifier is determined by the equation:

$-I_{\text{in}} = \frac{V_{\text{out}}}{R_{\text{f}}}$, so, $\frac{V_{\text{out}}}{I_{\text{in}}} = -R_{\text{f}}$

If the gain is large, any input offset voltage at the non-inverting input of the op-amp will result in an output DC offset. An input bias current on the inverting terminal of the opamp will similarly result in an output offset. To minimize these effects, transimpedance amplifiers are usually designed with field-effect transistor (FET) or Complementary Metal Oxide Semiconductor (CMOS) input opamps that have very low input offset voltages [27, 38, 53].

A TIA employs negative feedback to create a low input impedance. So it is the most essential current signal measurement tool for light sensing related operation. The feedback capacitor C_f is usually required to improve stability. The principal difference is that I_{in} sees a low impedance in Fig. 3.5 (a) and a high impedance in Fig. 3.5 (b). The virtual ground introduced by the TIA provides potentially a greater bandwidth and reduces nonlinear large voltage swings across it [63]

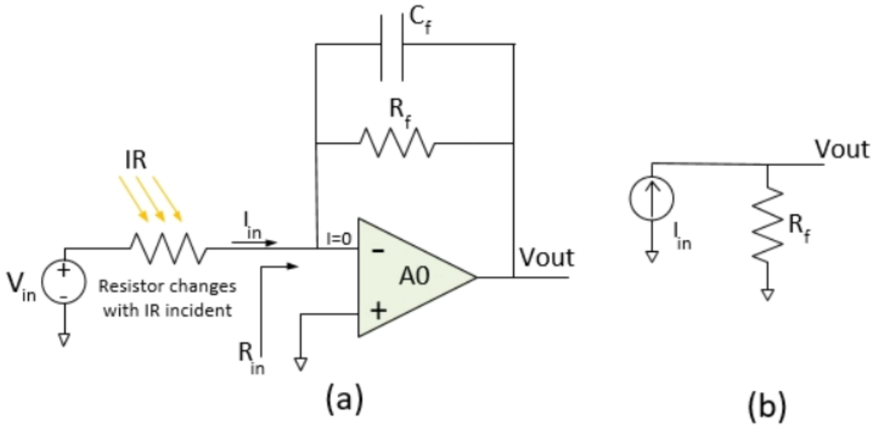

Figure 3.5: (a) Simplified form of transimpedance amplifier structure and (b) use of a resistor to convert current to voltage.

For microbolometer, low noise performance could be achieved with a pixel-parallel readout architecture in which the digitization takes place inside the pixel [77]. But for in-pixel design, we need right technology to match the size of layout to the pixel size. Designing such pre-amplifier at this size and properties is possible by using 3D circuit design in cadence in two tiers. By this technology 3D CMOS designs where transistors are no longer restricted to just a 2D plane, but can be stacked on top of each-other. In contrast to 'parallel' 3D integration that stacks several 2D wafers on top of each other using relatively huge and few vertical connections between the tiers, 'sequential 3D integration' builds the CMOS tiers on a single substrate using photolitography. This way, the density of vertical connections is of the same order of magnitude as the horizontal connections in 2D. So transistors of a circuit module can be placed freely in any tier with no significant disadvantages. This offers new opportunities to make tiers with different types of transistors and thus to make circuits that include different types of transistors, e.g transistors that are optimized for the digital signal domain in one and transistors that are optimized for the analog signal domain in another tier. So mixed signal circuits can be designed with highly optimized components. Optimized devices are not the only advantage though. In general, due to 3D placement the total interconnect wiring will be reduced enhancing speed and power efficiency. A very obvious example for this are systems-in-cube with a 2D sensor arrays integrated. When a 2D sensor array can have one or several connections per pixel connecting it to a next integrated CMOS tier, no sequential read-out of the pixels is necessary, reducing the signals' travel distances enormously resulting in power savings and noise-reduction. Fig. 3.6 shows Vision of a two tier(28nm transistors in bottom tier and 65nm transistors in top tier) 3D smart sensor interface, as it would also be suitable as a ROIC for a micro-bolometer [2].

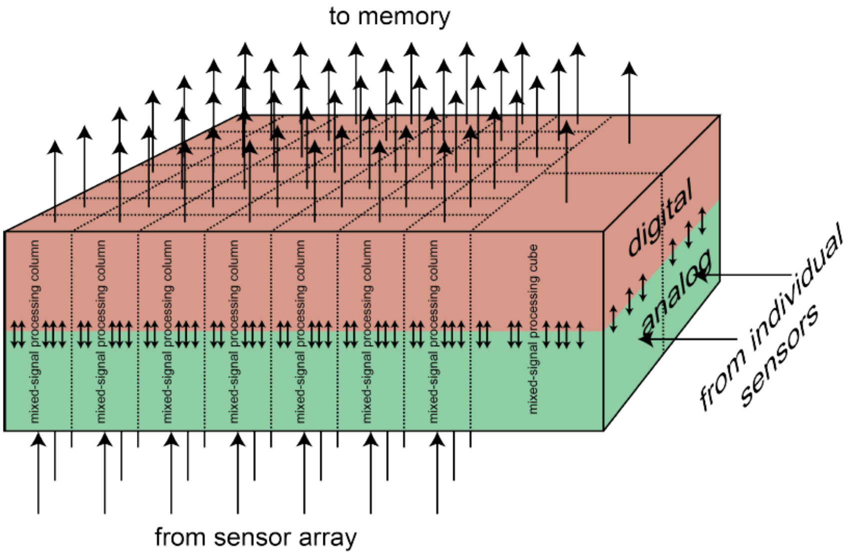

Figure 3.6: Vision of a two tier 3D smart sensor interface, also it is suitable as a ROIC for a micro-bolometer[2].

Our design aim is to use minimum amount of passive elements such as resistor and capacitor in the circuit for saving an area in layout. The gain of inverting configuration in operational amplifier is calculated below. Fig. 3.7 shows an inverting opamp configuration. As it is clear the higher R_f cause the higher gain while R_{in} is changing between 500kΩ till 400kΩ [45]. So for having enough gain , we should choose higher R_f. But actual resistor in layout takes so much places and can be challenging when our design has a size limitation. (R_{in} is bolometer resistance which is changing by IR incident.)

$$A_v = \frac{V_{out}}{V_{in}} = -\frac{R_f}{R_{in}}$$

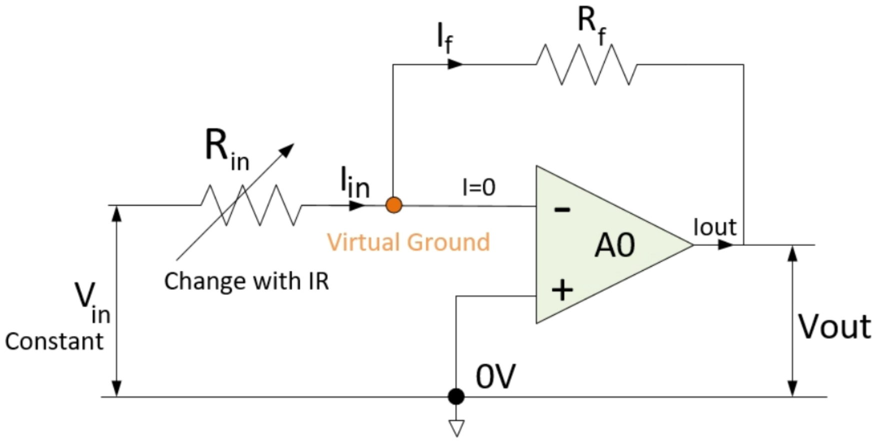

Figure 3.7: Inverting configuration of operational amplifier.

3.2.1 Opamp Design

For designing an operational amplifier, we used combination of differential pair, active load and current mirror. Fig. 3.8 shows the simple design of opamp by using active load and differential pair. default transistor size for bottom tier is (total gate width 80nm and gate length 30nm) and for top tier is (total gate width 89nm and gate length 67nm).

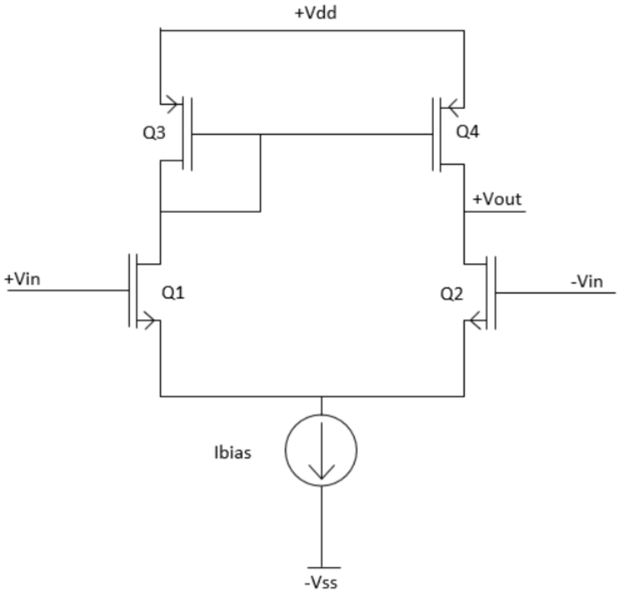

Figure 3.8: typical differential pair and active load combination as an Opamp.

In stead of ideal current source , we use current mirror (as on chip current source). For getting the $\frac{W}{L}$ ratio, we use variable width while keeping the length as a default and running the simulation to get the full voltage swing (proposed design is used W=800nm and L=67nm). The proposed Opamp is designed for top tier transistors. As we don't have some passive elements on top tier so we try to send all transistors to the top tier and placed other elements on bottom tier as shown in Fig. 3.9 (passive elements connected between V_{in-} and V_{out} as mentioned they are in the bottom tier, while V_{in+} is connected to the 500mV voltage source in the test bench model Fig. 3.11). Current source for supplying current mirror must has enough current for covering full supply voltage swing. (For the layout size consideration, transistors size keep the same for current mirror)

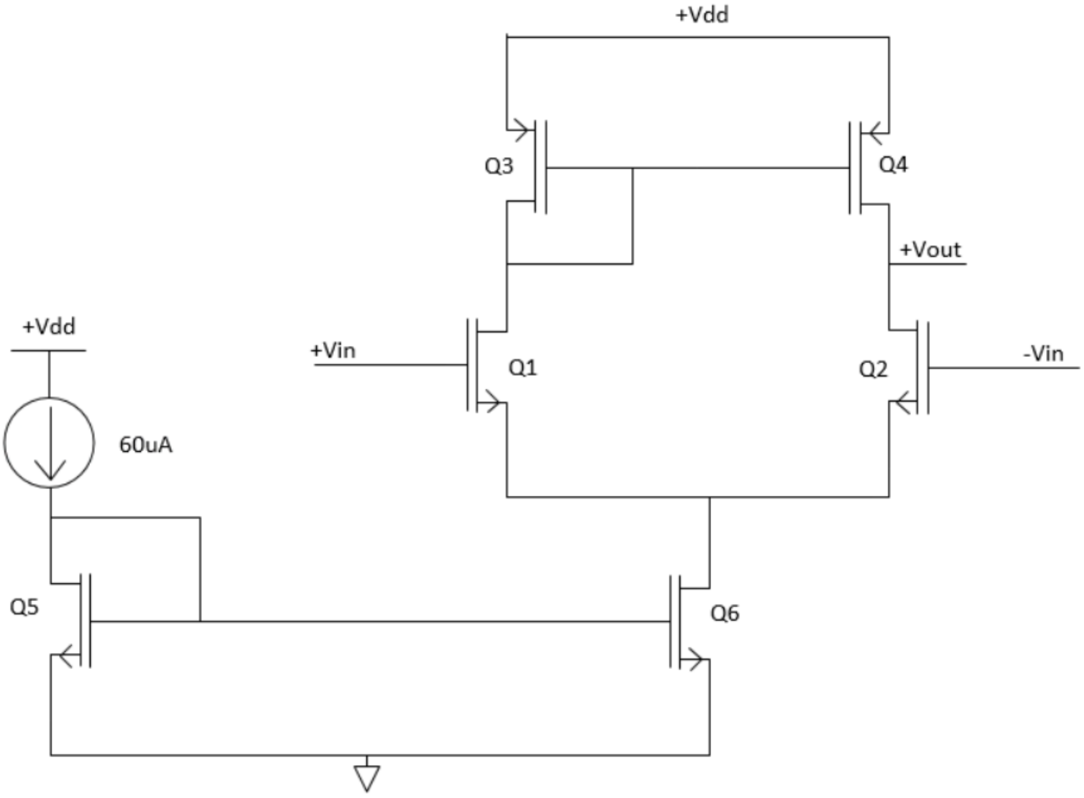

Figure 3.9: Top tier Opamp design.

3.2.2 Measurement

Microbolometer Resistance changes from 400$k\Omega$ till 500$k\Omega$ [45]. In Fig. 3.10 by applying -10 volt to the Bolometer (or -9.5v to inverting and +500mv to non-inverting pins, and it is not transistors supplying voltage) so the current will change between 20μA till 25μA by changing bolometer resistance. Injecting DC offset current to the inverting input will add DC voltage to the intended output signal which is desirable in this case for fully or major covering of supplying voltage V_{DD} (here is 1 volt). Injected current is the average of minimum and maximum current which is going through the bolometer 22.5μA.

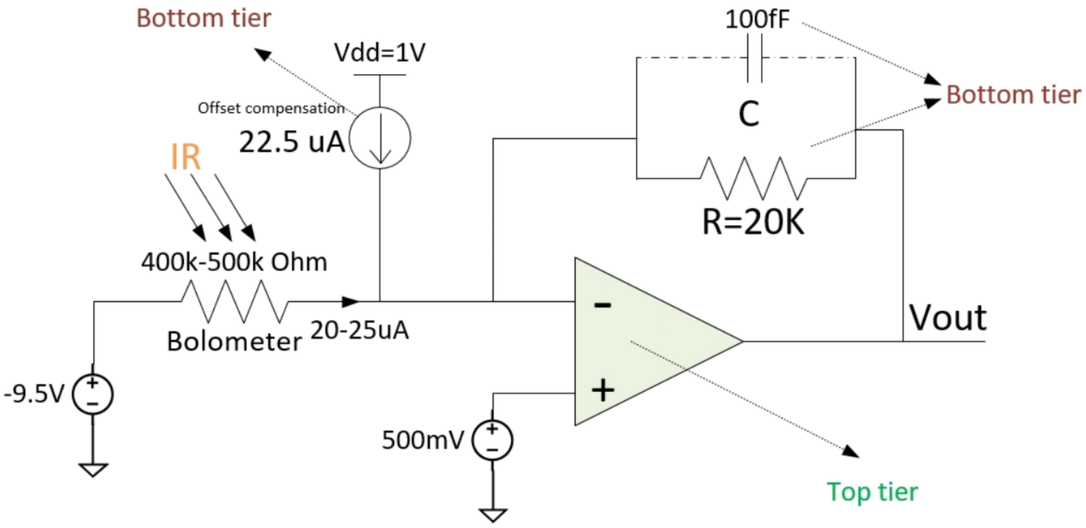

Figure 3.10: TIA with DC current offset compensation designed in different tiers.

For measuring the functionality of the TIA, the test bench is designed. Fig. 3.11 and 3.12 show the test best and DC simulation result. As we can see from Fig. 3.12 V_{out} is following almost full swing supply voltage by changing bolometer resistance R_{pix} from 400$k\Omega$ till 500$k\Omega$ [45]. Real passive elements also used in the circuit simulation for see how the circuit behaviour is closed to the reality. For resistor nwres(nwell resistance) and opppcres (p + op poly p) also for capacitor egncap is tested. In addition ideal DC cancellation current source is replaced with designed current source in the bottom tier to produce the supplying current almost on chip (for matching and implementation problems in real circuit, a potentiometer is used out off-chip to adjust the current to exact value).

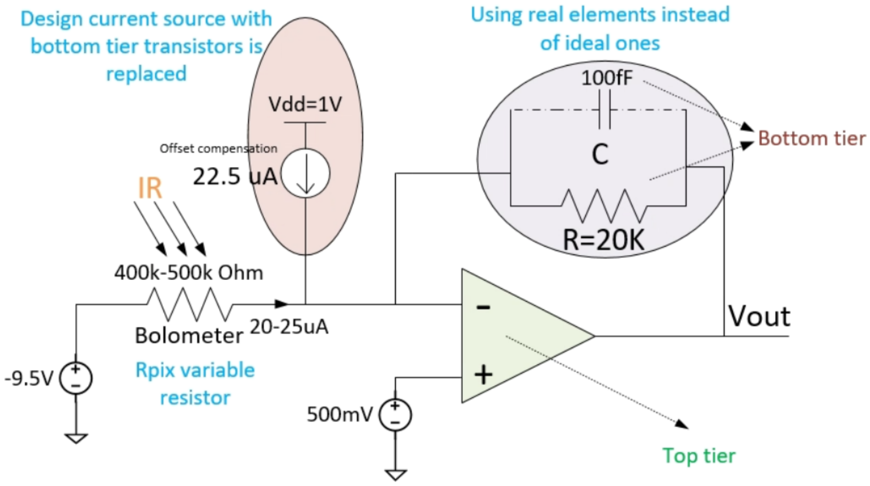

Figure 3.11: Test bench for measuring TIA parameter.

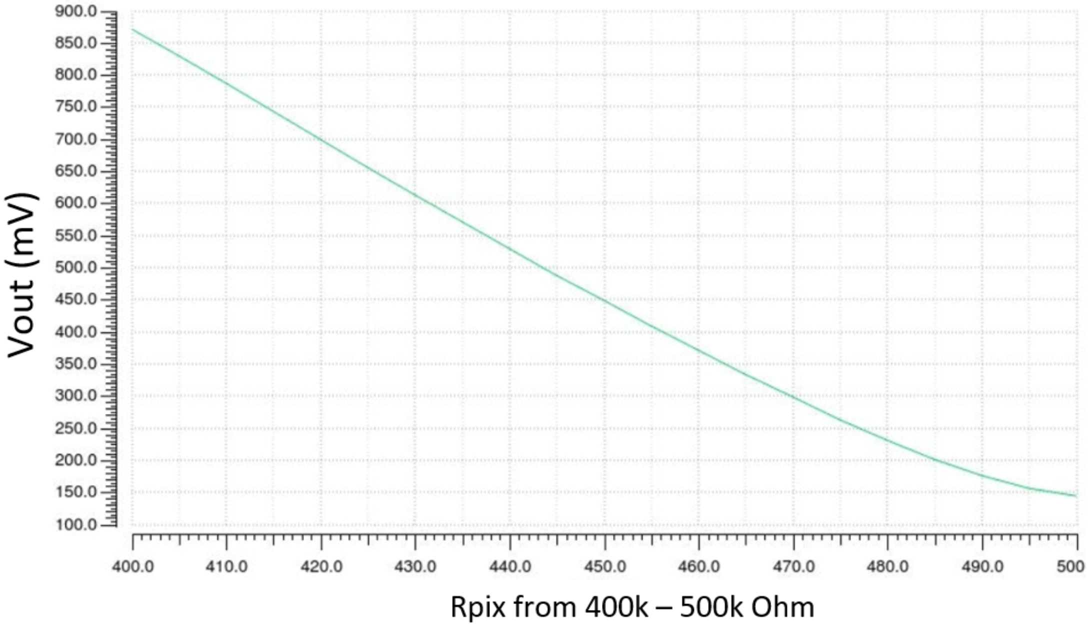

Figure 3.12: Output voltage based on bolometer resistance changing from $400k\Omega$ till $500k\Omega$.

As Fig. 3.12 shown, the output is not fully follow the supplying input (From 0v to 1V). It is close to the full swing but with some limits to linearity and cutting off above 0V mainly. Mismatching in transistors leads to non-linearity also as opamp input voltage goes above or under the certain amount (V_{ref} which is the voltage of non-inverting pin) the output goes to saturation and can not follow the input voltage.

3.3 Current source/sink

Current sources are one of the most important components in Analog Circuits. There are two main current sources used in this work. One in the Opamp configuration design and other for DC cancellation current. Usually, off-chip resistor is used to get a master bias current. An on-chip structure design is effected by process variation (mismatching between transistors and fabrications tolerances) can lead to the actual current to be quite different from what is simulated. This is important as we can not change anything in the post-production.

When a source of current flows from the highest positive potential (V_{DD}) into a load it is designated a current source while when the source of current flows from the load to the ground, it is designated a current sink. Current sources use off-chip potentiometer to adjust the precised current. Fig. 3.13 shows the topology design of current source/sink supply. In simulation, the width of transistors set as variable to get right current amount by swing it, while the off-chip resistor is set to calculated current. Fig. 3.14 shows the simulation result.

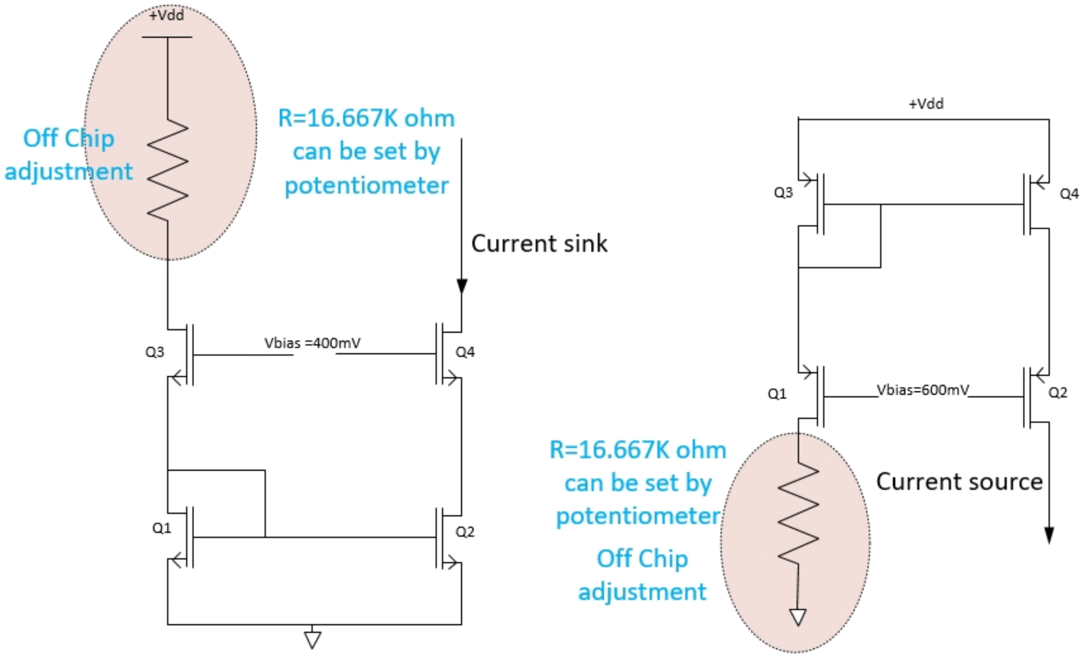

Figure 3.13: current source designed.

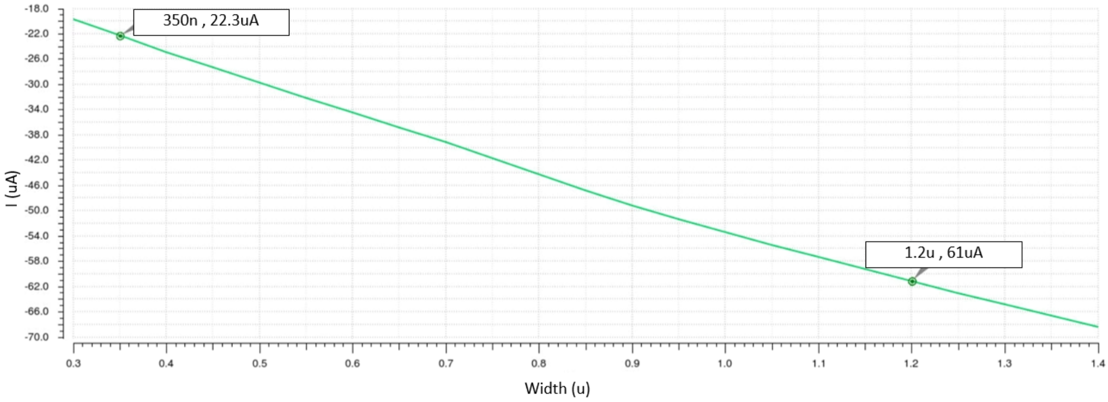

Figure 3.14: simulation result of current source for different transistor width.

3.4 Decoder

Generally, implementation of decoders occupy more space on chip. A conventional 2-4 decoder can be designed using two inverters and four AND gates which totally comprises of 28 transistors. Fig. 3.15 shows decoder at the gate level.
The transistor layout sizes can be reduced by using new mixed logic which uses Pass Transistor Logic (PTL) and Transmission Gate Logic. Usually, PTL has higher speed and occupies less area on the chip by applying the inputs directly to the MOSFET Transistors [71, 84, 86]. Transmission gate logic designs used NMOS and PMOS transistors that are connected as a parallel pairs where as the pass transistor designs uses individual either PMOS or NMOS transistors.

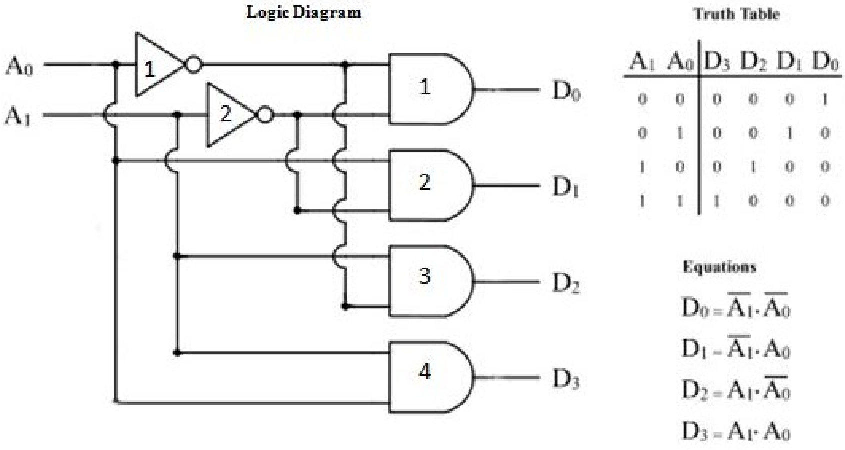

Figure 3.15: decoder gate level diagram.

In this work , we represented three types of decoders. But before explaining these three methods, some CMOS configurations will be defined. Fig. 3.16 shows "AND gate" and "OR gate" implementation with Transmission Gate Logic and Dual Value Logic.

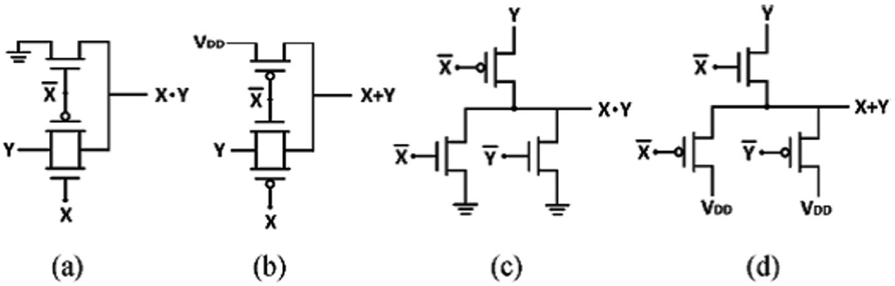

Figure 3.16: (a,b)Transmission Gate Logic for & , || - (c,d) Dual Value Logic for & , ||.

Decoder type 1 used a standard AND and NOT gates with CMOS design(AND gate uses 6T, NOT gate uses 2T). Fig. 3.17 and 3.18 show the decoder structure and simulation result.

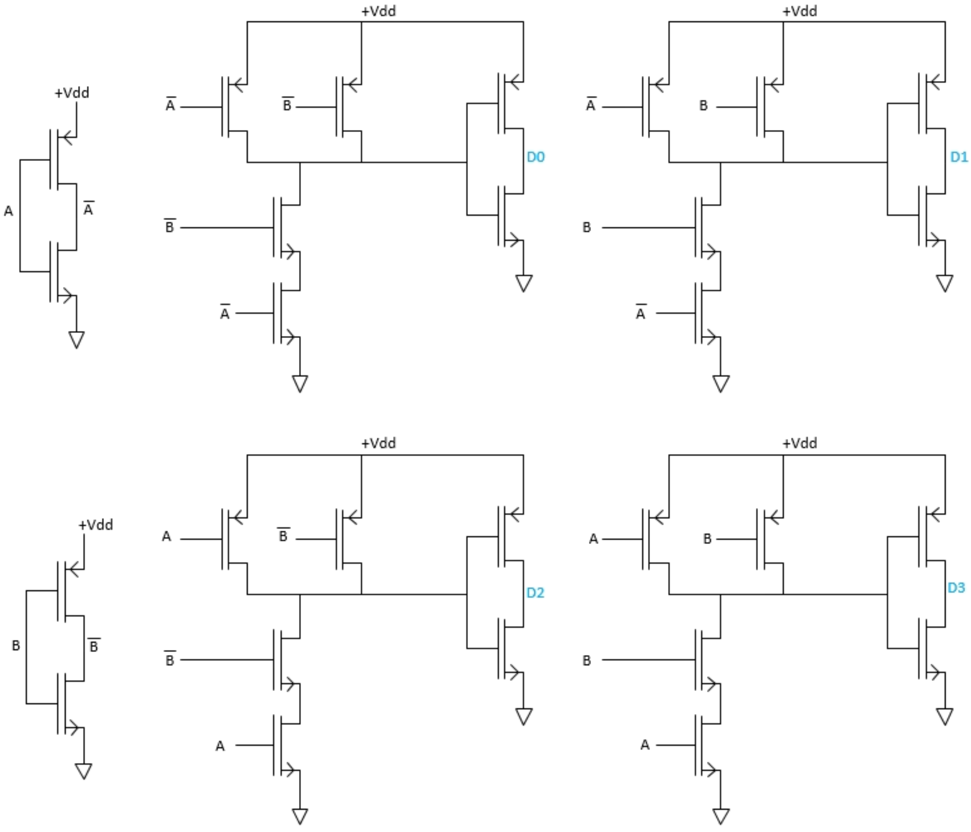

Figure 3.17: 2 to 4 line standard decoder (28-transistors).

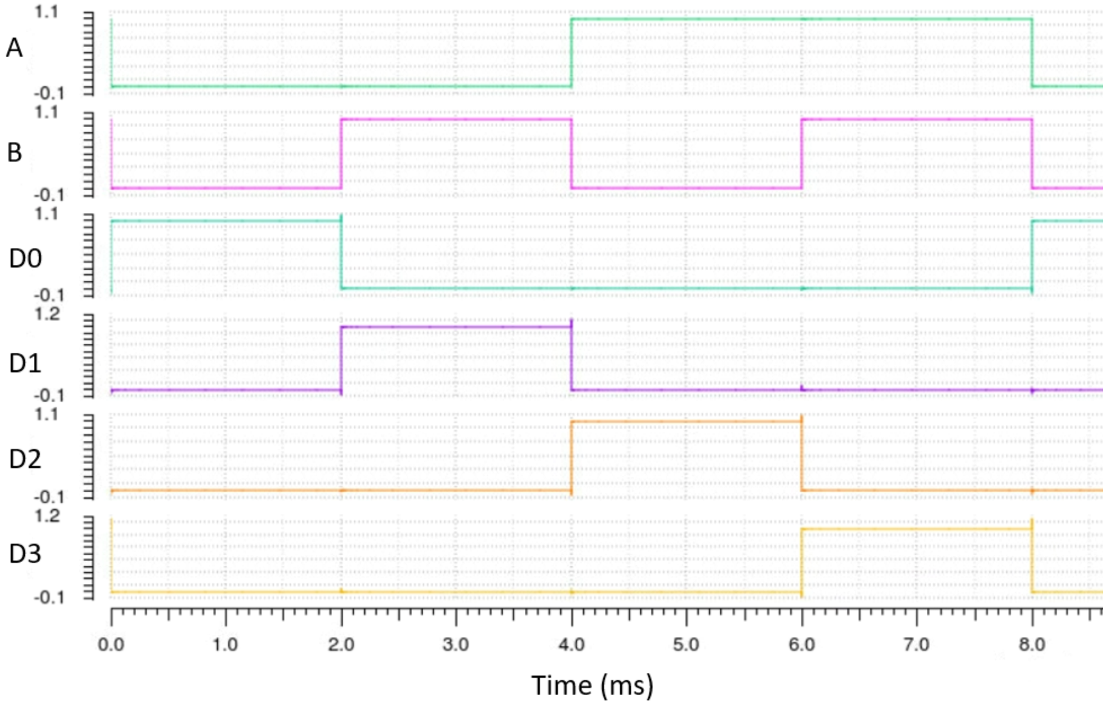

Figure 3.18: Simulation result for 2 to 4 standard decoder with 28T.

Decoder type 2 used mixed logic design technique, which is a combination of PTL, and DVL logic, we can get decoder module with minimum layout and low power consumption with a good performance. Fig. 3.19 shows the fundamental digital logic gates with 14 transistors for the 2 to 4 decoder. Transmission gate logic (TGL gate for D1 and D3) and Dual value logic (DVL for D0 and D2) is used beside a CMOS inverter. Fig. 3.20 shows the simulation result for 2 to 4 decoder with 14T. There are some glitches in the output waves as a result of propagation delay is not zero or do not have an equal delay for inputs or rising and falling time of input waves.

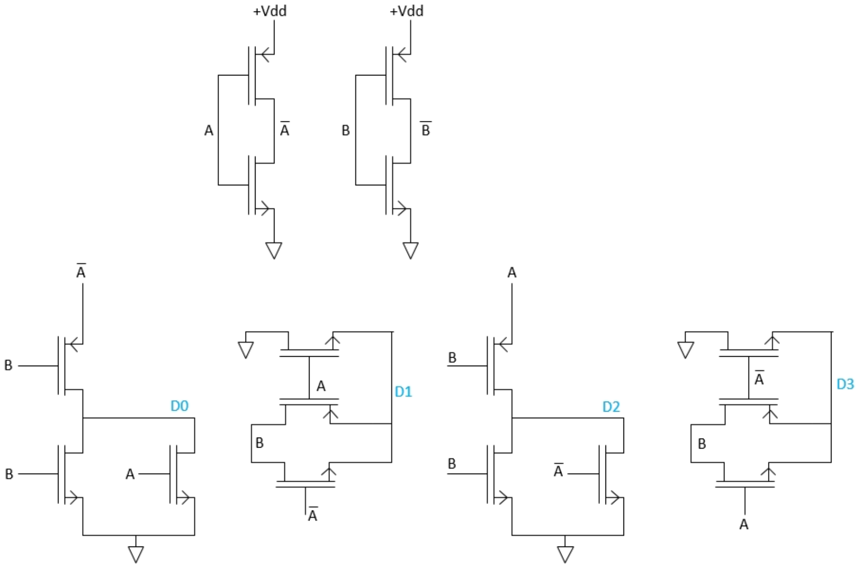

Figure 3.19: 2 to 4 line decoders (14-transistors).

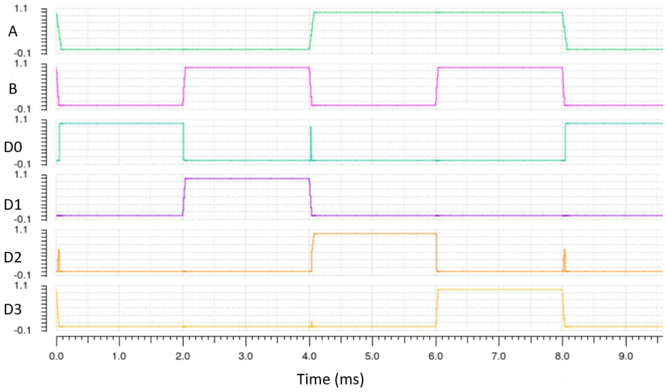

Figure 3.20: Simulation result for 2 to 4 decoder with 14T.

Decoder type 3, used 2 inverters with PTL configuration and 16T. Fig 3.21 shows the 2 to 4 decoder with 16T and Fig. 3.22 shows the simulation result. Some glitches exist in the output waves also.

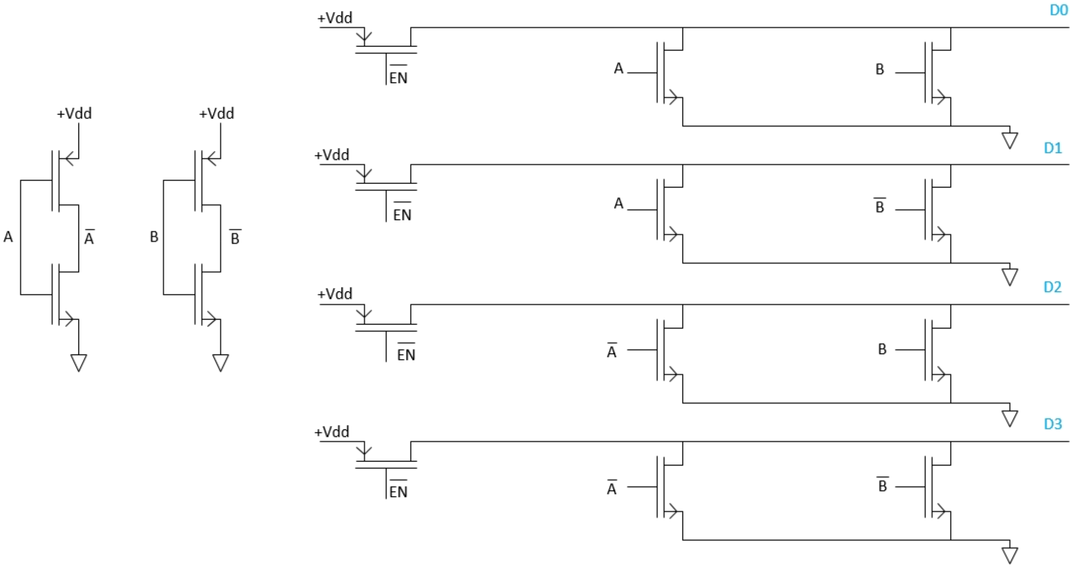

Figure 3.21: 2 to 4 line decoders (16-transistors).

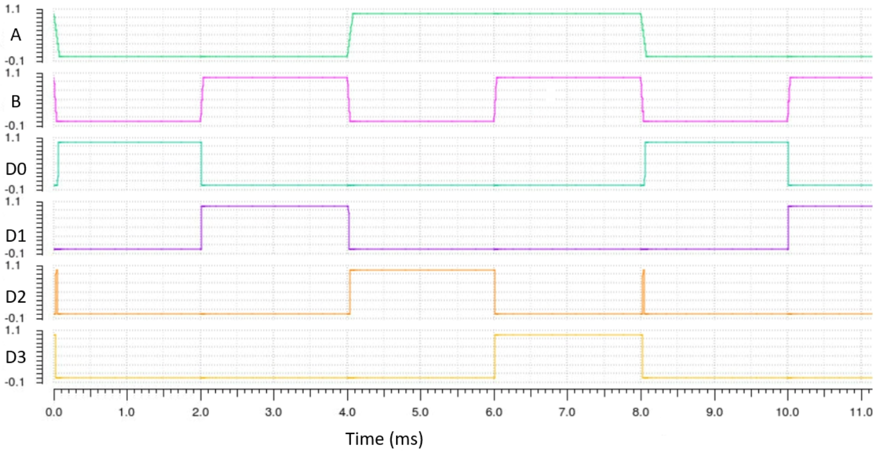

Figure 3.22: Simulation result for 2 to 4 decoder with 16T.

The structure of decoder for selection an addressed pixel in 4x4 pixel size is shown in Fig. 3.23

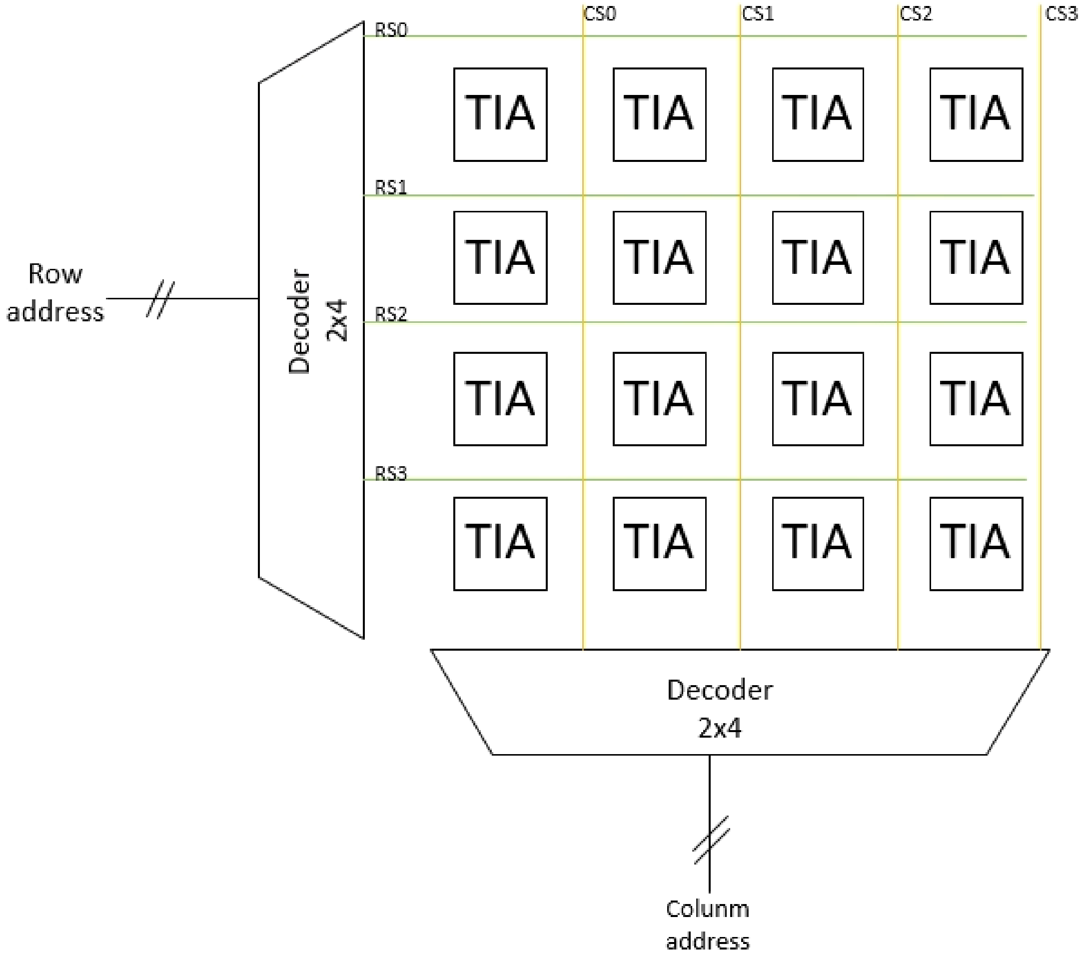

Figure 3.23: Decoder structure for selecting the addressed pixel.

3.5 Proposed Readout Integrated Circuit

Different read-out architectures are used to read pixels of an uncooled microbolometer FPA. These are classified as pixel-wise, column-wise, and serial readout architectures [19]. Fig. 3.24 shows Pixel-wise readout architecture for an N by M microbolometer array, where N is the number of columns and M is the number of rows. D, A, and I represent the detector, amplifier, and integrator, respectively. in this topology, each detector requires its own amplifier and integrator in pixel-wise readout. The detector resistance changes in all pixels can be amplified and integrated simultaneously with this configuration which results in low read-out bandwidth, therefore, the total noise voltage decreases. Also, the close placement of amplifiers to the detectors reduces the effect of interference in wire connections. This architecture is not preferred due to several reasons. Firstly, the total area for an amplifier and integrator pair is limited by the pixel area which is relatively small. Secondly, this architecture suffers from high power consumption due to the large number of amplifiers and integrators that work in parallel[19].

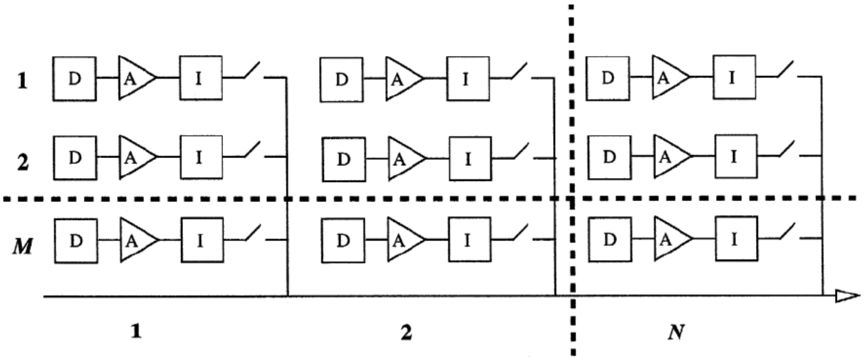

Figure 3.24: Pixel-wise readout [19].

The other type of architecture is the serial readout that is illustrated in Fig. 3.25 [19]. In this architecture, all the pixels are read out one by one, therefore, there is only one amplifier-integrator. Although it is compact in layout and it is power efficient, the main disadvantage of this architecture is that the bandwidth of the circuit is very high resulting in higher total noise voltage. Also, this architecture has low frame rates since each pixel is integrated and then read individually.

The last and the most widely used architecture is column-wise readout as illustrated in Fig. 3.26 [19]. This architecture is more practical than pixel-wise architecture since the read-out circuit area is not limited by the pixel area. Also, less number of amplifiers and integrators are implemented in this architecture; therefore, the total layout area and power consumption may not exceed the limits. In column-wise architecture, detector signals are read via row by row. In some cases, single readout channel may be shared by multiple FPA columns. This may be needed to decrease the average power consumption and total noise contribution of the readout channel since larger transistors

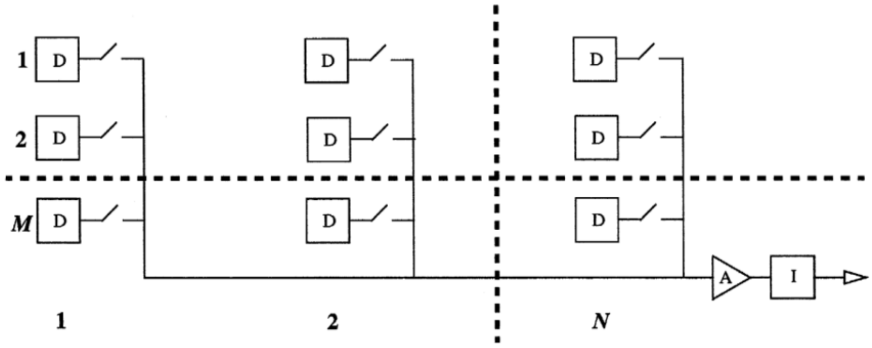

Figure 3.25: Serial readout.

can be implemented.

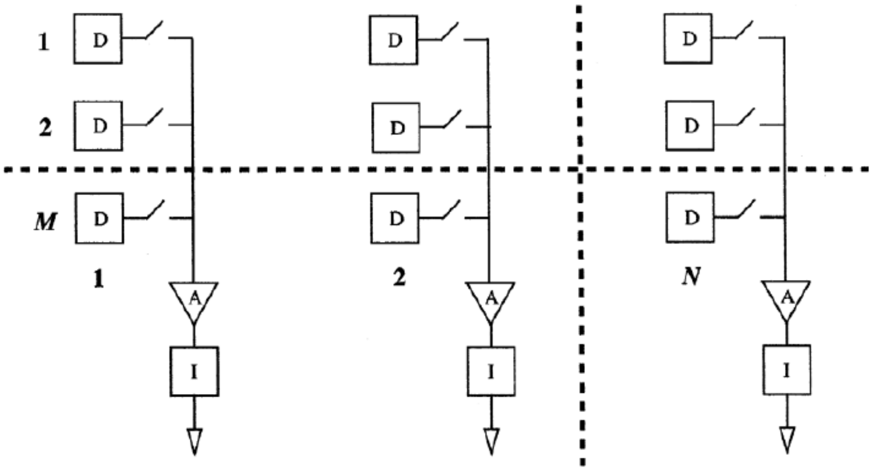

Figure 3.26: Column-wise readout.

This work is based on the designing of pre-amplifier with pixel-wise readout topology which has a lot of implementation limits specially with new pixel sizes, usually less than 17μm. Two types of pre-amplifier is designed and tested. Also layout size is evaluated for both amplifiers for adapting the design under each pixel.
By using the new 3D design process tool, in-pixel implementation of the pre-amplifier is possible. A ROIC also is designed for selecting the pixels with buffer and current amplification so the bolometer signal goes directly to the Trans-impedance amplifier (TIA) for pre-amplification which is followed by a source follower buffer then column and row selection (decoder) choose the cell to send the signal on the column bus of the ROIC. Fig. 3.27 shows the proposed ROIC diagram based on the pixel-wise design.

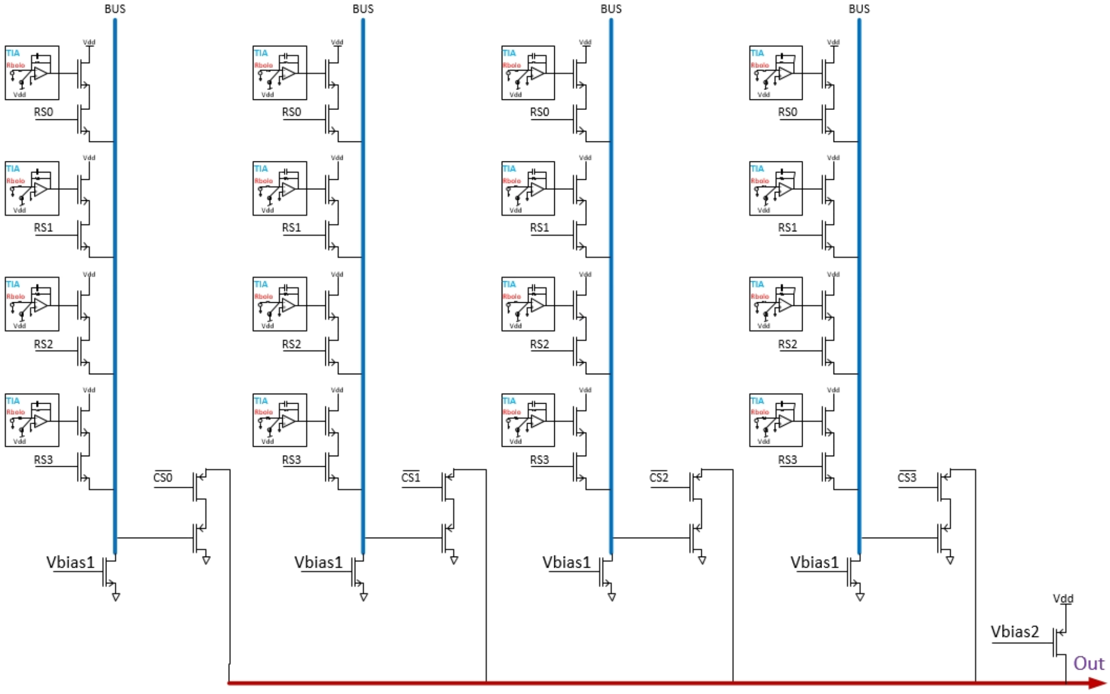

Figure 3.27: Proposed ROIC schematic.

A source follower (common drain) configuration is use as buffer with infinite current gain and approximately, voltage gain of one. The output of SF is lower than input with one V_{GS} for nfet source follower(Fig. 3.28). So the output shifted down by nfet SF and the result lift up by the readout output pfet SF (which has mirror effect of nfet). As we expect the final output readout will be from approximately 500mv to 800mv volt. Fig.3.29 shows the readout output result.

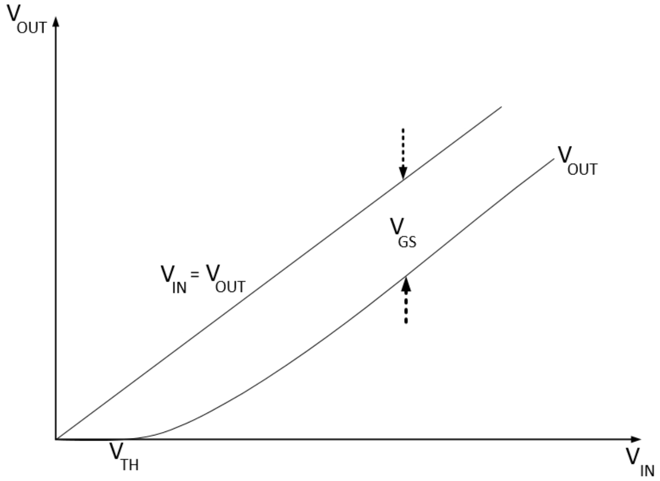

Figure 3.28: Variation of Vout with Vin for nfet source follower configuration.

Also the bolometer resistance is set for each pixel between 400kΩ till 500kΩ (divided in to 16). V_{bias1} for nfet is 400mV and V_{bias2} for pfet is 600mV. For generating decoder signal, pulse generator is used. Two for column decoder with values of 20ms and 10ms and two for row decoder with 80ms and 40ms. The transient analyse is run for 320ms. In the actual readout circuit, the clock signal apply to the logical gates which is producing the decoder addresses instead of using pulse generators.

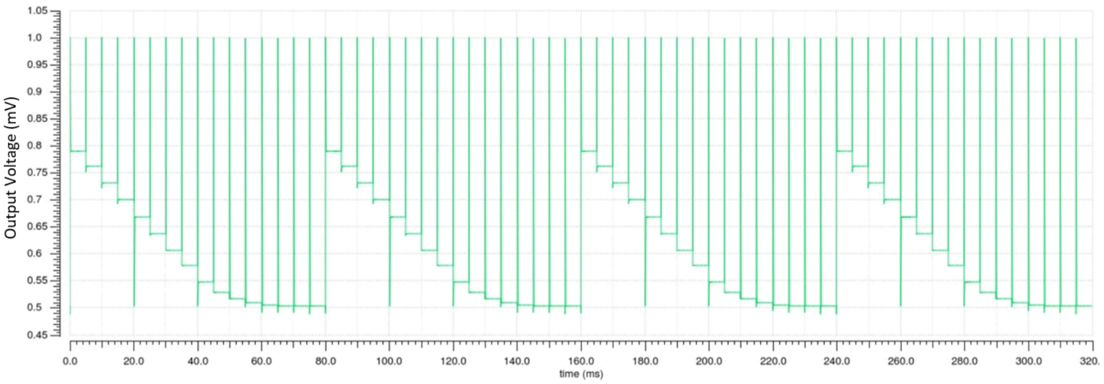

Figure 3.29: Simulation result of the ROIC with PTL decoder and 22.5μA DC compensation.

As Fig.3.29 shows, the output has many glitches with the same value for 6 or 7 pixels around 500mv which makes them not readable precisely. This output is a result of using Pass Transistor Logic (PTL) in decoder structure. In real logic, gates have a nonzero propagation delay resulting in spurious transitions or glitches (dynamic hazards). For reducing glitches, standard AND gate structure is used for decoder. The result is shown in Fig.3.30.

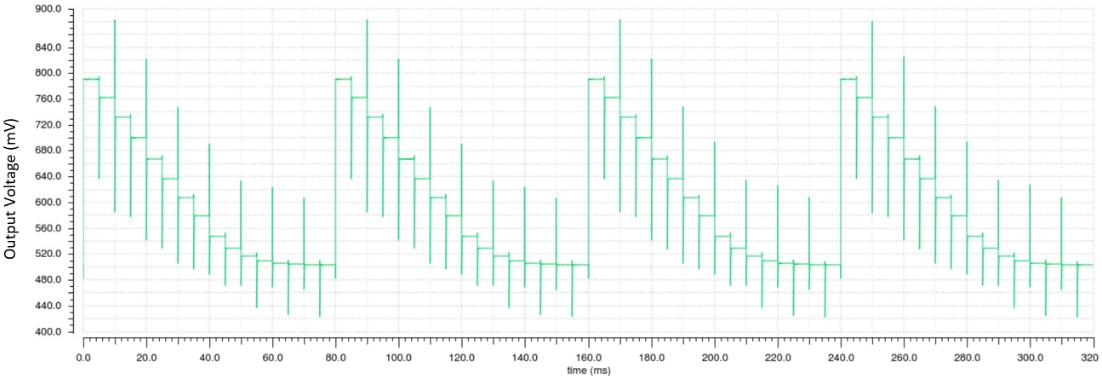

Figure 3.30: Simulation result of the ROIC with standard AND gate.

By adjusting DC offset current for each amplifier, we can set the amount of shifting up or down for SF nfet and pfet. Fig. 3 .31 shows the output result when the DC compensation is 21.5 μA.

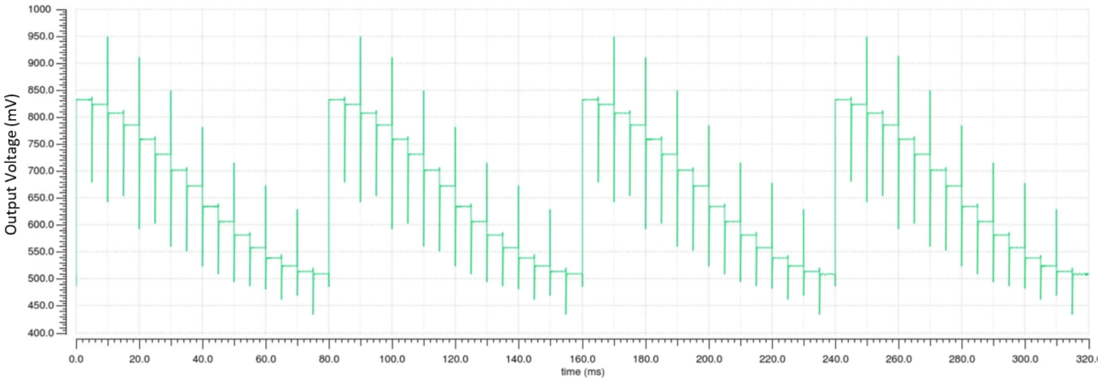

Figure 3.31: Simulation result of the ROIC with Standard AND gate and adjusting DC offset current (21.5μA).

Chapter 4

Layout

For the Layout, pixel size is limited to 17μm [45] in our work. For comparison purpose top tier and bottom tier TIA layout drew. As Fig. 4.3 and 4.4 show the difference result, top tier layout width is bigger by 3 to 4 μm. Some layout techniques are used to reduce mismatching and noise specially in amplifier design. Poor matching can result in non-idealities like amplifier offset, non-linearity and gain error. Common centroid layout techniques is widely used to minimize the effects of the linear gradients. Process gradients are systematic variations of a parameter over the wafer. Most process parameters are effected by process gradients. For example, the oxide thickness may vary systematically from one side of the wafer to the other. Similarly, for a transistor the threshold voltage may have a systematic variation.

Also using poly dummies to make sure matching elements see the same surroundings. Totally, we can say that The guard ring and diffusion (OD)/poly (PO) dummy improve the performance of MOSFET circuit [15]. For the top tier, metal layers M5 and M6 is used while for the connection of top tier to bottom tier via farming implemented instead of using single via , this can reduce the via's resistance and make better connections.

Fig. 4.1 shows Differential pair core of the Opamp common centroid with dummy poly and guard ring.

Fig. 4.2 shows the 2 to 4 decoder layout with 16T.

Fig. 4.3 shows top tier TIA layout which is placed under each pixel (with passive elements on bottom tier).

Fig. 4.4 shows bottom tier TIA layout.

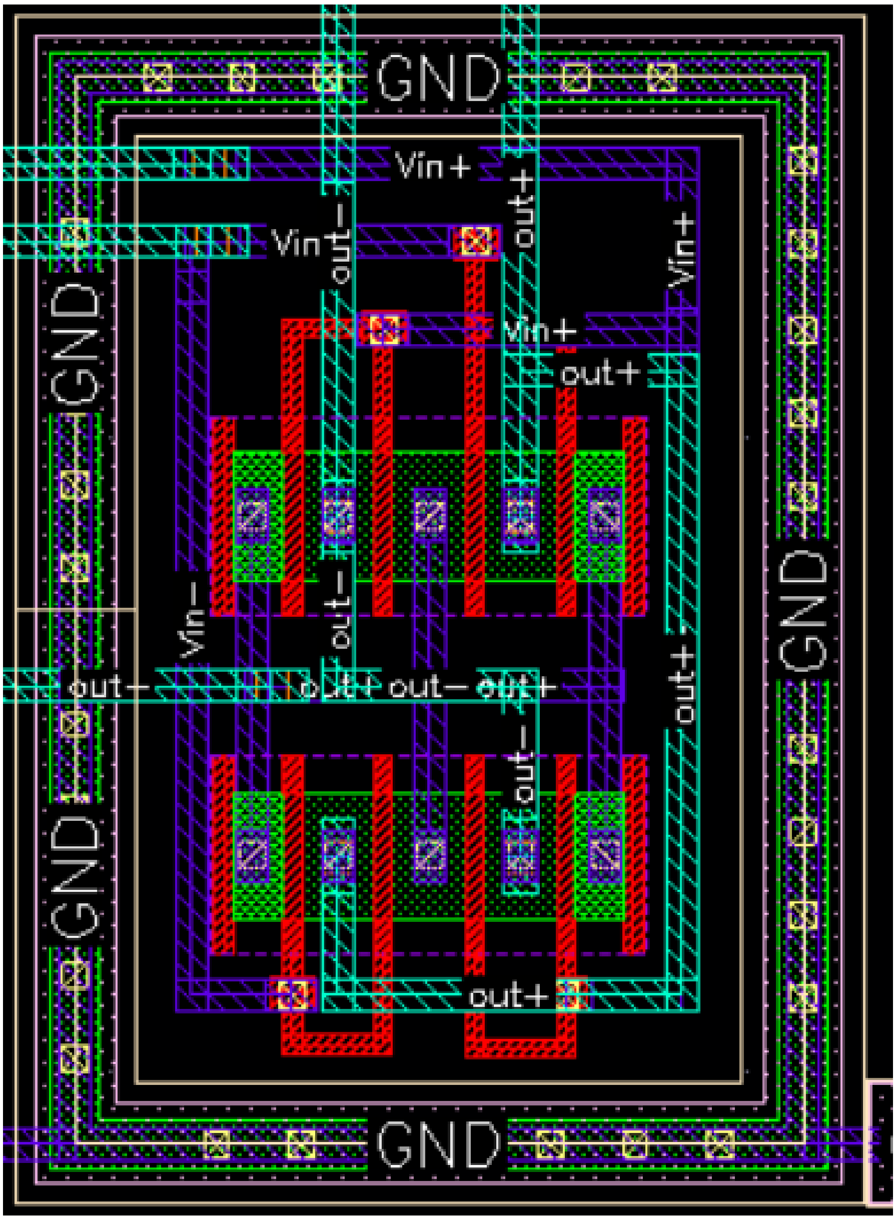

Figure 4.1: Differential pair core layout using ABBA configuration for pair transistors.

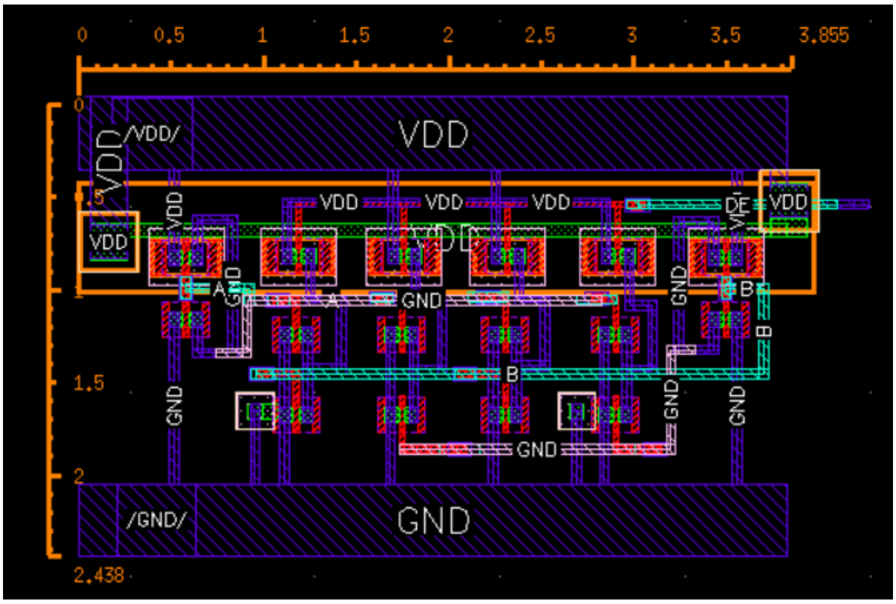

Figure 4.2: 2 to 4 decoder layout.

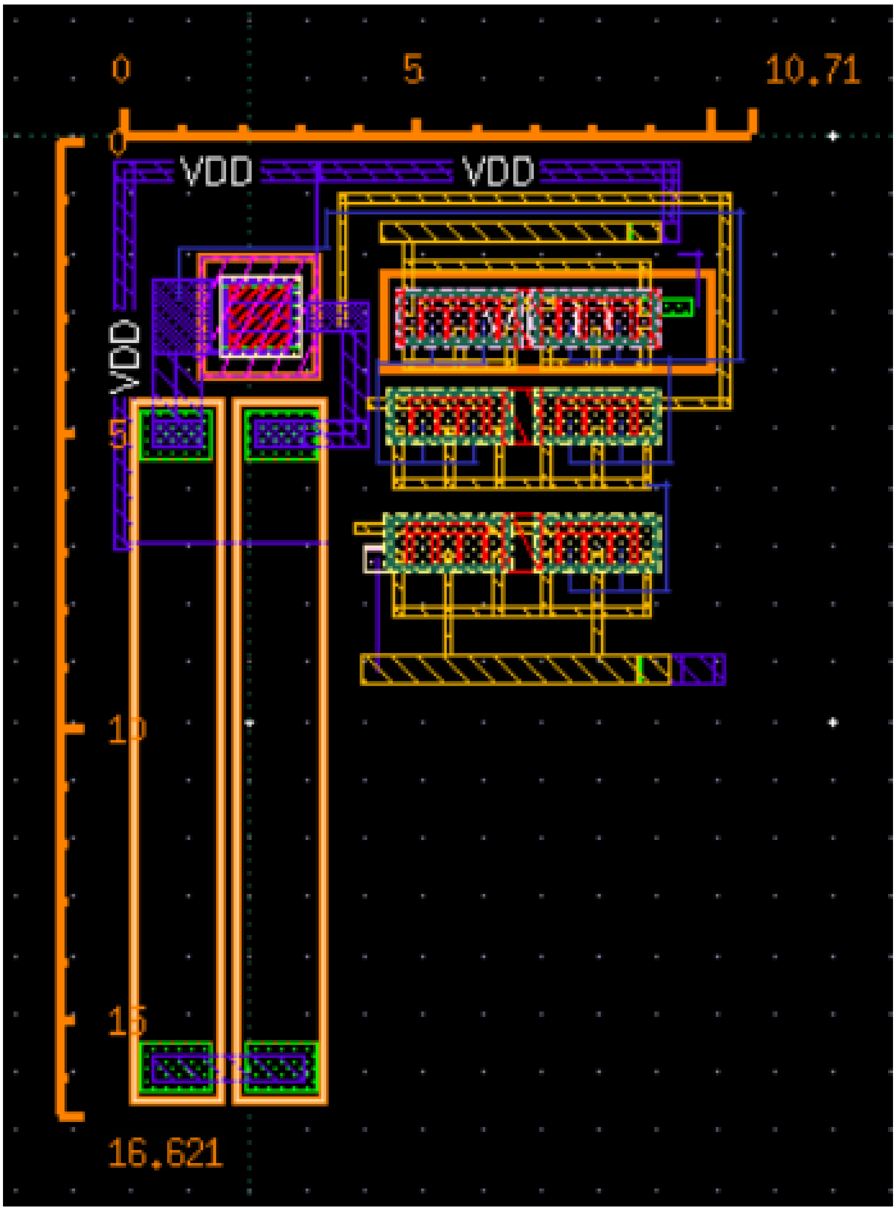

Figure 4.3: Top tier TIA layout.

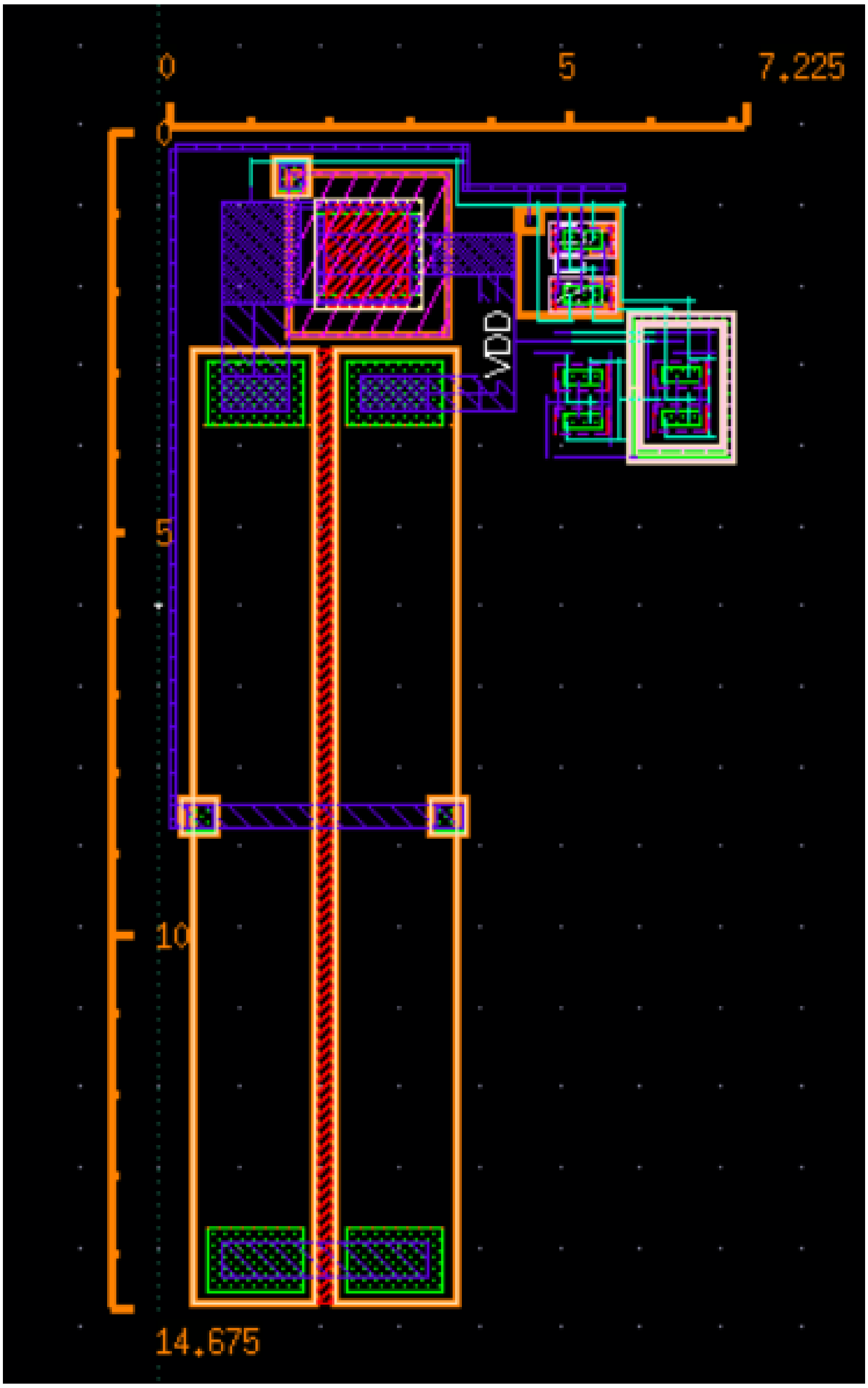

Figure 4.4: Bottom tier TIA layout.

Chapter 5

Conclusions

Pixel-wise readout configuration is implemented and functionality of this method by using TIA for each pixel is tested on 4x4 pixels array. Other parts of the readout (decoder, current sources, buffers) are designed and tested separately and within the ROIC. Although we have some glitches (related to the logical gates functionality) in the final result temperatures of 300K (26°C) to 370K (97°C) degrees would be reflected in an output voltage between 500mV and 850mV with adjusting DC current compensation. there are no statistical mismatch models for the top tier for doing Monte Carlo simulation, so that's a problem of the cadence tools. The Layout size is matched for each pixel with a good available place left for pixel at the size of 17μm [45].
As for future work , updating logical circuitry for generating decoder addresses with a clock as a system input, also building an ADC and memory cells as a digital storage at the pixel level is recommended.

Bibliography

[1] *16x16 Element MEMS Non-Contact Thermal Sensor for Use in Human Presence Sensors Utilizing Wafer-Level Vacuum Packaging Technology*. URL: http://www.omron.com/media/press/2013/05/e0529.html. May 29, 2013.

[2] *3D integrated circuit design*. URL: https://www.3dmuse.eu/. European Union Funding for Research and innovation.

[3] Rasim Caner alik and Emre Tunali. 'A Study on Calibration Methods for Infrared Focal Plane Array Cameras'. In: *SPIE* (2018). DOI: 10.5220/0006722402190226.

[4] Shahbaz Abbasi Arman Galioglua and Atia Shafique. 'A low power CMOS readout IC design for bolometer applications'. In: *Proc. of SPIE Vol. 10177* (2017). DOI: 10.1117/12.2262459.

[5] Norman B.Stevens. 'Semiconductors and Semimetals'. In: *Volume 5, 1970, Pages 287-318* (1970). DOI: 10.1016/S0080-8784(08)62818-5.

[6] R. Bannatyne. 'Digital Pixel Infrared Imaging Boosts Camera Speed and Performance'. In: *Vision Systems Design* (2020).

[7] G. Bieszczad and T. Sosnowski. 'Non-uniformity correction in microbolometer array with temperature influence compensation'. In: *MMS, vol XXI No. 4, pp. 709 718* (2014). DOI: 10.2478/mms-2014-0050.

[8] Paul R. Norton Bjørn F. Andresen Gabor F. Fulop. 'Infrared Technology and Applications'. In: *Proc. of SPIE Vol. 8353, 83531B · © 2012 SPIE · CCC code: 0277-786X/12* (2012). DOI: 10.1117/12.918916.

[9] F. W. Jih C. C. Hsieh and T. P. Sun. 'Focal-Plane Arrays and CMOS Readout Techniques of Infrared Imaging Systems'. In: *IEEE Trans. on Circuits and Systems for Video Tech., Vol. 7, No. 4, pp. 594-605* (1997). DOI: 10.1109/76.611171.

[10] R. Cannata. 'Design and Analysis of IR Focal Plane Electronics'. In: *SPIE Short Course Notes, Orlando* (1997).

[11] D.E. Carlson. 'Amorphous-silicon solar cells'. In: *IEEE* (1989). DOI: 10.1109/16.40936.

[12] RAMAZAN CETIN and OZAN ERTURK. 'Subwavelength perforated absorbers for infrared detectors'. In: *Optics Express 33700,Vol. 28, No. 22 / 26* (2020). DOI: 10.1364/OE.405100.

[13] T.-H. Yu; C.-Y. Wu; P.-Y. Chen; F.-W. Chi; J.-J. Luo; C. D. Chiang; Y.-T. Cherng. 'A new CMOS readout circuit for uncooled bolometric infrared focal plane arrays'. In: *IEEE* (2000).

[14] George S Chuan Li and Christopher H. 'Advancement in 17-micron pixel pitch uncooled focal plane array'. In: *SPIE, infrared technology and applications XXXV, Orlando* (2009). DOI: 10.1117/12.818189.

[15] Oscar Lau Chun-Chen Liu and Jason Y. Du. 'Complete DFM Model for High Performance Computing SoCs with Guard Ring and Dummy Fill Effect'. In: *ArXiv abs/1701.00460* (2017).

[16] DALSA Digital Cinema. 'Image Sensor Architectures for Digital Cinematography'. In: *03-70-00218-01* ().

[17] N. Coron, C. Cuesta and E. Garc. 'BGO scintillating bolometer: its application in dark matter experiments'. In: *IOP Publishing Ltd* (2010). DOI: 10.1088/1742-6596/203/1/012038.

[18] *Crew-1 Mission | Return*. URL: https://www.spacex.com/. Streamed live on May 2, 2021.

[19] C. Svensson D. Jakonis and C. Jansson. 'Readout architectures for uncooled IR detector arrays'. In: *Sensors and Actuators, vol. 84, pp. 220-229* (2000).

[20] S. Eminoglu D. Tezcan and T. Akin. 'A low-cost uncooled infrared microbolometer detector in standard CMOS technology'. In: *IEEE Transactions on Electron Devices* (2003). DOI: 10.1109/TED.2002.807453.

[21] S. Eminoglu D. Tezcan and T. Akin. 'A low-cost uncooled infrared microbolometer detector in standard CMOS technology'. In: *IEEE Transactions on Electron Devices, vol. 50, no. 2, pp. 494-502* (feb 2003). DOI: 10.1109/ted.2002.807453.

[22] A.C. Deb K.K; Ionescu and C. Li. 'Protein-based thin films: A new high-TCR material'. In: *Advanstar Communications. 17 (8): 52–55. Archived from the original on 2008-04-28* (2000).

[23] Maruyama T. Deguchi M. and Yamasaki. 'Design using Simulation Program for CCD Image Sensor'. In: *IEEE Transactions on Consumer Electronics,Volume: 38, Issue: 3, PP 583 - 589* (1992). DOI: 10.1109/30.156740.

[24] G.and Norgia Donati Martini. 'Microconcentrators to recover fill- actor in image pho-todetectors with pixel on-board processing circuits'. In: *Opt. Express 15, 18066–18075* (2007).

[25] W. J. Parrish; G. T. Kincaid; J. L. Heath; J. D. Frank. 'Lowcost 160 x 128 uncooled infrared sensor array'. In: *SPIE* (1998).

[26] D.B. Goldstein. 'Physical Limits in Digital Photography'. In: (2009).

[27] E. Gray and Campbell Searle. *Electronic Principles: Physics, Models and Circuits*. 1969. ISBN: 978-0471323983.

[28] M. J. Griffin and W. S. Holland. 'The influence of background power on the performance of an ideal bolometer'. In: *Infrared and Millimeter Waves, vol. 9, pp. 861–875* (1988).

[29] Fabrice Guellec. 'A 25µm pitch LWIR focal plane array with pixel-level 15-bit ADC providing high well capacity and targeting 2mK NETD'. In: *SPIE,Infrared Technology and Applications XXXVI* (2010). DOI: 10.1117/12.849684.

[30] Prachi Gupta. 'NETD Parameter in Thermal Imaging'. In: (2020).

[31] Kim H-Y. 'Mechanical robustness of FPA in a-Si microbolometer with fine pitch'. In: *TechConnect Briefs* (2010). DOI: 978-1-4398-3402-2.

[32] H. Bousack H. Soltner and H. Schmitz. 'Infrared receptors in pyrophilous ('fire loving') insects as model for new un-cooled infrared sensors'. In: *Beilstein Journal of Nanotechnology 2, 186* (2001). DOI: 10.3762/bjnano.2.22.

[33] Urban Halldin Henk Martijn and Jan Y. Andersson. 'A 640 by 480 Pixels Readout Circuit for IR Imaging'. In: *Analog Integrated Circuits and Signal Processing, Vol.22, pp.71-79* (2000). DOI: 10.1117/12.918916.

[34] W. Herschel. 'Experiments on the solar and on the terrestrial rays that occasion heat'. In: *Philosophical Transactions of the Royal Society. London* (1800).

[35] Tae Hyun Kim Ho Jung and Gyungtae Kim. 'Design and characteristics of a-Si-based micro-bolometers with shared-anchor structure in vacuum packaged systems'. In: *Springer* (2014). DOI: 10.1007/s00542-014-2073-3.

[36] F. Hooge. '1/f noise sources'. In: *IEEE Transactions on Electron Devices, vol. 41, no. 11, pp. 1926-1935* (1994).

[37] F. Hooge and L. Vandamme. 'Lattice scattering causes 1/f noise'. In: *Physics Letters A, vol. 66, no. 4, pp. 315-316* (1978).

[38] Horowitz and Hill. *The Art of Electronics*. 2015. ISBN: 9780521809269.

[39] Makoto Ikeda. 'Circuit Contributions to Performance of Imagers Transcript'. In: *IEEE solid states circuits society* (2018).

[40] *IR CAMERA MARKET - GROWTH, TRENDS*. URL: https://www.mordorintelligence.com/industry-reports/ir-camera-market.

[41] Christer Jansson. 'A high-resolution, compact and low-power ADC suitable for array implementation in standard CMOS'. In: *IEEE Transactions on circuits and systems - I: Fundamental theory and applications, Vol. 42, No. 11* (1995). DOI: 10.1109/81.477201.

[42] Hee Yeoun Kim and Kyoung Min Kim. 'Mechanical Robustness of FPA in a-Si microbolometer with fine pitch'. In: *Sensors and Transducers Journal, Vol.11, 56-63* (2011).

[43] J. Kim and C. Han. 'A New Uncooled Thermal Infrared Detector using Silicon Diode'. In: *Sensors and Actuators A 89, pp 22-27* (2001).

[44] Tae Hyun Kim and Gyungtae Kim. 'Design and characteristics of a-Si-based micro-bolometerswith shared-anchor structure in vacuum packaged systems'. In: *Springer, Microsyst Technol* (2014). DOI: 10.1007/s00542-014-2073-3.

[45] Taehyun Kim, Kimyung Kyung and Jae Hong Park. 'Development of microbolometer with high fill factor and high mechanical stability by shared-anchor structure'. In: *SPIE* (2012). DOI: 10.1117/12.918916.

[46] Taehyun Kim, Kimyung Kyung and Jae Hong Park. 'Sensors, Space Probes and Wi-Fi Cybersecurity'. In: *Maxfield, Max., Electronic Engineering Journal* (2020).

[47] M. Kimata. 'IR imaging" in Comprehensive Microsystems'. In: *vol. 3. Elsevior: Amsterdam, The Netherlands,* (2008).

[48] Masafumi Kimata. 'Trends in Small-format Infrared Array Sensors'. In: *SENSORS, 2013 IEEE* (2013). DOI: 10.1109/ICSENS.2013.6688495.

[49] P. W. Kruse. *Uncooled Thermal Imaging Arrays, Systems, and Applications*. SPIE. 2001. ISBN: 0-12-752155-0.

[50] Ko-Chi Kuo and Adrian Leuciuc. 'A linear MOS transconductor using source degeneration and adaptive biasing'. In: *IEEE Transactions on Circuits and Systems II Analog and Digital Signal Processing 48(10):937 - 943* (2001). DOI: 10.1109/82.974782.

[51] Sergei A. Kuznetsov1 and Andrey G. Paulish. 'Selective Pyroelectric Detection of Millimetre Waves Using Ultra-Thin Metasurface Absorbers'. In: *Scientific Reports , 6:21079* (2016). DOI: 10.1038/srep21079.

[52] K Lafevre. *Design of a Modified Cherry-Hooper Transimpedance Amplifier with Dc Offset Cancellation*. 2020. ISBN: 978-1-249-07817-3.

[53] K. Lafevre. *Design of a Modified Cherry-Hooper Transimpedance Amplifier with Dc Offset Cancellation*. 2020. ISBN: 978-1-249-07817-3.

[54] S. H. Black M. J. Hewitt and C. J. Nielsen. 'Infrared Readout Electronics: A Historical Perspective'. In: *Infrared Readout Electronics II, Proc. SPIE Vol. 2226, pp. 108-120* (1994). DOI: 10.1117/12.178474.

[55] R. Jimenez M. Moreno and R. Ambrosio. 'Microbolometers based on amorphous silicon germanium films with embedded nanocrystals'. In: *IEEE Transactions on Electron Devices, vol. 62, no. 7, pp. 2120-2127* (jul 2015). DOI: 10.1109/ted.2015.2434275.

[56] R. Jimenez M. Moreno and R. Ambrosio. 'Microbolometers based on amorphous silicon-germanium films with embedded nanocrystals'. In: *IEEE Transactions on Electron Devices, vol. 62, no. 7, pp. 2120-2127* (2015). DOI: 10.1109/TED.2015.2434275.

[57] American Society of Mechanical Engineers. 'Types of temperature measuring instruments'. In: *ASME* (2015).

[58] Nobili; Melloni. 'Recherches sur plusieurs phénomènes calorifiques entreprises au moyen du thermo-multiplicateur" [Investigations of several heat phenomena undertaken via a thermo-multiplier]'. In: *Annales de Chimie et de Physique. 2nd series* (1831).

[59] Barone 0F. B. Milton A. F. and Kruer M. R. 'Influence of nonuniformity on infrared focal plane array performance'. In: *Optical Engineering, Vol. 24, No. 5, pp. 855-862* (1985).

[60] Leopoldo Nobili. 'Description d'un thermo-multiplicateur ou thermoscope électrique [Description of a thermo-multiplier or electric thermoscope]'. In: *Bibliothèque Universelle* (1830).

[61] S. Chen P.Wang and H.Wang. 'High sensitivity 17μ pixel pitch 640x512 uncooled infrared focal plane arrays based on amorphous vanadium oxide thin films'. In: *IEEE Electron Device Letters, vol. 36,no. 9, pp. 923-925* (sep 2015). DOI: 10.1109/ted.2015.2451995.

[62] S. Chen P.Wang and H.Wang. 'High sensitivity 17u pixel pitch 640x512 uncooled infrared focal plane arrays based on amorphous vanadium oxide thin films'. In: *IEEE Electron Device Letters, vol. 36,no. 9, pp. 923-925* (2015). DOI: 10.1109/led.2015.2451995..

[63] Behzad Razavi. 'The Transimpedance Amplifier'. In: *IEEE SOLID-STATE CIRCUITS MAGAZINE* (2019). DOI: 10.1109/MSSC.2018.2881860.

[64] P. L. Richards. 'Bolometers for infrared and millimeter waves'. In: *Journal of Applied Physics 76* (1994). DOI: 10.1063/1.357128.

[65] M. Y. Tanrikulu S. Eminoglu and T. Akin. 'A Low-Cost 64 × 64 Uncooled Infrared Detector in Standard CMOS'. In: *Int. Conf. on Solid-State Sensors, Actuators and Microsystems (TRANSDUCERS'03), pp. 316-319* (2003).

[66] M. Y. Tanrikulu S. Eminoglu and T. Akin. 'A Low-Cost, Small Pixel Uncooled Infrared Detector for Large Focal Plane Arrays using a Standard CMOS Process'. In: *Infrared Detectors and Focal Plane Arrays VII, Proc. of SPIE, Vol. 4721, pp. 111-121* (2002).

[67] M. Y. Tanrikulu S. Eminoglu and T. Akin. 'Low-Cost Uncooled Infrared Detector Arrays in Standard CMOS'. In: *Infrared Technology and Applications XXIX, Proc. of SPIE, Vol. 5074* (2003).

[68] M. Y. Tanrikulu S. Eminoglu and T. Akin. 'Low-Cost Uncooled Infrared Detectors in CMOS Process'. In: *The 16th European Conf. on Solid-State Transducers (Eurosensors XVI), Prague, Czech Republic, pp. 263-264* (2002).

[69] Pierre Imperinetti Sebastien Becker and Jean-Jacques Yon. 'Latest pixel size reduction of uncooled IR-FPA at CEA, LETI'. In: *SPIE Vol. 8541, 85410C* (2012). DOI: 10.1117/12.974579.

[70] P. E. Howard; J. E. Clarke; A. C. Ionescu; C. C. Li; J. C. Stevens. 'DRS u6000 640x480 VO x uncooled IR focal plane'. In: *in Infrared Detectors and Focal Plane Arrays VII, E. L. Dereniak and R. E. Sampson, Eds. SPIE* (2002).

[71] M. Suzuki. 'A 1.5 ns 32b CMOS ALU in double pass-transistor logic'. In: *IEEE Int. Solid-State Circuits Conf.,pp. 90–91.* (1993). DOI: 10.1109/ISSCC.1993.280071.

[72] C. Chiang T. Yu and Y. Cherng. 'A new CMOS Readout Circuit for Uncooled Bolometric Infrared Focal Plane Arrays'. In: *IEEE* (May 2000). DOI: 10.1109/ISCAS.2000.856373.

[73] Anh Tung Doan Thang Duy Dao and Satoshi Ishii. 'MEMS-Based Wavelength-Selective Bolometers'. In: *Micromachines* (2019). DOI: 10.3390/mi10060416.

[74] *Thermopile Infrared Array and Thermal Imaging*. URL: http://www.heimannsensor.com/products_imaging.php.

[75] E. Mottin; A. Bain; J.-L. Martin; J.-L. Ouvrier-Buffet; S. Bisotto; J.-J. Yon; J.-L. Tissot. 'Uncooled amorphous silicon technology enhancement for 25 μm pixel pitch achievement'. In: *in Infrared Technology and Applications XXVIII, B. Andresen, G. F. Fulop, and M. Strojnik, Eds. SPIE* (2003).

[76] A. Tanaka; K. Chiba; T. Endoh; K. Okuyama; A. Kawahara; K. Iida; N. Tsukamoto. 'Low-noise readout circuit for uncooled infrared FPA'. In: *SPIE* (2000).

[77] V. Garg V. Ravinuthula and J. G. Harris. 'Time-mode circuits for analog computation'. In: *International Journal of Circuit Theory and Applications, vol. 37, no. 5, pp. 631-659* (2008). DOI: 10.1002/cta.488.

[78] J. L. Vampola. 'Readout Electronics for Infrared Sensors'. In: *The Infrared and Electro-Optical Systems Handbook, Vol. 3, Chapter 5, SPIE Optical Engineering Press, pp. 286-324* (1993).

[79] Kenton T. Veeder. 'Digital Converters for Image Sensors, Kenton T. Veeder'. In: *SPIE* (2015). DOI: 10.1117/3.1000639.

[80] K.P. VOLLMER M.and MOLLMANN. 'Infrared Thermal Imaging Fundamentals, Research and Applications'. In: *Wiley-VCH Verlag GmbH and Co,Weinheim* (2010).

[81] Hongchen; Xinjian Yi Wang and Jianjun Lai. 'Fabricating Microbolometer Array on Unplanar Readout Integrated Circuit'. In: *Infrared and Millimeter Waves. 26 (5): 751–762* (2005). DOI: 10.1007/s10762-005-4983-8.

[82] Jyun-Hao Su ; Wen-Kuan Yeh ; Wen-Teng Chang ; Ban-Li Wu ; Ju-Mei Lu; Jin-Hung Wang. 'Temperature coefficient of resistance related to amorphous silicon/metal contact design of microbolometers'. In: *IEEE* (2016). DOI: 10.1109/ICDCSyst.2016.7570626.

[83] Pezoa J.E. Wolf A. and Figueroa M. 'Modeling and compensating temperature-dependent non-uniformity noise in IR microbolometer cameras'. In: *MDPI AG* (2016). DOI: 10.3390/s16071121.

[84] X. Wu. ‘Theory of transmission switches and its application to design of CMOS digital circuits’. In: *Int. J. Circuit Theory Appl., vol. 20, no. 4,pp. 349– 356* (1992). DOI: 10.1002/cta.4490200402.

[85] Liang Xie Xiaojuan Xia and Weifeng Sun. ‘A High Performance CMOS Readout Integrated Circuit For IRFPA’. In: *SPIE* (2007). DOI: 10.1117/12.790751.

[86] K. Yano. ‘A 3.8-ns CMOS 16 × 16-b multiplier using complementary pass-transistor logic’. In: *IEEE J. Solid-State Circuits, vol. 25,no. 2,pp. 388–393* (1990). DOI: 10.1109/4.52161.

[87] Nezih Topaloglu; Patricia M. Nieva; Mustafa Yavuz and Jan P. Huissoonl. ‘A Novel Method for Estimating the Thermal Conductance of Uncooled Microbolometer Pixels’. In: *IEEE* (2007). DOI: 1-4244-0755-9/07.

[88] Wan W. Yuan X. and Zhao M. ‘New method for nonuniformity correction of solid state image sensor’. In: *Proc.SPIE* (1995). DOI: 10.1117/12.217397.

[89] Shiang-Feng Tang Yu-Zhen Deng. ‘Experiments on Temperature Changes of Microbolometer under Blackbody Radiation and Predictions Using Thermal Modeling by COMSOL Multiphysics Simulator’. In: *Sensors* (2018). DOI: 10.3390/s18082593.